

ELECTRIC VEHICLES - REVIEW OF TYPE-APPROVAL LEGISLATION AND THE IDENTIFICATION AND PRIORITISATION OF POTENTIAL RISKS

Ceri Donovan

Dr Huw Davies

Gerry Fung

Cardiff University School of Engineering

United Kingdom

Paper Number 13-0038

ABSTRACT

The introduction of electric vehicles provides opportunities for new mobility solutions. The extent to which these opportunities are realised depends on the accompanying regulatory framework. Current regulatory frameworks have developed around the internal combustion engine (ICE) and in response to observed problems - an example being the initial development of the FMVSS. For e-mobility, these frameworks need to be revisited and adapted for the new mobility paradigm. The problem faced by regulators is the accelerated pace of technology change is incompatible with the pace of regulatory development. Although the problems associated with the move to e-mobility are understood, the issue has been how to ensure that the transition to a regulatory framework is conducive to the introduction and continuing innovation in the e-mobility sector whilst avoiding technology lock-in. The approach taken here is to develop and trial a methodology that looks to prioritise the problems and to enable the regulator to focus on development of regulation in parallel to the uptake of e-mobility. The proposed approach consists of three phases. These are: a thematic analysis - to provide a measure of e-mobility development; a functional system breakdown - to identify the areas in which regulation is challenged; and a failure mode effect analysis - to prioritise the development of regulation in those areas in which are found to be deficient.

This work is ongoing and as such only the methodology is described in this paper with the use of exemplars. The work is part of the ENEVATE project, which is a JTS INTERREG IVB funded project.

INTRODUCTION

The pressures of rising fuel costs coupled with the need to meet ever stricter emissions targets, such as those outlined by Europe 2020 (European Commission, 2010), are driving the search for alternative propulsion methods for passenger cars. Of the competing technologies, electric vehicles (EV) seems to be the most viable proposition in the short term, in part due to its use of existing technologies. However, many of these technologies come from vastly different markets, such as mobile computing and smart phones and are being developed at a much quicker rate than is normal in the automotive sector. The regulatory framework that has been put in place is not reactive enough to encompass these new technologies as they come to market, so a new approach is needed.

As yet, the adoption of EVs has been slow, despite the fact that mainstream manufacturers have been producing models for several years. Research by the European Network of Electric Vehicles and Transferring Expertise (ENEVATE) has shown that a major barrier to adoption is the purchase cost – EVs that are currently on the market are too expensive for the average motorist (Davies et al, 2012). Ensuring that regulations do not place restrictions that inhibit new, cheaper and more efficient technologies reaching marketplace will mean that the demand for EVs will be enhanced, as they will become a more realistic alternative to the current internal combustion engine (ICE) powered cars.

Streamlining the type approval process also makes the market more appealing to smaller manufacturers. Those that already produce EVs tend towards lightweight electric vehicles (LEV) that are classed as a quadracycle (European classification L6e/L7e). These are appealing to

urban dwellers as they are ideal for city use where space is at a premium and journeys may be shorter. However LEVs do not require the same level of safety testing and they are also lower performance vehicles, which may lead to poor perception of EVs in general by the media and general public.

Initial work has been undertaken in updating the regulatory framework in response to EVs beginning to emerge in the transport mix. In Europe the most notable review of the type approval process was carried out by the UK's Transport Research Laboratory on behalf of the European Commission (Visvikis et al, 2010), whilst in the US the American National Standards Institute (ANSI) Electric Vehicles Standards Panel (EVSP) has produced a standardization roadmap (American National Standards Institute, 2012). Whilst both of these documents give comprehensive reviews of existing standards and where there might be gaps, there is no method of prioritising where effort should be concentrated to achieve the biggest gains and, as a result, accelerating e-mobility.

Currently, regulations are developed in response to problems rather than anticipating them. Further problems arise as there are relatively few EVs currently in use, resulting in limited data with which to detect operational faults.

In order to pre-empt how regulations should be developed and where effort should be targeted, this paper proposes a three stage process to identify and prioritise potential gaps in the regulations.

METHODOLOGY DEVELOPMENT

A new methodology is proposed to both identify areas where problems might arise and prioritise these in order that the greatest gains might be achieved. It will also create a dynamic framework in which to develop regulations in the future. The methodology uses a novel combination of techniques that form a three stage process comprising of a thematic analysis, a functional system breakdown (FSB) and a failure mode and effects analysis (FMEA). The thematic analysis provides the context by exploring the themes surrounding vehicle safety and how related technologies are developing. It does this by examining a variety of qualitative sources of data. A functional system breakdown is then used to decompose the vehicle into sub systems and

mission modules, to which the appropriate regulations can be attached. This provides a method of sorting the complex regulatory framework. Critical pathways are then highlighted in the FBS based on the thematic analysis and deficiencies in the current regulations that have been identified. Finally applying an FMEA will allow the deficiencies to be prioritised in terms of severity of failure mode and probability of occurrence of the identified gaps in the regulatory process.

Thematic Analysis

Thematic Analysis is a qualitative research technique focusing on examining and recording themes within a set of data that may come from a variety of sources. These might include interviews with experts and stakeholders, literature reviews, conference proceedings and the media. (for example see Rossen et al, 2012). A lack of empirical data relating to incidents where failures have occurred means alternative sources must be used to gauge safety related issues. An overview on safety aspects and also emerging technology trends can be sought from literature reviews and conference proceedings. Detailed expert opinion can be gained from interviewing stakeholders and industry experts.

The analysis consists of a three stage process of thematizing, data collection and analysing & transcribing, which are described as follows:

Thematizing This bounds the area of the analysis by describing what themes should be included, and those that should not. As the aim is to identify areas where electric vehicles may not necessarily be covered by current regulations, the themes will be the areas of concerns where EV safety may be a potential problem. Hybrid and fuel cell vehicles have not been included, although there will inevitably be some overlaps in technologies that may warrant investigation in order to further streamline the type approval process. Also, charging infrastructure has not been fully included in order to keep the main focus on vehicle technology. Again, this is an important area that should be considered in future studies as it can have major impacts on safety, for example when charging takes place in domestic properties or in public places.

Data Collection The next stage is data collection, in which relevant source material needs to be gathered. As there is little data available on safety issues arising from incidents involving EVs, alternative methods are needed. A more general overview can be gained from scientific literature reviews, conference proceedings and other documents such as roadmaps and policy documents. This can also provide some insight to any new technologies that are currently in development. In order to obtain a more detailed opinion on relevant issues, semi-structured stakeholder interviews should be undertaken. Here industry experts such as legislators, manufacturers and safety testing organisations are asked a series of open questions in order to elicit their opinion, but still retaining some structure and context in order that comparisons can be made between responses. A detailed description of interviewing techniques can be found in Johnson, 2002. By drawing upon networks such as ENEVATE, a wide range of experience and opinion can be gathered. In particular, the work already carried out by ENEVATE on surveying supply chain stakeholders (Pannkoke and Ernst, 2012) can be used to identify emerging technology development trends. This work is ongoing and does not form part of the example described in this paper, but will be reported at the ENEVATE final conference, November 2013.

Analysing & Transcribing After reviewing all the information that has been gathered from various sources, the data is then analysed. This is done by examining the text in detail and highlighting the emerging and recurring themes. By recording the occurrence of each theme, patterns begin to emerge, highlighting where opinion lies with regards to the issues being explored. Themes can also be grouped where similarities occur, and ranked according to how often they are highlighted in order to gauge the importance of a theme.

Functional System Breakdown

Stage two of the methodology is a functional system breakdown (FSB). Today's vehicles are incredibly complex and in most cases regulations only apply to specific parts of the vehicle. In order to make sense of the regulations in relation to the vehicle and highlight areas of concerns, a method of sorting is required, for which FSB is ideal.

An FSB starts with the top level primary function of the system – in this case the vehicle. This is then decomposed into multi level sub systems, such as drivetrain and structures. These are further broken down until they reach mission modules, each of which has its own function such as the battery in an EV or fuel tank in an ICE vehicle. The function of the module missions affects the performance of the sub systems, which in turn determines the operation of the primary function – for example the fuel tank or battery supplies energy into the drivetrain which then powers the vehicle. Some examples and methods of FSB can be found in Stone & Wood, 2000 and Pailhès et al 2011. A basic FSB outline is shown in *Figure 1*

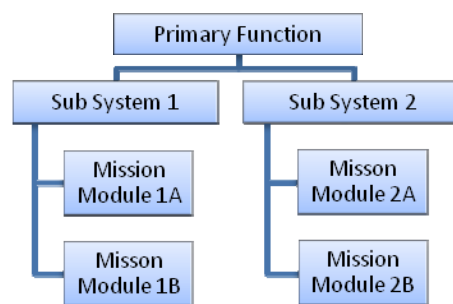


Figure 1 outline functional system breakdown.

The level of detail contained in the FSB can vary depending on the context and it could potentially include the component level as the mission modules. Whilst this might highlight areas where new technologies may appear, it also should not be over prescriptive as tightly specifying components could exclude future innovations.

For this methodology two FSB diagrams should be produced, one for a standard passenger ICE powered vehicle (e.g. European category M₁) and one for an equivalent class EV. For each level in the diagram the appropriate regulations should be identified, where they exist. By comparing the FSB diagrams the areas that require new regulations can be highlighted. In addition the FSB for the EV can be compared with the thematic analysis results. This will further identify the areas where there may be gaps in the regulations. As a result a number of critical pathways can then be devised. These are subsequently used to determine areas of concern and the relevant regulations can be investigated.

Failure Mode and Effects Analysis

The final step is to take an area highlighted by the critical pathways and apply a failure mode and effects analysis (FMEA). This is done in order to prioritise where the most gains can be made and allocate available resources appropriately. An FMEA is more normally used to identify areas of risk or potential failure within a system or process. To do this three criteria are applied: severity, occurrence and detection. Each of these is given a ranking (usually numerical). By multiplying the values a final score is achieved, highlighting the areas that are most at risk to developing a fault. The standard procedure for conducting an FMEA in Europe is outlined in IEC 60812:2006. (CENELEC, 2006). FMEA is routinely used in many industries, including the automotive industry (for example Chrysler et al, 1995). It can also be applied to processes as diverse as healthcare (Latino 2004) and web based systems (Zhou and Stålhane, 2004), which highlights the adaptability of the procedure.

The automotive industry generally uses a scoring system ranging from 1 to 10, with clearly defined criteria to guide the application of the ranking. These will be used for the proposed methodology as they are widely used and understood (e.g. Chrysler et al, 1995). The scores as listed in IEC 60812:2006 for severity are described in Table 1 and scores for occurrence are shown in Table 2.

Table 1
FMEA Severity Scores

Severity	Criteria	Score
None	No discernible effect.	1
Very minor	Fit and finish/squeak and rattle item does not conform. Defect noticed by discriminating customers (less than 25 %).	2
Minor	Fit and finish/squeak and rattle item does not conform. Defect noticed by 50 % of customers.	3
Very low	Fit and finish/squeak and rattle item does not conform. Defect noticed by most customers (greater than 75 %).	4

Low	Vehicle/item operable but comfort/convenience item(s) operable at a reduced level of performance. Customer somewhat dissatisfied.	5
Moderate	Vehicle/item operable but comfort/convenience item(s) inoperable. Customer dissatisfied.	6
High	Vehicle/item operable but at a reduced level of performance. Customer very dissatisfied.	7
Very high	Vehicle/item inoperable (loss of primary function)	8
Hazardous with warning	Very high severity ranking when a potential failure mode affects safe vehicle operation and/or involves non-compliance with government regulation with warning.	9
Hazardous without warning	Very high severity ranking when a potential failure mode affects safe vehicle operation and/or involves non-compliance with government regulation without warning.	10

Source CENELEC 2006

Table 2
FMEA Occurrence Scores

Occurrence	Score	Frequency
Remote: Failure is unlikely	1	≤ 0.010 per thousand units
Low: Relatively few failures	2	0.1 per thousand units
Moderate: Occasional failures	3	0.5 per thousand units
	4	1 per thousand units
	5	2 per thousand units
	6	5 per thousand units
High :Repeated failures	7	10 per thousand units
	8	20 per thousand units
Very high: Failure almost inevitable	9	50 per thousand units
	10	≥100 in thousand units

Source CENELEC 2006

The automotive industry also uses a score of 1 to 10 to rank the probability of detection of a given fault, again with defined criteria for each score. However for the proposed methodology, detection relates to whether or not a potential fault in a mission mode is covered by existing regulations. In

order to simplify the process, a value of 0 is given if the mission module is covered by a standard and 1 if it is not. The resulting score will then be zero if the module is adequately covered and it will not be included in the final prioritisation. Those that are not covered by existing standards will have a score based on severity multiplied by risk, so in principle those with the highest scores would be given highest priority once the modules are put in ranking order.

One of the drawbacks is that the values used for the ranking may in many cases be subjective, as evidence based on failure rates may not be available due to the small number of EVs currently in use. Where available evidence from other sources may be used – for example, if a technology has been used for a different application then data from this can be used to determine the score. This should only be done with the caveat that automotive use may place different demands on the technology, particularly where safety critical systems such as braking are involved. Expert opinion may also be used; ideally a consensus of opinion should be reached by multiple stakeholders where possible.

EXAMPLE APPLICATION

In order to demonstrate the proposed methodology a worked example has been carried out for this paper. The example has been kept deliberately simple by focusing on one potential area for concern to highlight the methodology rather than the outcome. Work is ongoing by the ENEVATE project team in order to further validate the methodology and develop realistic applications, which will be reported at the ENEVATE final conference, November 2013.

Thematic Analysis

In order to obtain a high level overview of potential areas of concern, data was gathered from proceedings taken from worldwide EV related events from 2010 to present. This gives a broad consensus of areas of concern, not just relating to vehicle technologies and systems but also to the general usage of EVs, with the aim of highlighting where potential failures might arise. A second data set was taken from the standards review undertaken by TRL and the ANSI roadmap. By comparing these two data sets a gap analysis can be

undertaken in order to determine any areas that have not been considered by these reviews. The themes that became apparent are summarised in Table 3. Those shown in bold are themes that were not covered by the TRL summary and ANSI roadmap.

Table 3
General Thematic Analysis using Conference Proceedings

Theme	Count
Aftermarket standards	7
Battery - recycling and reuse	11
Battery safety - design	2
Battery safety - general	13
Battery safety - misuse	3
Battery Safety - monitoring	3
Battery safety - protection	3
Battery storage	8
Battery testing methods	7
Emergency Response procedures	10
Standards - Charging	12
Standards - electrical safety	7
Standards for batteries	6
Standards for Charging interoperability	9
Standards for retrofit systems	1
Standards for vehicles	9
System integration	1
Training for mechanics, salvage operators	3
Vehicle - infrastructure interface	3
Vehicle crash testing	8
Vehicle Labelling	5
Vehicle testing and compliance	1
Wireless Technology	4

It can be seen from the initial thematic analysis that battery safety, issues around charging infrastructure and battery recycling and reuse are major issues. Emergency response procedures were also seen as important, with issues such as vehicle identification, battery disconnect and personal protective equipment mentioned as problem areas. This applies not just to first responders such as fire service personnel, but also second responders such as recovery teams. Of the issues that did not receive

coverage in the standards review and roadmap, the most prominent relates to standards for aftermarket parts, which may also include conversion of ICE vehicles to EV. There were also issues around the vehicle to infrastructure interface. With vehicles increasing using “smart” technology and the possibility of downloading information or software upgrades straight onto the vehicle, there needs to be protection put in place to guard against faults or potentially malicious software becoming embedded in the vehicle’s electronic control systems.

A final data set examined vehicle specific topics, so that a comparison to be made with the functional system breakdown. The data used for this was the proceedings of the 22nd Enhanced Safety Vehicle Conference (ESV22). The proceedings of previous ESV conferences were discounted, as EV were not explicitly discussed. The results of the analysis are shown in Table 4.

Table 4
Vehicle Thematic Analysis using ESV22 Proceedings

Theme	Count	Context
Collision	8	Frontal, Rear, side impact, protection zone
Energy Storage	7	Lithium-ION Battery Technology, cause of failure, thermal runaway
Control	4	High Voltage Shutdown System
Occupant	4	Protection from electric component(before and after crash)
Electrical safety	3	Protection from electricity
Leakage	2	Leakage of hydrogen, Battery acid.
Fire	2	Overheating battery or rupture of fuel tank can be source of fire
Pedestrian	2	Warning sound of EV approaching to prevent impact with pedestrian
Abuse	1	Misuse of the vehicle
Structure	1	Battery Pack
Recharge process	1	Recharging battery

The results show that collision and energy storage were the two main issues being discussed by experts in the field at the conference. This was followed by the control system, protection of the occupant from electrical components and electrical safety. Hence, the complete thematic analysis has shown that the patterns suggest collision and energy storage are the areas that attract the most concern, with control also being an important factor.

It should be noted that this is only a small part of the thematic analysis that would be required to conduct a comprehensive review of technology trends and safety issues. Work will continue under ENEVATE in order to obtain a fuller picture by examining a wider range of literature and conducting stakeholder interviews.

Functional System Breakdown

Figure 2 and Figure 3 shows the functional system breakdown of a standard passenger ICE vehicle and an EV. As the FSB for the whole vehicle becomes increasingly large it decomposes to the lower levels, the figures show only the breakdown for the drivetrain sections for each vehicle. By comparing the two diagrams, there are clearly differences in the drivetrain section, for example the energy storage method for ICE and EV is fundamentally different. An ICE vehicle uses a fuel tank to store the fuel and it is governed by FMVSS 301 Fuel System Integrity. On the other hand, for EVs the energy storage method is a battery, which can be based on various chemistries such as Lithium-ion or lead acid. FMVSS 305 regulates the affects of failure in a battery powered vehicle, by regulating the amount of spillage of electrolyte in the event of a crash and stipulating isolation of electrical components to protect against electric shock. It is important that any such regulation is written independently of issues such as battery chemistry in order that future technology developments are not precluded.

There are several critical paths that could be defined within the EV FSB. From the thematic analysis, the main areas of concern for EV were collisions, energy storage, control system and occupant protection. By following the critical pathways, gaps in regulations which may cause concern are identified. For the purposes of this illustrative example, the critical path relating to the battery has been chosen to demonstrate the proposed methodology, and is shown in *Figure 4*. Here it can be seen that the critical pathway from the mission module (in this case the battery) to the primary function (the EV) takes in several sub systems, namely the battery management system, the motor and the drivetrain. All of these could be affected by a fault in the battery, which in turn could cause the vehicle to malfunction. The regulations that are highlighted by the critical path are shown in Table 5.

Table 5
Critical path for battery mission module

Regulation Number	Area Regulated	Level
ECE-68	Measurement of the max speed, inc EV	Vehicle
UNECE-100	Electric power trained vehicles	Vehicle
ECE-84	Measurement of Fuel Consumption (Liquid Fuel)	Control
UNECE-85	Measurement of net power	Control
UNECE-GTR5	Technical requirements for on-board diagnostic systems (Currently Diesel Heavy Vehicles)	Battery Management
FMVSS 305	Electric Powered Vehicles, Electrolyte Spillage and Electrical Shock Protection	Battery

Of these regulations several currently only apply to ICE powered vehicles, but relate in some respects to similar functions that are carried out by the equivalent EV mission module, so may have the potential to be adapted. For example, UNECE-GTR5 currently relates to on board diagnostics for diesel powered heavy vehicles, but the regulation states that:

“the gtr has been structured in a manner that facilitates a wider application of OBD to other vehicle systems in the future” (UNECE-GTR5, 2007)

ECE-84 relates to the measurement of fuel consumption, so could also be a useful regulation if applied to EV, as monitoring the amount of “fuel” in the form of charge remaining in the battery is an crucial factor in the operation of the vehicle.

Again this is only a sample of the full FSB that would be required to fully understand the vehicle’s systems. A more detailed FSB will be undertaken by the ENEVATE project team at Cardiff University in order to fully explore the potential issues.

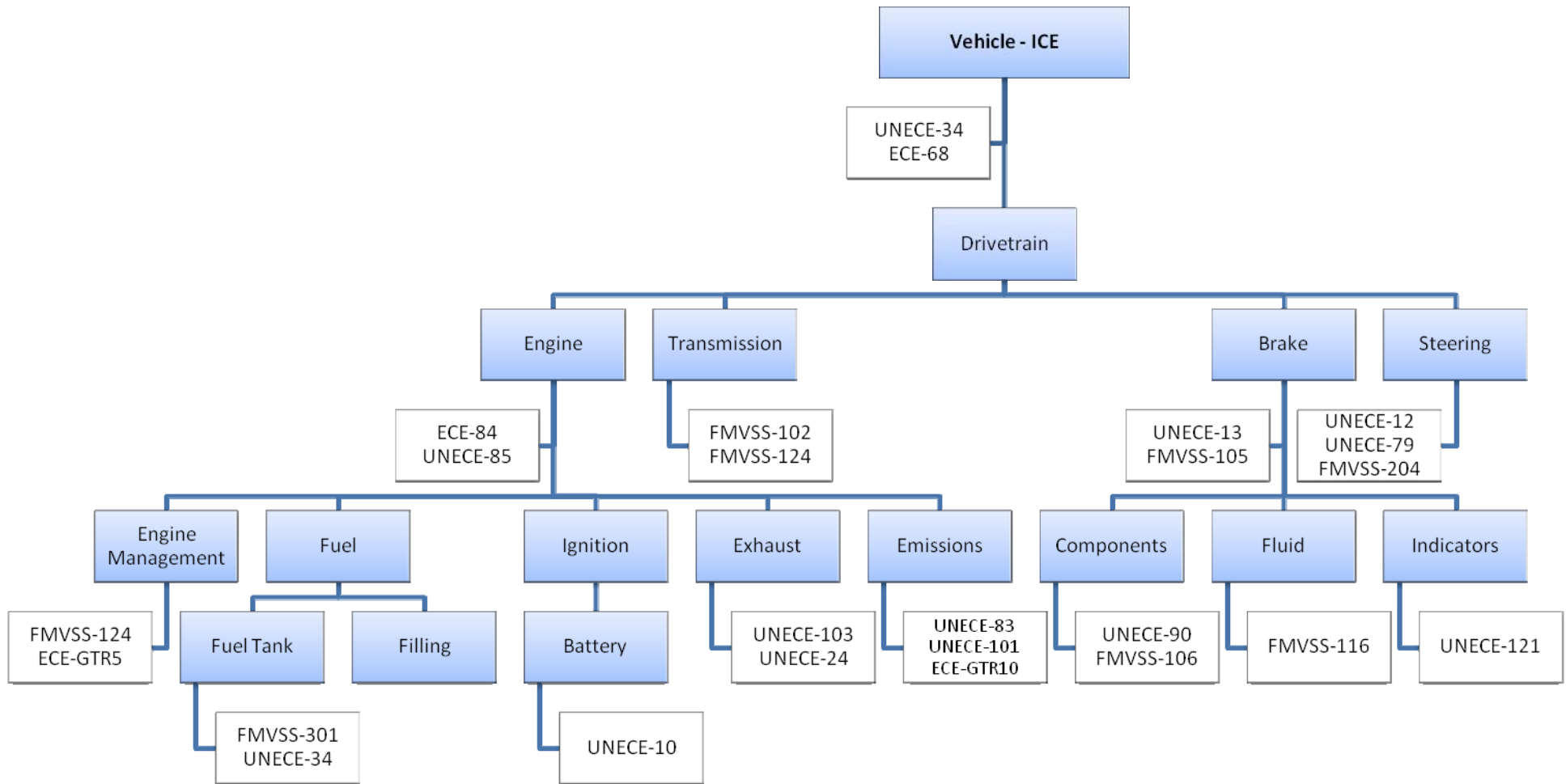


Figure 2 functional breakdown system for a standard passenger ICE drivetrain with relative regulations.

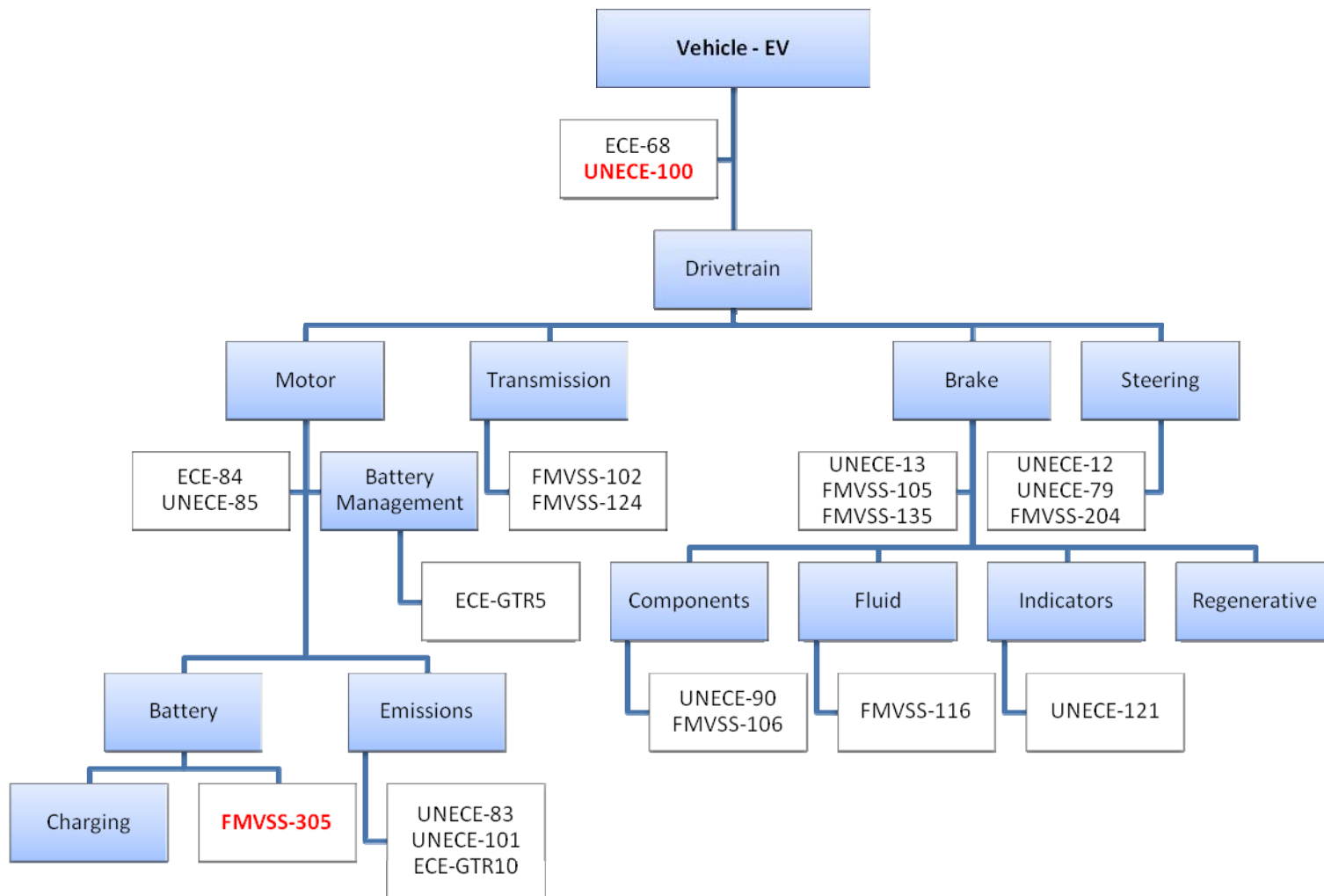


Figure 3 functional system breakdown for electric vehicle drivetrain.

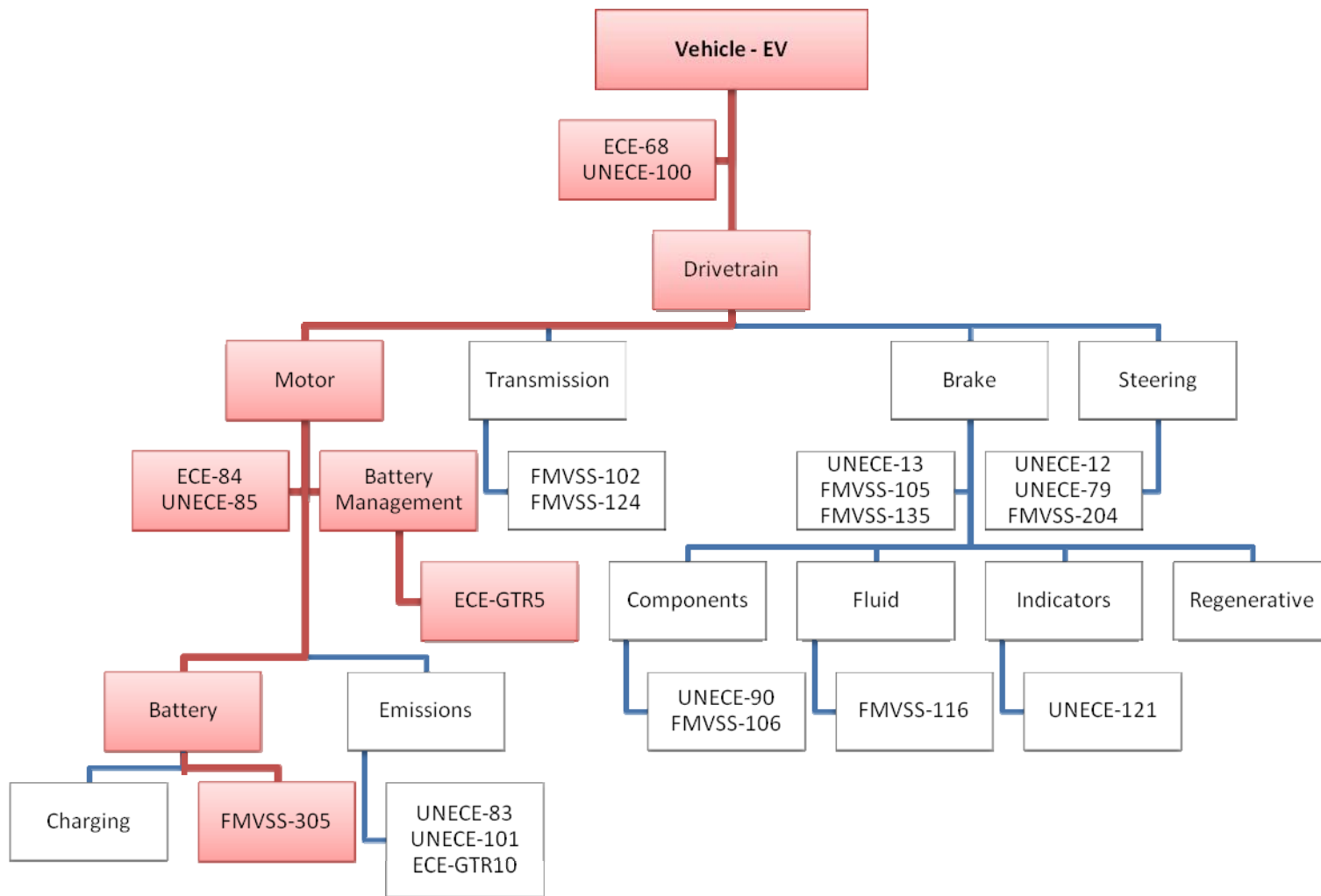


Figure 4 critical path for the battery mission module.

Failure Mode and Effects Analysis

In order to apply the failure mode and effects analysis, some potential failure modes needed to be identified. For the purpose of this illustrative example a list was taken from the battery guide produced by Axion. This list may not cover all possible battery failure modes, but is used to generate a comparison whereby the modes that are listed can be ranked in order to demonstrate the methodology being proposed.

Once the list of failure modes had been identified the severity and occurrence of each mode was ranked according to the criteria outlined in Table 1 and Table 2. As already described, these values are largely subjective, although evidence has been used to guide the judgements made wherever possible. This was more achievable for the occurrence ranking, as information from other domains could be used for guidance. In many cases the failure mode relates to a high severity ranking as the failure may result in events such as thermal runaway in the battery pack, potentially resulting in fire.

The final stage was to compare the failure modes with the identified standards in order to determine if there was adequate coverage. The failure modes were graded for coverage with 0 or 1 accordingly, in order to rule out those that were already included in existing regulations. The resulting example FMEA is shown Table 6.

From the table it can be seen that some aspects are already adequately covered by regulations. Pressure venting for any gases given off by the battery are covered in UNECE-100 section 5.1.1.2, and fuses are covered by section 5.1.1.3 of the same standard. FMVSS-305 states that if the vehicle is involved in a crash, the battery should not enter the passenger compartment.

Of the remaining failure modes, the highest score has been given to flame retardant cover. There have been some incidents in pure EVs and also hybrid vehicles where vehicles have caught fire (e.g. Smith 2012). This suggests that this is a potential area for concern. Next are cell isolation and shutdown separator followed by current interrupt devices. These are all crucial safety aspects that help protect the battery from events such as thermal runaway and short circuit. Whilst these may have

been tested in other applications such as mobile phone and laptop devices, the demands placed on a battery by vehicular use may be very different. The final failure modes relate to the battery management system and PCT resistors, which present similar issues.

DISCUSSION

One of the main drawbacks of the regulation process is that effects over time are not taken into account, in particular with regards to battery chemistry and components (Doughty 2012). This can affect the vehicle in two ways. Firstly it can take a period of time for a fault to manifest itself, as was the case with the Volt fire incident, where the vehicle caught fire some weeks after crash testing (Smith 2012). There may also be longer term issues that may arise as the battery degrades after years of use, which would not come to light after short term use of the vehicle. Whilst it may be possible to learn some lessons from other mobile technologies, there may be faults that are specific to the demands of automotive use and safety critical systems. Whilst the proposed methodology provides a prioritisation at a given point in time, it also has the benefit of being easily adaptable into a living document. The process would not need to be started from scratch - by repeating the thematic analysis and updating the initial FSB and FMEA, the resulting prioritisation can be updated as required.

The example in this paper has concentrated on high level regulations that are directly required for type approval such as FMVSS and UNECE regulations. There are many more standards such as SAE and ISO standards that could be used to verify the safety of EV systems and components. The ENEVATE team at Cardiff University will continue to verify the methodology by using a more detailed thematic analysis and FSB coupled with an expanded set of standards and regulations to create a more detailed picture of the current state of the regulatory process.

Table 6
Example Failure Mode and Effects Analysis for Battery Safety Regulation Ranking

Sub System	Mission Module	Severity	Occurrence	Standard	Coverage	Total	Notes
Cell level safety devices	Current interrupt device (CID) - safety components to protect the cell from excessive internal pressure - the CID will break and electrically disconnect the cell	8	2	-	1	16	Failure rate ~1:10000 (Doughty 2012)
	Shut down separator: The separator between anode and cathode has the ability to close its pores as a result of thermal runaway	9	2	-	1	18	
	Pressure vent	8	2	UNECE-100 (5.1.1.2)	0	0	No action needed
	Flame retardant cover	9	3	-	1	27	There have been incidents of vehicle fires e.g. Volt (Smith 2012)
External circuit devices	Positive Temperature Coefficient (PTC) resistors (Low power only) exhibit an increase in resistance at a specified temperature. They are suitable for a wide range of applications, in particular including overcurrent protection devices, switches and additionally as heaters	7	1	-	1	7	PTCs are used in other applications, lessons learned can be applied to EV application
	Fuses	7	3	UNECE-100 (5.1.1.3)	0	0	No action needed
	Cell isolation to prevent a chain reaction of cell events	9	2	-	1	18	Some cell elements such as short circuits are difficult to replicate in test environment (Doughty 2012).
BMS Software	The software monitors all key indicators coupled to control actions (e.g. cooling, power disconnect)	7	1	-	1	7	ECE GTR5 could cover BMS, but does not at present. BMS used in other applications, but is more complex in EV.
	The hardware provides a fail-safe back-up, including a switch-off in case of software failure	8	1	-	1	8	
Battery location	This should be outside the passenger compartment and behind the vehicle firewall	9	1	FMVSS-305 (S5.2)	0	0	No action needed

Sub system and mission module data taken from Axion “Our Guide to Batteries”

SUMMARY

Electric vehicles present new opportunities that need to be managed in a timely manner in order to achieve their highest potential. The mismatch between the rate of change of technology and the time taken to update the regulatory framework as a reaction to new technology and problem areas could hinder the development of new e-mobility concepts. As EVs are an evolving technology it is also crucial that regulations are not specified in such a way that new technologies cannot be used in the future and technology lock-in is avoided.

In order to focus the development of standards in relation to EV a three stage methodology has been described and applied to an example illustrated by the battery and related systems. The thematic analysis provided the context by highlighting discussion on topics relating to battery safety. The functional system breakdown for a conventional ICE powered vehicle and an EV were compared and a critical path devised that showed how battery related issues relate to the vehicle's operation. This also highlighted what regulations were already in place and those that may need reviewing. Finally a list of potential battery failure modes was used to create an illustrative FMEA and prioritise any outstanding issues in order to focus where the biggest gains might be made.

Work will continue to create a more detailed analysis in order to verify the methodology and produce meaningful output. Further results will be presented at the ENEVATE final conference in November 2013.

ACKNOWLEDGEMENTS

This work forms part of the JTS INTERREG IVB funded European Network of Electric Vehicles and Transferring Expertise (ENEVATE)

REFERENCES

Axeon "Our Guide to Batteries",
<http://www.axeon.com/Technology/Our-Guide-To-Batteries.aspx>, UK

American National Standards Institute, 2012 "Standardization Roadmap for Electric Vehicles", Version 1.0 prepared by the Electric Vehicles Standards Panel

CENELEC, 2006 "Analysis techniques for system reliability – Procedure for Failure Modes and Effects Analysis (FMEA)" IEC 60812:2006, European Committee for Electrotechnical Standardization, Brussels

Chrysler Corporation, Ford Motor Company, General Motors Corporation, 1995 "Potential Failure Mode and Effects Analysis (FMEA)" Second Edition, Carwin Continuous Ltd, UK

Davies, H., Nieuwenhuis, P., Wells P., Newman D. and Donovan, C., 2012, "ENEVATE Project - Electric Vehicle Market Drivers and E-Mobility Concepts", proceedings of the European Electric Vehicle Congress, Brussels

Doughty, D., H. Pesaran, A. A., 2012 "Vehicle Battery Safety Roadmap Guidance" National Renewable Energy Laboratory, Subcontract Report NREL/SR-5400-54404, USA

European Commission, 2010 "Europe 2020 A strategy for smart, sustainable and inclusive growth", Communication from the Commission COM(2010) 2020 final, Brussels

Johnson, J. M., 2002 "In-Depth Interviewing. In handbook of interview research: Context and Method". Jaber F. Gubrium and James A. Holstein, eds. Thousand Oaks, CA: Sage

Latino, R. J., 2004 "Optimizing FMEA and RCA efforts in health care", American Society for Healthcare Risk Management Journal, Vol 24, No 3 pp 21-28, USA

Pailhès, J., Sallaou, M., Nadeau, J. P., Fadel, G. M., 2011, "Energy Based Functional Decomposition in Preliminary Design" Journal of Mechanical Design. Vol 133

Pannkoke, K., and Ernst, C., 2012, "ENEVATE – Accelerated Introduction of Electric Vehicles in North West Europe" proceedings of the European Electric Vehicle Congress, Brussels

Rossen, C. B., Sørensen, B., Jochumsen, B. W. and Wind, G., 2012 "Everyday life for users of electric wheelchairs – a qualitative interview study", Disability and Rehabilitation: Assistive Technology, 7(5): 399–407, UK

Smith, B., 2012 “Chevrolet Volt Battery Incident Overview Report”, National Highway Traffic Safety Administration, Report No DOT HS 811 573, USA

Stone, R. and Wood, K., 2000, “Development of a Functional Basis for Design”, Journal of Mechanical Design, Vol. 122, pp 359 – 370

UNECE-GTR5, 2007 “Technical Requirements for On-Board Diagnostic Systems (OBD) for Road Vehicles” Global technical regulation No. 5, ref ECE/TRANS/180/Add.5, Geneva

Visvikis, C., Morgan, P., Boulter, P., Hardy, B., Robinson, B., Edwards, M., Dodd, M., and Pitcher, M., 2012 “Electric vehicles: Review of type-approval legislation and potential risks”, Client Project Report CPR810, Transport Research Laboratory, UK

Zhou, P. and Stålhane, T., 2004, “Using FMEA for early robustness analysis of Web-based systems”, Proceedings of the 28th Annual International Computer Software and Applications Conference, IEEE

A STUDY ON MECHANICAL CHARACTERISTICS OF LITHIUM-POLYMER POUCH CELL BATTERY FOR ELECTRIC VEHICLE

Hyung Yun Choi

HongIk University, Mechanical System Design Engineering Department
Korea, Republic of

Inhyeok Lee

Hankook ESI
Korea, Republic of

June Soo Lee, Young Man Kim, Hyunjin Kim

SK Innovation
Korea, Republic of
Paper Number 13-0115

ABSTRACT

In order to characterize deformation and failure behaviors of Lithium-Polymer pouch cell battery and its components, various mechanical tests were performed. Uniaxial tensile properties of electrodes, separator, and pouch cover were obtained from coupon tests. Effects of temperature and strain rate on the mechanical behavior were also investigated. The three-point bending tests with and without pouch vacuum were performed to quantify the stiffening effect due to the pouching vacuum as well as quantifying the bending rigidity and failure load of the pouch cell. Static and dynamic pin drop tests were also carried out to investigate the failure mode and impact energy threshold for the perforation. The vibration responses, i.e., natural frequencies of pouch cell were obtained from impact hammer and shaker excitation tests. A finite element model of pouch cell using shell and membrane elements was also constructed. The same number of stacking layers in separator/electrode assembly was represented in the model. The solid state electrolyte that occupies very tiny volume between layers in the pouch was modeled by tied option of which the normal and shear moduli were calibrated from the three-point bending simulation.

INTRODUCTION

The Lithium-Polymer battery is widely adopted RESS (Rechargeable Energy Storage System) in electric vehicle and becomes a key component especially considering the safety issue. The pouch cell, a common design of Lithium battery is in a vacuum packed thin plate shape in which many stacking layers of thin cathode and anode electrodes are alternately winded by a long ribbon of polyolefin separator. This separator/electrode assembly including widespread solid-state electrolyte between each layer are sealed inside a flexible thin plastic/aluminum pouch cover. Multiple cells are assembled to a module level and several modules are further joined together into a battery pack in various

shapes to be installed at the safest position in electric vehicle, e.g., in a tray shape under floor or in a fuel tank shape behind the rear seat.

Sahraei et al [1] reported their effort on a FE modeling of pouched Lithium ion cell. Their model predicted force-displacement relations for bending, axial and through thickness compressions, and also onset of short circuit during a punch loading. However the outcome of the model simulation is rather limited to the overall behavior of the pouch cell than local stress and strain level because their model was built with lumped solid and shell elements to model layers of electrodes, separator, and electrolyte altogether.

In this study, comprehensive mechanical tests were performed to characterize deformation and failure behavior of Lithium-Polymer pouch cell and its components. Effects of temperature, strain rate, and anisotropy on the mechanical behavior were also investigated. Vibration characteristics were examined by impact hammer and shaker excitation tests to secure in situ natural frequencies and associated mode shape of the pouch cell. In addition, there was an effort to build a detailed finite element model of LB pouch cell in this study. Precise geometry of pouch cell and its components to the level of single layers of separator and electrode were reconstructed. A unique modeling approach was employed to represent the mechanical behaviors of solid-state electrolyte which needs an extra numerical treatment due to its very thin and complicated mechanical properties. Using this FE model of pouch cell, virtual simulation of mechanical deformation and failure of pouch cell is attempted in both component and assembly levels to validate against test results.

CHARACTERIZATION OF MECHANICAL BEHAVIOR

In this study, used but serviceable Lithium Polymer pouch cells of 10Ah capacity designed for a serial hybrid vehicle were procured for various mechanical

tests. In order to avoid possible electric short circuit during tests, all cells were completely discharged and further disassembled into components, i.e., electrodes and separators for the coupon test. The stained solid-state polymer electrolyte on electrodes and separator layers was totally washed out using ethylene carbonate solution but the coating layers on

electrodes were preserved as undamaged. Then they were hung up to dry in a hood with ventilation system. Table 1 lists mechanical tests performed to characterize deformation and failure behaviors of Lithium polymer pouch cell battery at each individual component level as well as at integrated pouch cell unit.

Table 1 List of tests to characterize mechanical behaviors of Lithium Polymer pouch cell battery

Test	Specimen	Test parameters	Objective
Tension	Coupons of Electrodes, separator, pouch cover	Temperature, Strain rate, anisotropy	Basic tensile properties of each component
Bending	Pouch cell unit	Temperature, Strain rate, vacuum	Flexural stiffness and strength
Quasi static pin penetration	Electrodes, separator, pouch cover	Temperature(3), Strain rate(2)	Failure threshold of each component
Drop impact penetration	Pouch cell unit	Drop height	Failure threshold
Impact Hammer	Pouch cell unit	-	Modal frequency
Shaker excitation	Pouch cell unit	Excitation direction, Boundary condition	Vibration response

Tension test

Uniaxial tension test was performed to characterize basic tensile properties of each component in Lithium Polymer pouch cell battery. The temperature standard in ASTM E8M-09 was adopted using an environment chamber with 1kN load cell and visual extensometer (Instron UTM 5569). Test coupon was cut into a dumbbell shape in a size of total length of 120mm, grip width of 25mm, gauge length of 40mm, and gauge width of 10mm as specified in KS-M3054. There were three test parameters, i.e., temperature (-40°C, 22°C, 65°C), strain rate (1mm/min, 50mm/min for electrodes, 490mm/min for separator and pouch cover), and loading direction (anisotropy, 0°, 45°, 90°). Tensile test with each condition was repeated for three times to obtain mean and standard deviation values of elastic modulus, yield strength, tangent modulus, failure strength, and failure strain of each component. Some of representative stress-strain curves are introduced in Figures. 1-6.

Figure 1 shows representative engineering stress-strain relations of all components at room temperature (22°C), lower strain rate (1 mm/min), and longitudinal direction (0°). The initial elastic moduli of two electrodes, cathode (Al) and anode (Cu) were similar to each other. However cathode specimen showed higher yield and failure strengths but lower failure strain than anode did. The separator exhibited the lowest modulus but highest failure strain.

Two electrodes, cathode and anode showed temperature and strain rate dependencies as in

Figures. 2 and 3. However there was no noticeable anisotropy found from the tensile response of electrodes. Both electrodes exhibited increasing failure strength and decreasing failure strain at lower temperature as shown in Figure 2. The maximum applicable strain rate to electrodes in our test was 50mm/min (c.f., 490mm/min for separator and pouch cover) due to the measurement limit of the visual extensometer and the brittle behavior of electrodes, especially at a low temperature. It was found that there was a large variation in the measured failure strain at the higher strain rate and thus became to be hard to conclude any strain rate effect on electrodes.

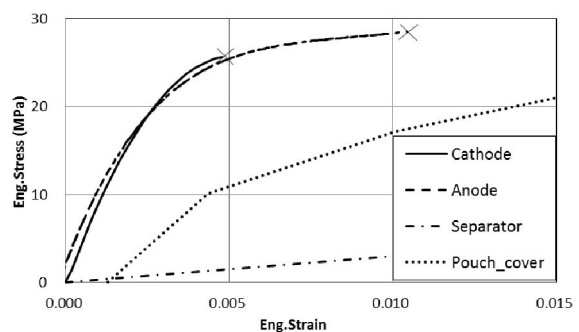
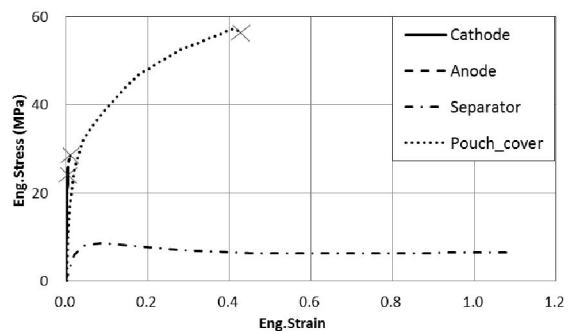


Figure 1. Normalized engineering stress-strain curves of electrodes, separator, and pouch cover (top) and zoomed initial portion (bottom) (temperature: 22 °C, strain rate: 1mm/min, anisotropy: 0°)

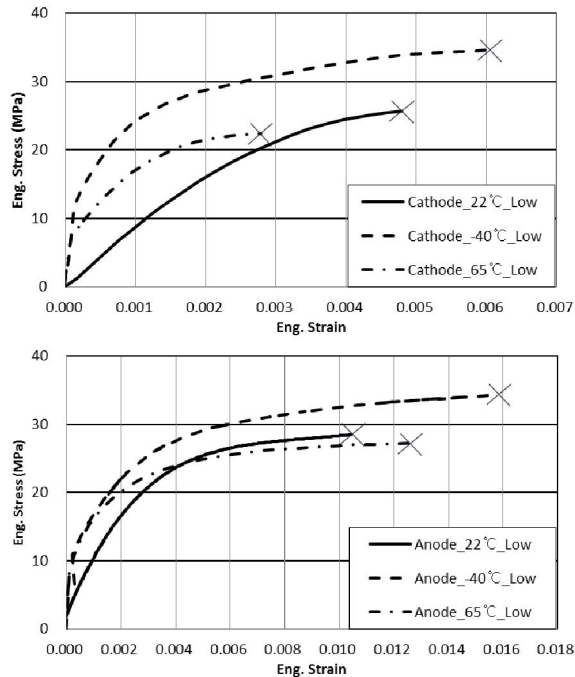


Figure 2. Temperature effect on tensile stress-strain relationship of electrodes, cathode (top) and anode (bottom), strain rate: 1mm/min, X: failure point

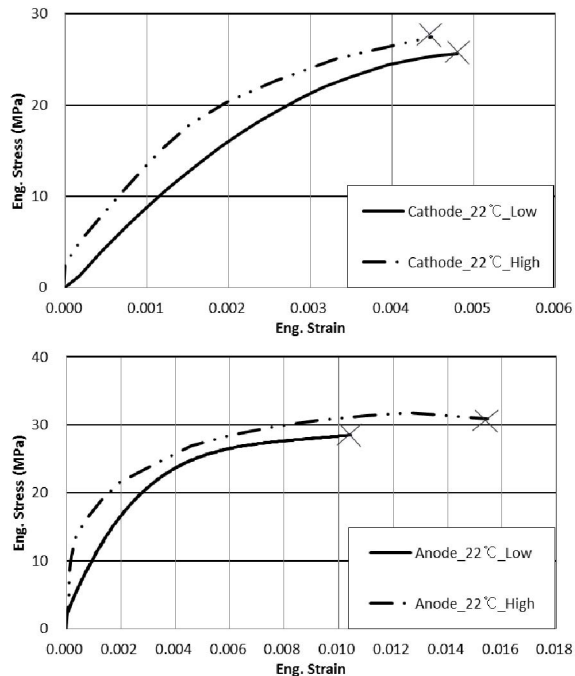


Figure 3. Strain rate effect on tensile stress-strain relationship of electrodes, cathode (top) and anode (bottom) at temperature: 22 °C, Low: strain rate 1mm/min, High: strain rate 50mm/min, X: failure point

For separator and pouch cover, elastic modulus and failure strength and strain increased with the temperature as shown in Figure 4. Due to the capacity limit of the UTM machine used in this study, it was not possible to elongate the separator specimen up to the failure point at all temperature conditions.

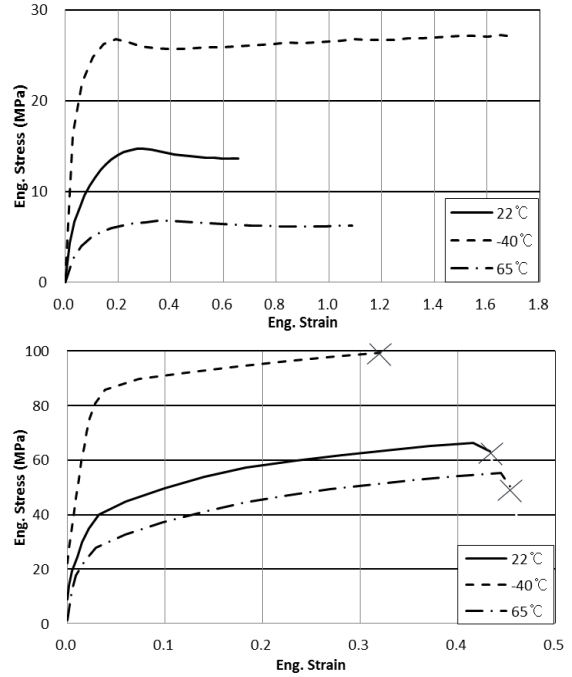


Figure 4. Temperature effect on tensile stress-strain relationship of separator (top, anisotropy: 45°, strain rate: 1mm/min) and pouch cover (bottom, anisotropy: 0°, strain rate: 490mm/min), X: failure point

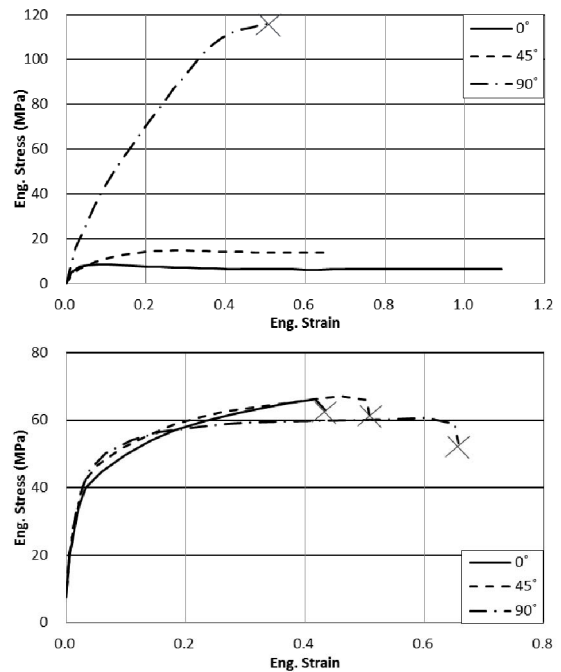


Figure 5. Anisotropy of separator (top, temperature: 22 °C, strain rate: 1 mm/min) and pouch cover (bottom,

temperature: 22 °C, strain rate: 490mm/min)

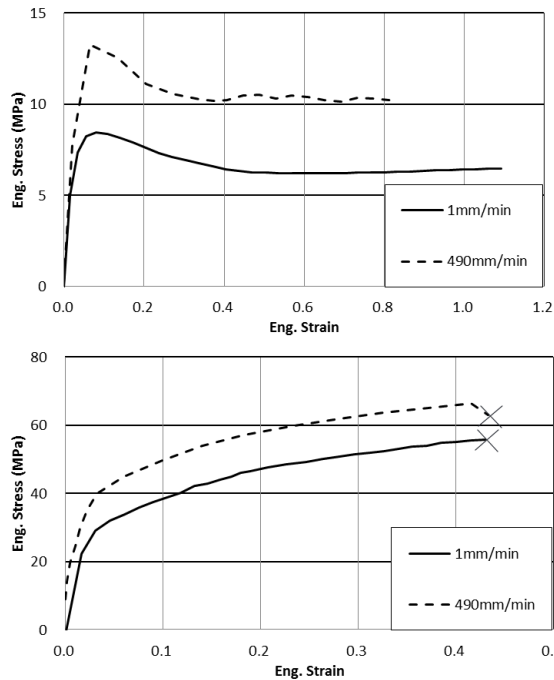


Figure 6. Strain rate effect tensile stress-strain relationship of separator (top, anisotropy: 0°, temperature: 22 °C) and pouch cover (bottom, anisotropy: 0°, temperature: 22 °C), X: failure point

Three-point bending test

Bending rigidity of the LB pouch cell depends on the degree of pouching vacuum. Also, the bonding strength between separator and electrodes is affected by the phase change of electrolyte which plays an adhesive role in a mechanical point of view. The bending stiffness and strength of the pouch cell is also largely influenced by this bonding strength. In order to characterize a bending stiffness and strength of the LB pouch cell taking the effect of pouching vacuum into consideration, three-point bending test complying KSMISO-14125 was performed. Three temperatures (-40 °C, 22 °C, 65 °C) and two loading speeds (1mm/min, 490 mm/min) were respectively applied as test conditions. Figure 7 shows representative force-displacement relationships from three-point bending test of LB pouch cell. Both bending stiffness and strength decreased at higher temperature. Strain rate increased both bending stiffness and strength, i.e., the ultimate bending force.

Impact hammer and shaker excitation tests

Vibration characteristics of LB pouch cell were obtained from impact hammer and shaker excitation tests. A vertical impact force was applied at a corner of LB pouch cell with a free boundary condition. As shown in Figure 8, a Frequency Response Function (FRF) was acquired from the uniaxial acceleration

measured at the diagonally opposite point from the same loading direction of hammer impact.

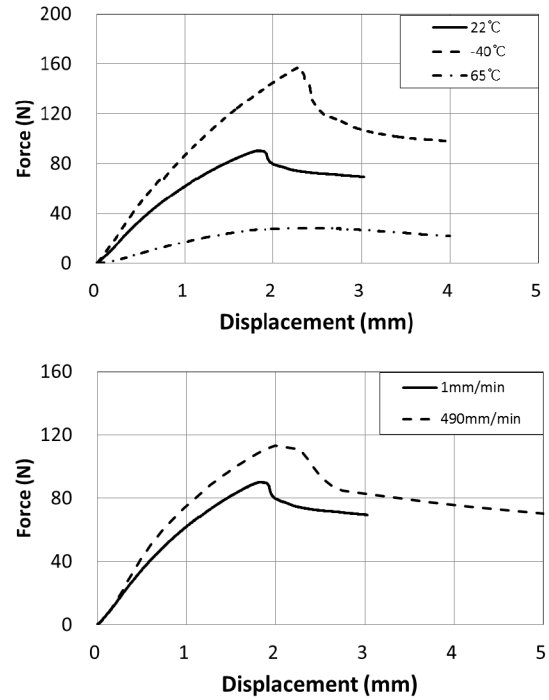


Figure 7. Force-Displacement relationship from three-point bending test of LB pouch cell; Temperature (top) and strain rate (bottom) effects

The bandwidth for natural frequency measurement in our impact hammer test was over 250 Hz and it thus became to pass beyond the range for the durability test. The durability test of battery system is usually carried out in a pack level with up to 200 Hz frequency range, which focuses on the evaluation of joining strength between lead electrode taps and separator/electrode assembly inside the cell and between cells. The main objective of the hammer impact test in our study was to identify natural frequencies of LB pouch cell as listed in Table 2.

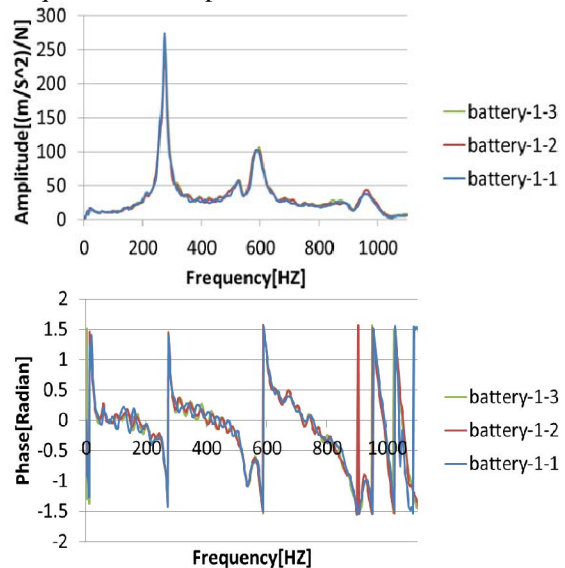


Figure 8. FRF amplitude (top) and phase of a LB pouch cell (bottom)

Table 2 Natural frequencies of LB pouch cell measured from hammer impact test

Mode	Specimen				
	#1	#2	#3	#4	Average
1st	274	284	266	244	267
2nd	-	-	-	474	474
3rd	590	602	592	-	595
4th	954	1000	945	950	962

Figure 9 is a schematic drawing of LB pouch cell describing the connection between lead electrodes and stacked layers of separator/electrodes assembly inside pouch cell by a simple elastic spring. The frequency range employed for the investment of pouch cell durability, i.e., below 200 Hz may be largely affected by this joining stiffness (i.e., spring constant in Fig. 11) between internal component (separator/electrodes assembly) and lead electrode taps and the mass of internal component. In order to characterize this dynamic property, a shaker excitation test was also performed with adopting same boundary conditions as when cells are assembled in a modular level of battery system.

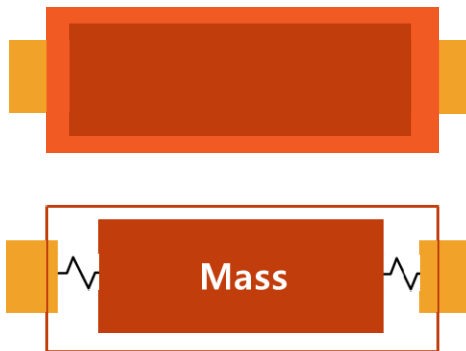


Figure 9. Schematic drawing of LB pouch cell to depict cell assembly for its dynamic response

Two kinds of clamping boundary conditions were respectively used in the shaker excitation test; 1) two edges in longitudinal directions, and 2) all four edges of pouch cell. There were three excitation directions, longitudinal (X), transverse (Y), and vertical (Z) directions, respectively. Two pouch cell specimens were used for each condition to check repeatability of

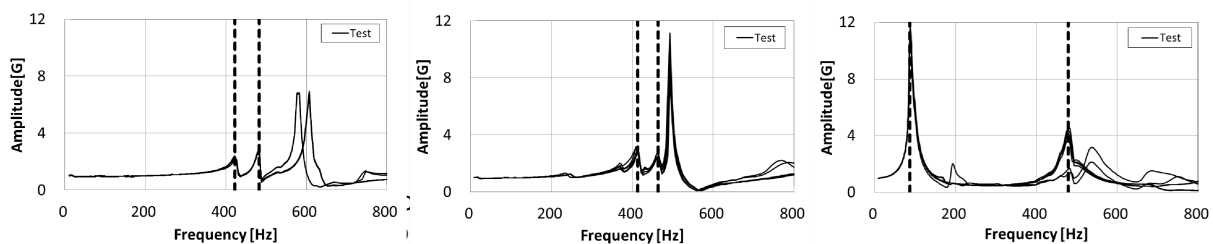
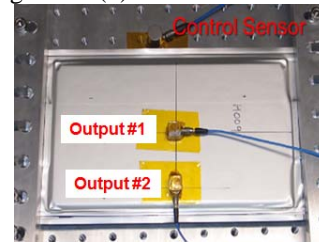


Figure 11. Acceleration response along three excitation directions with two-edge clamping boundary condition; longitudinal (left), transverse (middle), and vertical (right)

the test. Figure 10(a) shows mounted control sensors which is a uniaxial accelerometer that monitors excitation signals and two triaxial accelerometers which sense vibration response output of the pouch cell specimen. The configurations of fixed boundary conditions and excitation directions of shaker test are shown in Figure 10 (b).



(a) Accelerometer sensors

Boundary condition	Excitation direction		
	X	Y	Z
Two-edge clamping			
Four-edge clamping			

(b) Boundary conditions and excitation directions
Figure 10. Accelerometers for excitation control and output measurement and the boundary conditions and excitation directions at shaker test

Excitation frequency range was selected from 10 to 2000 Hz in sine sweep signal with 5min/sweep speed considering durability test condition and the capacity limit of the test machine (shaker: LDS, controller: B&K V875-440 LPT 600 COMBO). The magnitude of excitation was set to 1G which is one third of the required condition in the durability test. Acceleration profiles in frequency domain measured from two sensors for three excitations are shown in Figure 11. The resonant frequencies were selected where the amplitude of output signal became twice than that of input excitation amplitude. First two natural frequencies with all test conditions, i.e., two boundary conditions and three excitation directions are summarized in Table 3.

Table 3 Modal frequencies of LB pouch cell from shaker test

Mode / Excitation direction	Two-edge clamping			Four-edge clamping		
	X	Y	Z	X	Y	Z
1 st (Hz)	422	414	87	414	422	268
2 nd (Hz)	483	464	478	469	478	476

Quasi static pin penetration test

In order to characterize failure thresholds, especially in a penetration mode of LB pouch cell components, a quasi-static pin penetration test was performed. A spike shaped pin with 4.5 mm diameter was used as a penetrator on circularly clamped cell components with 45mm diameter as shown in Figure 12. Representative force-displacement curves of electrodes, separator and pouch cover are shown in Figure 13.



Figure 12. Test setup for quasi-static pin penetration test

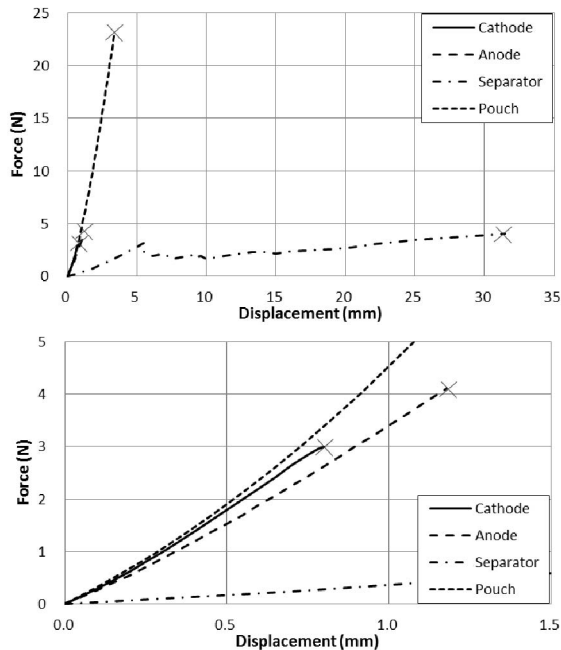


Figure 13. Force-displacement curves from quasi static pin penetration test at 22 °C (top) and zoomed initial portion (bottom)

Pin drop impact test

The characteristic of dynamic perforation of LB pouch cell was obtained from pin drop impact test (see Figure 14). Drop weight was fixed to 1.78 kg

and drop height was varied from 1m to 3m high. Total ten drop impacts were performed to find out the threshold height to perforate the pouch cell. Threshold height was found to be between 1.3m and 1.4m which corresponds 22.7J and 24.4J in drop energy. Perforation shape of a pouch cell from the pin drop impact test is shown at Figure 15.



Figure 14. Test setup for drop impact on pouch cell

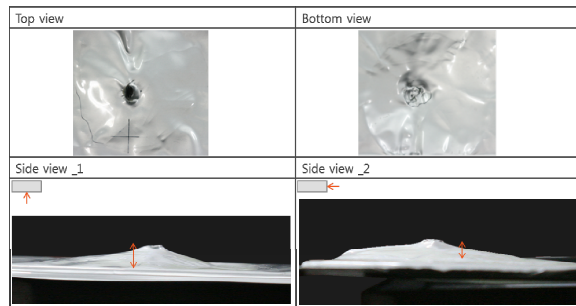


Figure 15. Perforation of pouch cell from drop impact test; impact mass 1.78 kg, impact height 1.4 m

FE MODELING OF LITHIUM-POLYMER BATTERY POUCH CELL AND ITS VALIDATION

Detailed stacking sequence and winding of separator/electrodes in LB pouch cell is shown in Figure 16. The thickness of each component was directly measured from the disassembled cell specimen except the electrolyte layer

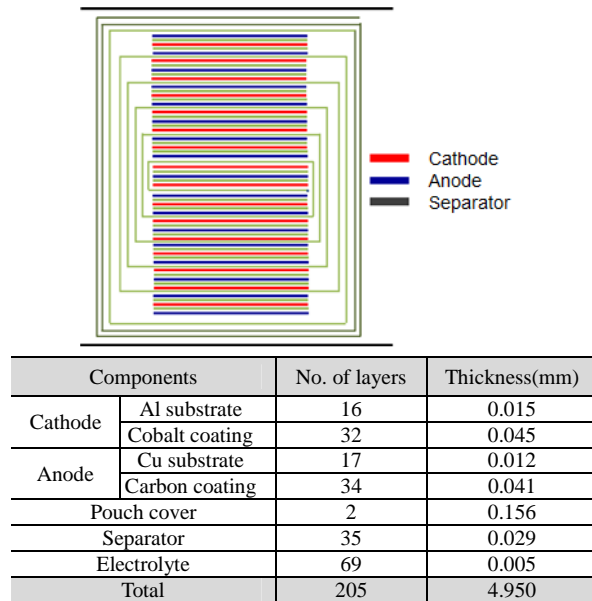


Figure 16. Schematic drawing and detailed thickness distributions of separator/electrode assembly in LB pouch cell

In an aspect of finite element modeling, the most unique approach of this study could be the electrode and electrolyte models in a pouch cell structure. The electrodes are made of very thin pure metal substrates (Al for cathode and Cu for anode) coated by Lithium compound (Cobalt compound for cathode and Carbon compound for anode) and their thicknesses are around 0.1mm. Each electrode layer was modeled by three stacking shell elements, i.e., middle element represented pure metal substrate and upper and lower elements for coating layers, respectively. The nodes of three layered shell elements are rigidly tied together for all degree of freedoms. The solid-state electrolyte polymer layer was only 0.005mm thick in a pouch cell and therefore the direct measurement of mechanical property and assigning a physical element in the FE pouch cell model became quite difficult. So, the layers of electrolyte were modeled by a link element (Material type #304 in Pam-Crash [4]) which connected nodal points by a penalty spring with normal and shear stiffness. The contribution of binding strength of electrolyte in separator/electrode winding assembly depends on this normal and shear stiffness which are to be determined from a three-point bending analysis. The spacing of shell elements through the thickness direction is schematically presented in Figure 17. As mentioned in the previous section, pouching vacuum plays an important role in the mechanical integrity of the pouch cell. Thus, upper and lower sides of pouch cover were rigidly tied together to numerically represent the pouching vacuum inside the cell as shown in Figure 18. Mechanical properties, such as elastic modulus, yield strength, tangent modulus,

and failure strength obtained from tension tests in above section were assigned into pouch shell components. The total number of nodes and elements of finite element pouch cell model in Fig. 20 were 134,086 and 126,256, respectively.

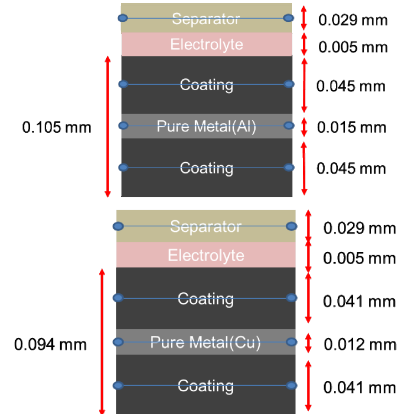


Figure 17. Spacing of shell elements through the cell thickness direction, Cathode (top) and Anode (bottom) in separator/electrode winding assembly

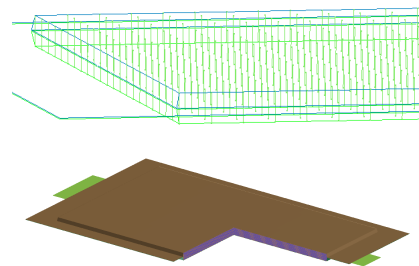


Figure 18. Tied link between upper and lower pouch cell covers to represent pouching vacuum condition (top), Lithium polymer battery finite element model with a quarter cut (bottom)

Three-point bending simulation

A three-point bending simulation was performed with unpouched separator/electrodes assembly to estimate the normal and shear stiffness of tied link which represent the thin layers electrolyte. (Figure 19 left) The stiffness of tied link was determined to match the simulated force-displacement relationship against the test measurement. Thereafter, the modeling of electrolyte was validated with two other conditions in pouch cell level, i.e., with and without pouching vacuum (Figure 19 right). The force-displacement relationships from simulation were compared with test measurements for various pouching conditions are shown in Figure 20. It is noted that one of test result of depouched cells was found to have very lower reaction force than the other two test results. The effect of pouching vacuum on the mechanical integrity of pouch cell can be seen from the Figure 21 which displays two folded center region of the cell with and without pouching vacuum conditions. It was found that the

pouch cell slightly inflated and the cover got wrinkled when the vacuum was absent. The pouching vacuum thus restrained a formation of internal vacant space, i.e., the separation of pouch cover from the internal separator/electrode assembly even at the extreme deformation of the pouch cell.

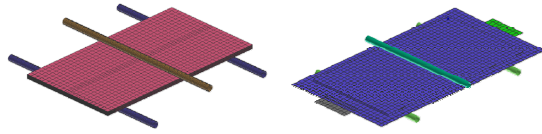


Figure 19. Finite element models for three-point bending simulation; unpouched internal separator/electrodes assembly (left) and pouch cell unit (right)

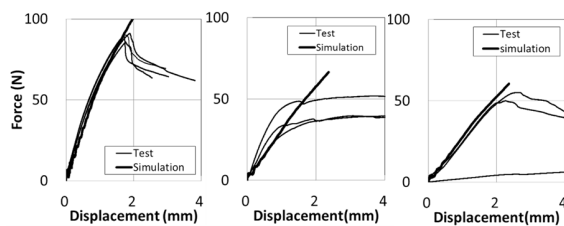


Figure 20. Comparison of test and simulation results of 3-point bending test: effects of pouching and pouching vacuum (loading speed 1mm/min at 22°C) pouched cell with vacuum (left), pouched cell without vacuum (middle), and depouched cell (right)

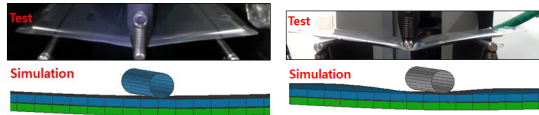


Figure 21. Effect of pouching vacuum on bending behavior of pouch cell. Test and simulation are in the same state at peak force.

Effects of temperature and loading speed on three-point bending characteristics of LB pouch cell are shown in Figure 22. A significant reduction in bending stiffness and ultimate bending force at higher temperature was found, but the threshold displacement was not much affected. Slight increases of peak bending, i.e., ultimate force were found at higher loading speed. Simulation results correlate quite well with the test results for all test parameters. To simulate effects of temperature and loading speed, relevant mechanical properties of pouch cell components obtained in tension coupon tests were applied.

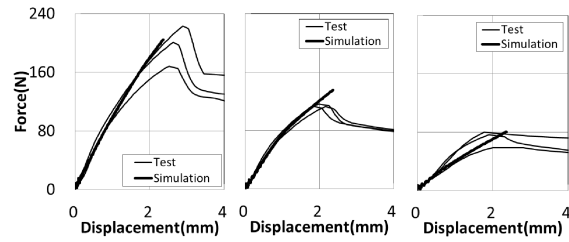
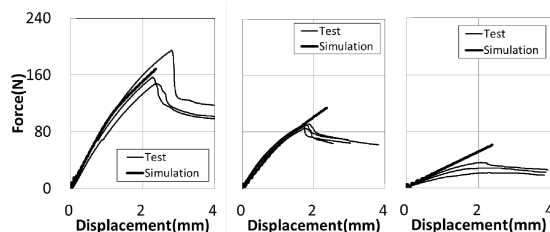


Figure 22. Comparison of test and simulation results of three-point bending test: effects of loading speed and temperature: top 3 graphs, -40 °C (left) 22 °C (middle) 65 °C (right) at 1 mm/min and bottom 3 graphs, -40 °C (left), 22 °C (middle), 65 °C (right) at 490 mm/min.

Impact Hammer and shaker simulations

The same FE model used for the three-point bending simulation was also employed for the impact hammer simulation to analyze modal frequencies of the LB pouch cell. Same impact loading and output acceleration measurement conditions used for the test were applied in the simulation as shown in Figure 23. The resonant frequencies for acceleration amplitude in frequency domain correlate well with the test measurement as listed in Table 4.

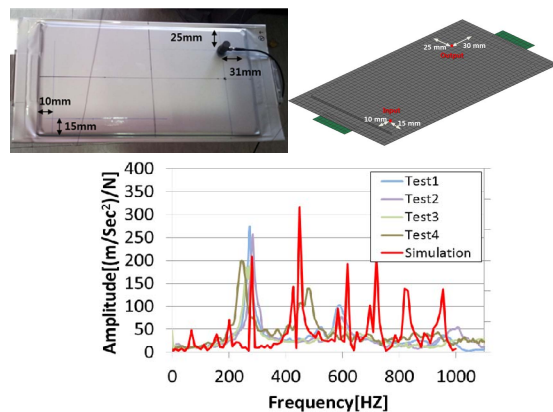


Figure 23. Impact hammer test and simulation setup and result

Table 4 Comparison of natural frequencies from impact hammer test and simulation

Mode	Natural frequency[Hz]		Error [%]
	Simulation	Test	
1st	281	267	5.2
2nd	449	474	5.3
3rd	618	595	3.9

A more practical vibration response of pouch cell was simulated taking the clamping boundary condition into account. A white noise as shown in Figure 24 was created for a sine sweep input signal with frequency range of 10-2000Hz and 1G amplitude which were same as the test condition. Since acceleration input cannot vibrate the object but only bring a rigid body motion in an explicit analysis, it

was needed to convert the white noise acceleration profile to the velocity input as in Fig. 26.

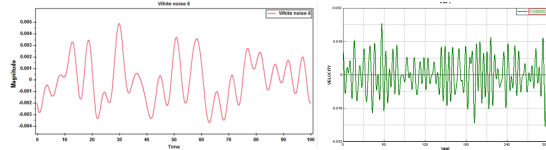


Figure 24. White noise input signal used in shaker vibration simulation; Acceleration profile (left) and converted velocity profile (right)

Figure 25 shows compared vibration responses of pouch cell between test and simulation of shaker excitation. As discussed in the previous section, only vertical excitation with two-edge clamping boundary condition resulted in the natural frequency within the range of durability concern which was 87 Hz, the first mode frequency. Therefore the simulation was focussed on the same boundary and loading conditions. The simulated first two natural frequencies correlated well with the test measurement as list in Table 5.

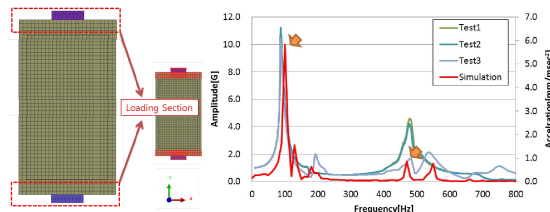


Figure 25. Two-edge clamping boundary condition (left) and acceleration response in frequency domain to the vertical direction excitation (right).

Table 5 Comparison of natural frequencies from shaker excitation test and simulation

Mode	Natural frequency[Hz]		Error [%]
	Simulation	Test	
1st	100	87	12.7%
2nd	470	478	1.7%

DISCUSSION AND LIMITATIONS

Tension coupon test

Since used LB pouch cells with no available information on the number of charge and discharge cycles were employed as test specimen in this study, it was speculated that some degree of mechanical degradation might have occurred at both component and cell levels due to the thermal cyclic loading. Extend of degradation would be unevenly distributed likewise the temperature distribution. Therefore the coupon specimen was consistently extracted at the center portion of the disassembled single layer sheets of separator and electrode to avoid the possible effect of regional degradation differences. The repeatability of electrode was not so good, especially at the higher strain rate and at the lower temperature test conditions. The identification of yield point from stress-strain curve of cathode became a bit obscure

due to the short elastic strain region. And the fracture strain of cathode was unusually higher at low temperature than at room and high temperatures. Both electrodes did not show any anisotropy. It was not clear to judge the effects of temperature and strain rate on elastic properties of separator due to the lacking repeatability. Fracture strength and strain of separator were certainly showed their dependencies on temperature, strain rate, and loading direction (i.e., anisotropy); Fracture strength of separator decreased with temperature (i.e., $-40^{\circ}\text{C} > 22^{\circ}\text{C} > 65^{\circ}\text{C}$), increased with strain rate ($490\text{mm/min} > 1\text{mm/min}$), and decreased from transverse to longitudinal direction of the cell ($90^{\circ} > 45^{\circ} > 0^{\circ}$). The effects of temperature, strain rate, and loading direction on fracture strain of the separator were precisely opposite to those on fracture strength. Pouch cover showed a similar trend as separator for temperature and strain effects but showed an isotropic behavior.

Impact hammer and shaker excitation tests

Among the four pouch cell specimens for the impact hammer test, 2nd modal frequency was detected from only one pouch cell (specimen #4 in Table 2) but the following 3rd mode, on the other hand, was found alone with the other three pouch cells (specimen #1-3 in Table). This result might come from the impact hammer test condition and the feature of pouch cell used in this study. It was speculated that the accelerometer sensor was placed by chance at one of 2nd mode's nodal positions where the detection of corresponding mode became quite difficult. However, the pouch cell specimen #4 might have different nodal position of the 2nd mode due to the variation of vibration characteristics made in fabrication process. A more refined outcome might be obtained when adopting miniature impact hammer and accelerometer system to analyze the modal shape together with the frequency. Since LB pouch cell has inhomogeneous and nonlinear vibration characteristics, a supplementary shaker excitation test was performed to investigate its further vibration characteristics with more stable loading and boundary conditions. The first natural frequency measured at shaker test, 87Hz with two-edge clamping condition along the out of plane excitation was far lower than the first mode from the impact hammer test (265Hz) and fell within the range of durability concern. Therefore the resonant issue to vehicle level vibration would be with the assembled battery module or pack rather than the design of single detached LB pouch cell.

Finite element modeling of LB pouch cell

Because of thin characteristics of solid-state electrolyte evenly spaced between separator and electrodes layers, each layer of electrolyte was modeled by a link element that connected nodal

points of adjoining elements by a penalty spring with normal and shear stiffness. A force-displacement relation from a three-point bending test for depouched separator/electrode assembly was used to calibrate those normal and shear stiffness of penalty spring in the electrolyte link element. However, a four-point bending could have been a more effective test for separate calibration of normal and shear terms since four-point bending contains a pure bending region where no cross sectional shear stress and strain exist. At first the modeling of pouching vacuum was attempted by applying an external pressure on the pouch cell cover but no good correlations were obtained against test results. It was quite difficult to gauge the degree of vacuum from a completed pouch cell product. And the vacuum for a used cell would not be same as in the initial state due to the internal gas formed during charge and discharge cycles during the service. Therefore the both top and bottom sides of pouch cover was rigidly tied together to model the tight adherence between pouch cover and internal component developed by a pouching vacuum. This modeling was well validated against the three-point bending test result of the pouch cell with and without pouching vacuum. However the tied option cannot properly represent the rigidity change of pouch cell with the degree of the pouching vacuum that is a critical drawback of this approach. The virtual simulation of impact hammer and shaker excitation tests using the finite element model of pouch cell was aimed to predict just natural frequencies. It is expected to extend the simulation to corresponding amplitudes by including damping ratios of each component of pouch cell, which is our future plan.

CONCLUSION

Mechanical characteristics of Lithium-Polymer battery pouch cell were investigated. Tension tests with coupon specimen were performed to measure elastic modulus, yield strength, fracture strength and strains of electrodes, separator, and pouch cover. Effects of temperature, strain rate, and loading direction were also examined. Three-point bending tests on depouched and pouched cells with and without pouching vacuum were conducted to assess stiffness and ultimate strength together with effects of pouching vacuum on its rigidity. Quasi-static and dynamic pin penetration tests were carried out to quantify threshold failure forces of each component and pouch cell, respectively. Vibration characteristics of pouch cell were identified with impact hammer and shaker excitation tests. A virtual simulation model with finite elements is also constructed and validated against test results. A module and pack level tests and computer simulations are scheduled as a following step. Based on this information, further enhancement on the mechanical integrity of pouch

cell design will be attempted.

REFERENCES

- [1] Elham Sahraei, Rich Hill, Tomasz Wierzbicki, Calibration and finite element simulation of pouch lithium-ion batteries for mechanical integrity, 201, 307– 321, Journal of Power Sources, 2011
- [2] Ping Liu, Elena Sherman, Alan Jacobsen, “Design and Fabrication of Multifunctional Structural Batteries”, 646~650, Journal of Power of Sources, 2008
- [3] Stephanie Golmon, Kurt Maute, Martin L. Dunn, “Numerical modeling of electrochemical-mechanical interactions in lithium polymer batteries”, 1567~1579, Computers and Structures, 2009
- [4] Pam Visual Performance Solution Solver Reference Manual, ESI Group, 2012

WELDING CHARACTERISTICS AND MODELING OF LITHIUM-POLYMER BATTERY FOR ELECTRIC VEHICLE

Jang Ho, Ahn

Hankook ESI
Korea, Republic of

Hyung Yun, Choi

Hongik University
Korea, Republic of

Joon Soo, Lee

Dong Gwan, Bae

SK Innovation
Korea, Republic of
Paper Number 13-0143

ABSTRACT

The fatigue life is a major issue of weld joints due to a severe thermal exposure during the welding process. Welded joints experience highly localized heating and cooling from welding processes. As a result, the material properties around the welding joints can be in significant variations after welding. The prediction of fatigue life and crack propagation in welding parts of pouch cell type lithium polymer battery is the main objectives of this study. The series spot welding and laser welding processes between different electrode materials (Cu and Al) were virtually processed using a finite element method and validated against the metallography of welding specimen.

INTRODUCTION

Lithium-polymer battery is mainly used for Rechargeable Energy Storage System(RESS), the main energy source for electrical vehicles. In this study, weld characteristics of spot welded connections between lithium-polymer battery pouch cells for electric vehicles are investigated with finite element modeling. The final objective of welding simulation is to determine fatigue lifecycle at the welding area. In general, fatigue lifecycle at the welding area is vulnerable due to a phase transformation and residual stress induced by thermal effects. [1] In this study, the series spot welding process is used for welding between electrodes materials of pouch cells and virtually processed using a finite element method. The welding characteristics such as material properties and residual stress can be used as initial conditions for fatigue life cycle assessment or crack propagation analysis.

MATERIAL PROPERTIES

Spot welding is a resistance welding process welded by a contact resistance between sheets and electrodes and a resistance of material to apply current between two electrodes. [2] Sheets are held together under pressure exerted by electrodes. A large amount of heat can be delivered to a very small area and therefore welding occurs without excessive heating to remainder part of components. But heat affected area and molten area are exposed to inhomogeneous heating and cooling process and this thermal cyclic loading brings a metallurgical change such as a phase transformation, recrystallization, re-solution of precipitation. These metallurgical changes effect on mechanical characteristics on the welding area. In case of Cu and Al, typical metals used for electrodes of lithium-polymer battery, a softening due to a recrystallization and re-solution occurs at the heat affected and molten area.[3](See Figure 1)

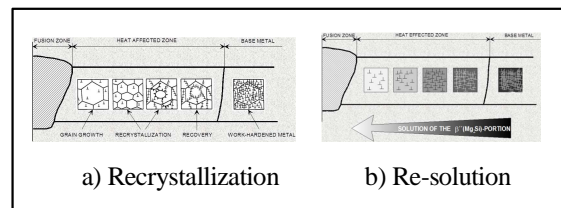


Figure 1. Schematic illustrations for recrystallization and precipitation kinetics in Al and Cu alloys during the welding process.

To capture the softening material properties at heat affected and molten zone, specimens of Cu and Al are heat-treated at 500°C and 300°C then cooled in furnace. Tensile coupon test for intact and heat-treated specimens were performed at room and elevated temperature conditions. Yield strength of intact and heat-treated Cu and Al specimens at various temperatures are shown in Figure 2.

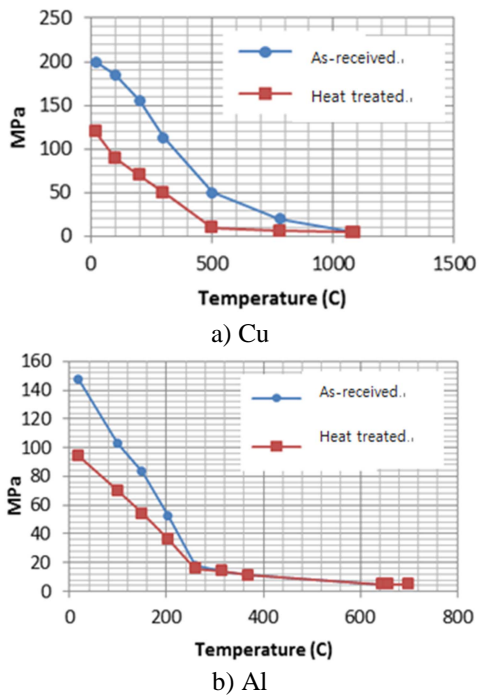


Figure 2. Comparison of yield strength for intact and heat treated Cu and Al with temperature.

FINITE ELEMENT MODELING OF SERIES SPOT WELDING PROCESS

Schematic diagram for series spot welding process is shown in Figure 3. Electrodes are located in parallel and each contact area can be welded simultaneously with one electrical circuit in a series spot welding process. Unlike a vertical electrical current movement in a conventional direct spot welding process, the electrical current flows through the longitudinal direction of plates in a series spot welding process.

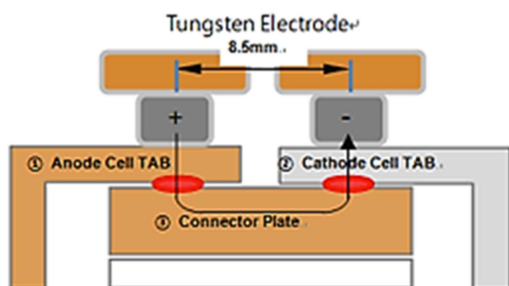


Figure 3. Schematic diagram of electrode for series spot welding.

The thicknesses of Cu and Al sheets are 0.3mm and 0.64mm, respectively. Tungsten electrode with 4mm tip diameter and a DC inverter type with a current profile as shown in Figure 4 which is employed in this study.

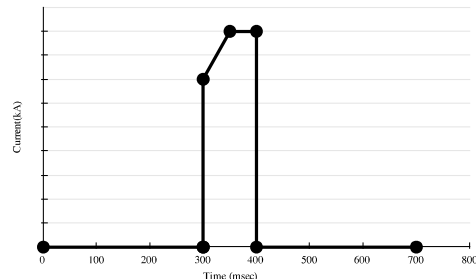


Figure 4. Current profile for Cu-Al welding process.

The spot welding wizard module in SYSWELD [4], which supports a full coupling computation between Electro-Thermo-Metallurgical-Mechanical processes for conventional direct spot welding process, was modified and applied to construct a modeling of series spot welding. Due to a complexity of coupling process between Electro-Thermo-Metallurgical-Mechanical processes of spot welding process, a 2D axisymmetric FE model was assumed and a dummy electrode was introduced to reproduce an electrical current flow in series spot welding process as shown in Figure 5.

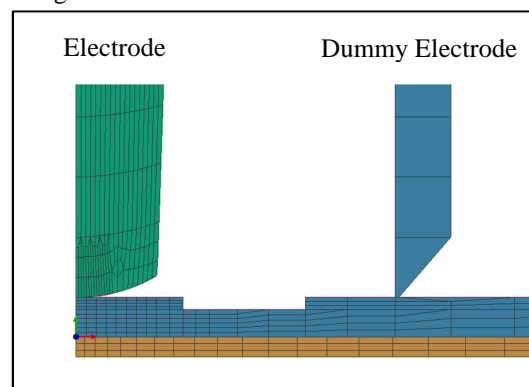


Figure 5. 2D axisymmetric mesh model for series spot welding process.

The main tungsten electrode is modeled at the center of axisymmetric mesh model while a dummy electrode reproducing electrical current flow is placed at the right side. The tip shape of dummy

electrode is modified to make same contact area by comparing real and dummy electrodes.

Electrical and mechanical boundary conditions are shown in Figure 6. Electrical current from process condition is applied at the top surface of the electrode and squeezing force is applied at the same surface where the electrical current is applied. For the dummy electrode, an exit of electrical current condition is given on the top surface of and squeezing force is also applied. The thermal and electrical contact resistance is assigned to the interface between electrodes and sheets. Regarding the mechanical contact, a sliding contact method is initially applied to the interface between sheets and electrodes. When temperatures of nodes at the interface exceed the melting point of alloys, the contact method automatically changes from a sliding into a sticking. [5]

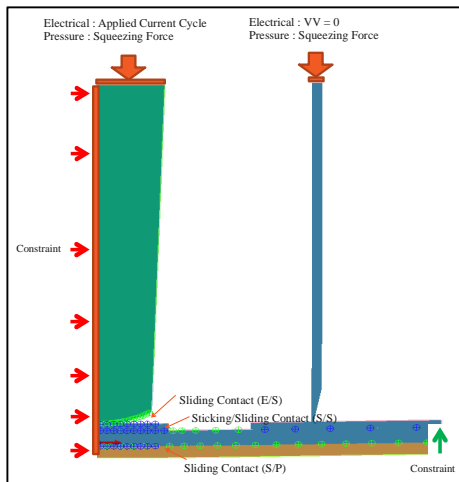


Figure 6. Applied boundary conditions.

RESULTS AND DISCUSSIONS

Validation against experimental results

Electrical potential distribution of a series spot welding process is shown in Figure 7. Electrical potential difference between electrodes is predicted about 1.508V, which is in good agreement with measured range which is between 1.5 and 1.6V.

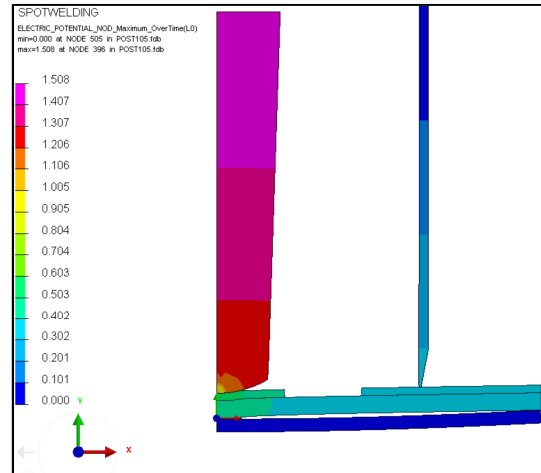


Figure 7. Electrical potential distribution in a series spot welding process.

To verify series spot welding simulation, maximum temperature distribution of whole spot welding cycle is compared with experimental results. The sectioned series spot welding specimen is grinded and polished. To reveal grain structures, the polished surface is etched by a nitric acid solution and analyzed by an optical microscope. (See in Figure 8.) [6]

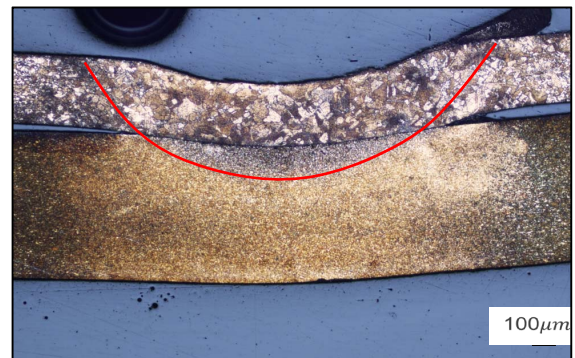


Figure 8. A micrograph of Cu-Cu series spot welding specimen.

More heat is induced at the upper sheet due to a high electrical resistance between tungsten electrode and sheet interface. Therefore the recrystallization and grain growth is observed at the upper Cu sheet. Molten zone shape is displayed with red line in Figure 8.

Predicted maximum temperature distribution of Cu-Cu series spot welding process is shown in Figure 9.

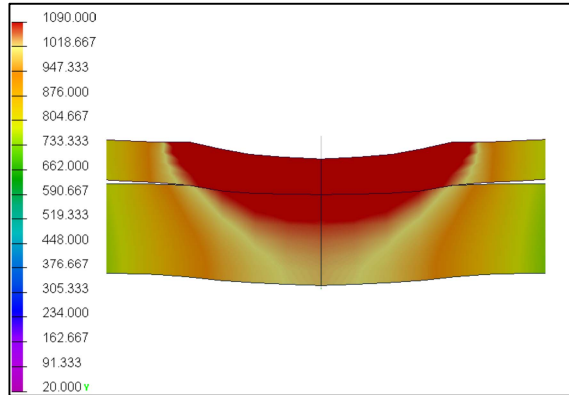


Figure 9. Maximum temperature distribution.

Temperature above melting temperature during welding process is depicted as a red region in Figure 9 and the comparison with micrograph of a specimen Figure 8 is in good agreement.

Series spot welding simulation results

Series spot welding simulations are conducted for 4 welding process conditions of Cu and Al electrode in lithium polymer battery pouch. Phase distribution results are shown in Figure 10 for Cu-Cu-Cu welding process.

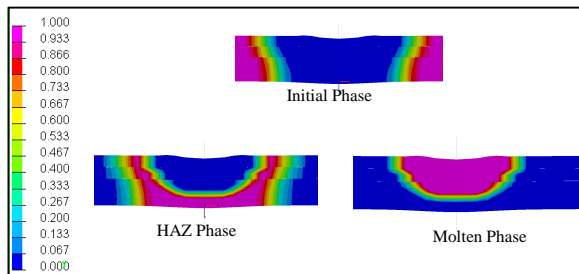


Figure 10. Phase distribution after welding for Cu-Cu-Cu sheet.

Molten zone is created across 3 sheets which ensure that applied electrical current is enough to weld 3 sheets simultaneously. Predicted yield strengths are shown in Figure 11 for Cu-Cu-Cu sheet.

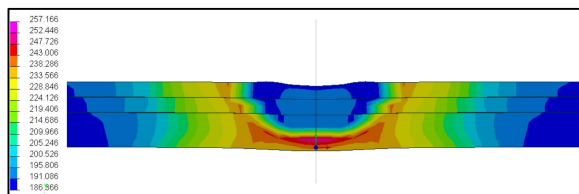


Figure 11. Yield strength distribution after welding for Cu-Cu-Cu sheet.

Because of re-melting and recrystallization in the molten zone, yield strength decreased. But yield strength increased in the heat affected zone due to work hardening effect. Residual stress distributions quantified by Von-mises and longitudinal stress of Cu-Cu-Cu sheet are shown in Figure 12.

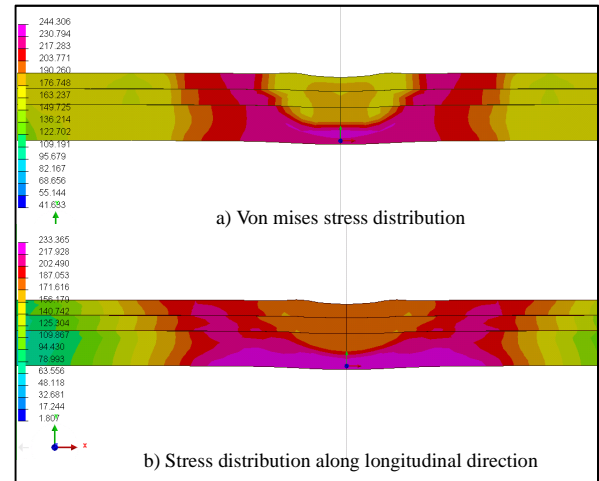


Figure 12. Von-mises stress distribution and stress distribution along longitudinal direction (x) after welding for Cu-Cu-Cu sheet.

A deformation that occurred during welding process from squeezing forces by electrodes and the thermal gradient in heat affected zone is constrained therefore tensile residual stress is observed at longitudinal direction. These material changes occurred at molten and heat affected zone would influence on fatigue life and fracture properties of lithium polymer batteries in service.

CONCLUSIONS

2D axisymmetric finite element modeling method for series spot welding process is proposed. A dummy electrode method is used to simulate electrical current flow in a series spot welding process. Thermo-metallurgical and mechanical characteristics of weld joint between Cu and Al electrodes of Lithium-Polymer battery are computed and validated against experimentally measured electrical potential values, macrographs and hardness values. Computed values with the proposed 2D axisymmetric methods were in good agreement against the experimental results. Further studies to predict fatigue life of weld joint, which take account into welding effect based on this study, are scheduled as a following step.

REFERENCES

- [1] YW Shi, BY Chen, JX Zhang, "Effects of welding residual stresses on fatigue crack growth behavior in butt welds of a pipeline steel", Engineering fracture mechanics, Vol 36 Issue 6, 1990, 893-902
- [2] Z. Feng, S.S. Babu, M.L. Santella, B.W. Riemer, J.E. Gould, "An incrementally coupled Electrical-thermal-mechanical model for Resistance Spot Welding," Proc. 5th International Conference on Trends in Welding Research, Pine Mountain, USA, 1998.
- [3] Grundlagen und Werkstoffe , "Aluminium Taschenbuch Band 1", Aluminium-Zentrale Düsseldorf, 15. Auflage, 1995
- [4] ESI Group, "SYSWELD User's manual", 2012.
- [5] V. ROBIN, A. SANCHEZ, T. DUPUY, J. SOIGNEUX, J.M. BERGHEAU, "Numerical Simulation Of Spot Welding With Special Attention To Contact Conditions", Journal of Materials Processing Technology, Volumes 153-154, 10 Nov 2004, 436-441
- [6] NJ Nelson, "Copper etching process and solution", US Patent 4,632,727, 1986

A STUDY OF ELECTRO-MAGNETIC COMPATIBILITY ABOUT ELECTRIC VEHICLE'S CHARGING MODE

Sung-Bum KIM

Jin-ju KANG, Jae-sung AN, Joong-ho BAE, Jong-Hyun LEE

Korea Automobile Testing and Research Institute

Republic of KOREA

Paper Number 13-0297

ABSTRACT

Eco-friendly car market, which involves hybrid car, electric vehicle, plug-in electric vehicle, hydrogen fueled cell vehicle is expected to be extended locally and abroad amid the high price of petroleum and the enhancement of regulations on environments. Electric vehicles (EV), called Zero Emission Vehicles (ZEV) are perceived as an alternative by using the battery due to all kinds of regulations on cars. In order to avoid problems with electromagnetic interference, Extensive Electromagnetic Compatibility (EMC) and components of vehicles are being developed.

As the electric cars are the ones that need recharging after driving, it may cause social problems when electromagnetic waves are over-generated while battery is being recharged at our home or work places. So the electric cars need to be evaluated by two methods. One is driving mode with no charging on the power grid which is the existing test method from old times. The other is the RESS in charging mode coupled to the power grid. Recently various researches are discussing about battery recharging methods of electric cars. However, according to vehicle's manufacture, the charging type and the position of inlet in vehicle are quite expensive. Real experiments of several electric vehicles were conducted in EMC chamber in KATRI lab. This study shows the differences in the test results of two different methods (driving & charging mode) and provides proper test setup according to the location of inlet.

INTRODUCTION

Recently, many kinds of electric & electronic devices have been equipped in vehicles. There is an Electromagnetic Compatibility in one of the test methods to improve safety of these electric & electronic devices. Due to development and propagation of Eco Friendly Vehicle (EFV), it has tightened the various regulations about these vehicles.

'Electro-Magnetic Compatibility' test can be divided broadly into two types: 'Electro-Magnetic Interference' test and 'Electro-Magnetic Immunity' test. The 'Electro-Magnetic Interference' test, in turn, can be classified into the broadband test, which measures the electromagnetic waves from the engine, the ignition system, the motor in a car, and the narrowband test, which gauges those from electronic control unit built in a car. On the broadband test, internal combustion engines are evaluated in 1500 idle RPM state, with all electronic component being operated while the electric cars and hydrogen fueled cell vehicle being fixed in 40 kilometers per hour are checked if emit electromagnetic waves are exceeding their acceptable limit. Immunity tests are used for confirming whether cars and electronic component malfunction are due to the electromagnetic waves from outside or not. Domestically, the automobile safety standard related with electromagnetic waves has been applied since 1997. [1] However, as the electric cars are the ones that need battery charging after driving, they can cause social problems as mentioned earlier.

Recently, WP.29(Working Party 29), GRE(Working Party on Lighting and Light-Signaling) and UN-affiliated organizations are discussing the battery recharging method.[2] Through this study, by analyzing the results of Electro -magnetic Interference test on neighborhood electric vehicle, electric vehicle and a large-sized electric bus in the middle of recharging, This research shows the necessity of its introduction of additional test methods about battery charging mode of EV's.

EVALUATION OF ELECTRIC VEHICLES

Test Facility and Vehicles

absorber-lined shielded enclosure

The test is performed in shielded enclosure room with internal ceiling and walls which made with radio frequency-absorbing materials. It is illustrated in Figure 1.



Figure 1. Test Facility

Chassis Dynamometer

The Chassis dynamometer can control driving and rotating condition of the test vehicle as figure 2.



Figure 2. Chassis Dynamometer

EMI Receiver and Antenna

Test Equipments are EMI receiver and broadband antenna.

FCC or CISPR prefers the use of turned and half-wave dipoles for measurement of radiated emissions. From the standpoint of rapid and efficient gathering of data over the frequency range of the radiated emission limits of 30 MHz~1GHz, the tuned half-wave dipole is not an attractive measurement antenna. Its length must be physically adjusted to provide a total length of $\frac{1}{2}\lambda$ at each measurement frequency. Also, in the measurement of the vertically polarized emissions at the lowest frequency of the limit, 30 MHz, the dipole length is 5 m. More practical measurement is the use of broadband antennas.

The infinite biconical antenna is constructed with two cones of half angle θ_h with a small gap at the feed point.

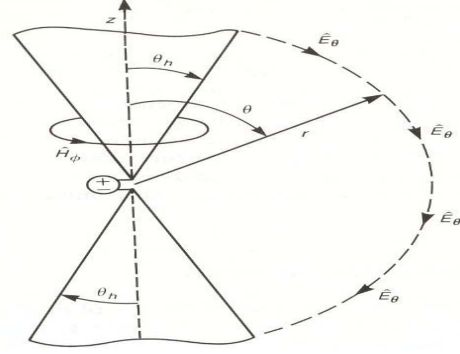


Figure 3. The infinite, biconical antenna

A voltage source feeds the antenna at this gap. A spherical coordinate system is appropriate to use for the analysis here. In the space, surrounding cones (assumed to be free space), $J = 0$, and symmetry suggests that the fields are Faraday's and Ampere's laws can be solved to give the forms of the fields [3]

$$\hat{H}_\phi = \frac{H_o}{\sin \theta} \frac{e^{-jBor}}{r} \quad (1).$$

and

$$\hat{E}_\theta = \frac{\beta_o}{\omega \epsilon_o} \frac{H_o}{\sin \theta} \frac{e^{-jBor}}{r} = n_o \hat{H}_\phi \quad (2).$$

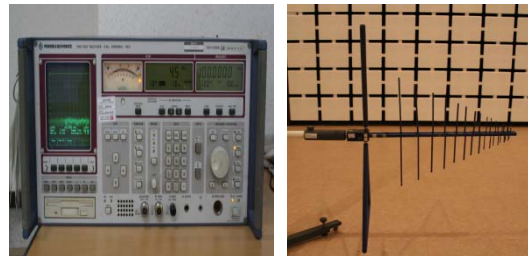


Figure 4. Test Receiver and Antenna.

Test Vehicles

The electric vehicles launched in the domestic are used to evaluate in this study. The test vehicles are EV, NEV and EV-bus. The NEV(Neighborhood Electric Vehicle) is that the maximum speed and the total weight of the vehicle never exceed 60

kilometers per hour and 1,316 kilograms respectively and they can only be driven on the road that government permitted

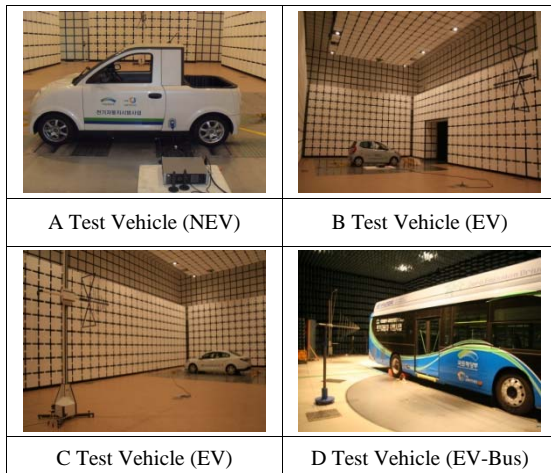


Figure 5. Picture of Test Vehicles

The existing EMC test methods of the vehicles

Many countries are emphasizing their EMC(Electro Magnetic Compatibility) regulations around the world. An electronic system in vehicle that is able to function compatibly with other electronic systems and not produce or be susceptible to interference is said to be electromagnetically compatible with its environment. A system is electromagnetically compatible if it satisfies three criteria [1]

1. It does not cause interference with other systems.
2. It is not susceptible to emissions from other systems.
3. It does not cause interference with itself.

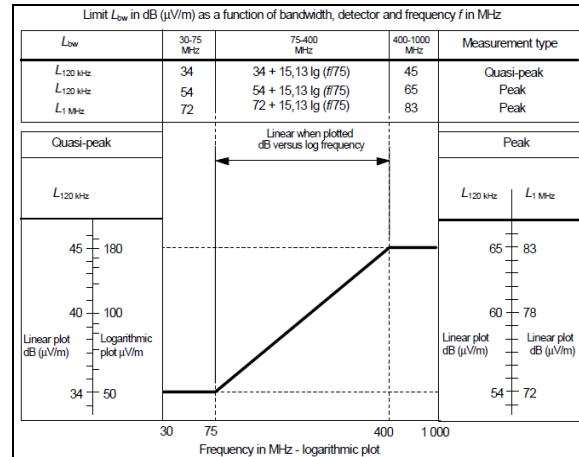
This vehicle EMC applies to components to be fitted in these vehicles with the limitation given. It covers requirements regarding the immunity to radiated and conducted disturbances for functions related to direct control of the vehicle, related to driver, passenger and other road user’s protection and related to disturbances, which would cause confusion to the driver or other road users(EMS) and requirements regarding the control of unwanted radiated and conducted emissions to protect the intended use of electrical or electronic equipment at own or adjacent vehicles or nearby, and the control of disturbances from accessories that may be retrofitted to the vehicle(EMI). [4]

Emission test (EMI)

The limits in this International Standard are designed to provide protection for broadcast receivers in the frequency range of 30 MHz to 1000MHz when used in the residential environment. The vehicle shall comply with both

average limits when the vehicle is in “key-on, Engine-off” mode(Narrowband test) and quasi-peak(or peak) limits when in “Engine-Running” mode(Broadband test). [5]

Table 1.
Peak and quasi-peak detector limits



At each measurement frequency, measurements shall be taken for horizontal and vertical polarization. The horizontal distance between the reference point of the antenna and to the nearest metal part of the vehicle shall be $10 \pm 0.2\text{m}$, as an alternative measurement may be made at a distance of $3 \pm 0.05\text{m}$. For an antenna distance of 10m, the center of the antenna shall be $3 \pm 0.05\text{m}$ above the ground surface. For an antenna distance of 3m, the height shall be $1.8 \pm 0.05\text{m}$. Measurements are made on the left and right sides of the vehicle. [6]

The “key-on, Engine-off” mode operating conditions are as follows:

1. The ignition switch is switched on.
2. The engine shall not be operating
3. The vehicles electronic system shall be all be in their normal operating mode.

The “Engine-Running” mode operating conditions are as below according to vehicle type.

1. Vehicle with an internal combustion engine is tested with engine operated $1,500 \pm 150\text{ rpm}$. (Number of cylinders >1)
2. Vehicle equipped with an electric propulsion motor is tested with the vehicle driven on a dynamometer with a constant speed of 40 km/h.

Immunity test (EMS)

This test scope specifies a vehicle test method for determining the immunity of passenger cars and commercial vehicles to electrical disturbances from off-vehicle radiation sources. The test is performed in an absorber-lined shielded enclosure, the aim being to create an indoor electromagnetic compatibility testing facility that simulates open field testing. Testing consists of generating radiated electromagnetic fields using antenna sets with radio frequency (RF) sources capable of producing the desired field strength over the range of test frequencies.

The RF power required to achieve the required field strength is determined during the field calibration phase. Calibration is performed without a vehicle in the test location. The specific test level is calibrated periodically, using an unmodulated sinusoidal wave, by recording the forward power required to produce a specific field strength for each test frequency. [7], [8] The vehicle is in an unladen condition except for necessary test equipment and the engine normally turns the driving wheels at a steady speed of 50 km/h.

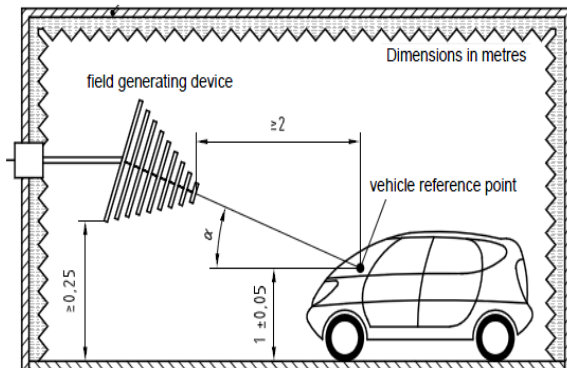


Figure 6. Example of test set-up

The EV's Charging experiment

The EMC test for EV charging mode is implemented as illustrated in Figure 6. The experiment uses the informal document of Electromagnetic compatibility for fourth stage in the Directive ECE/Trans/WP.29/GRE/2010/54 [9].

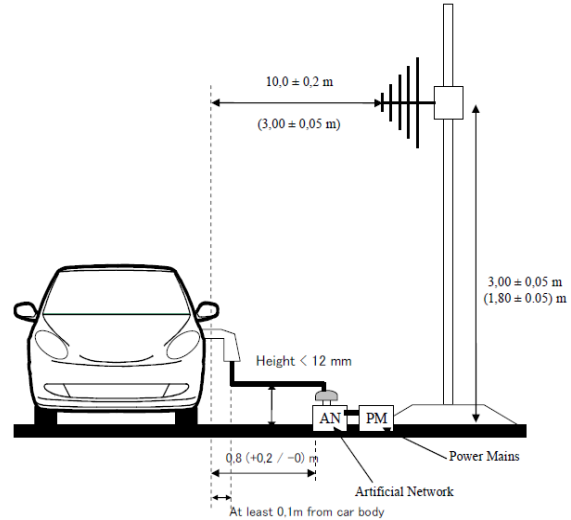


Figure 7. Vehicle in configuration "Charging mode"

In order to ensure that whether occurs in electromagnetic emission in charging mode in comparison with driving mode and how arrange test setup in case of the inlet located on the front or rear (the inlet located on the left or right is measured like figure 6) and 2 inlets in same vehicle for slow charger, we preformed the 4 kinds of EVs in the facility in Figure 1.

This study shows the differences in the test results of two different methods (driving & charging mode) and provides proper test setup according to the location of inlet and bidirectional inlet position.

Table 2.

Specifications of test vehicles

Name	A Test Vehicle (NEV)	B Test Vehicle (EV)	C Test Vehicle (EV)	D Test Vehicle (EV-Bus)
Overall L×W×H(mm)	3,210×1,575×1,560	3,585×1,595×1,540	4,750×1,810×1,460	10,995×2,490×3,325
Curb weight(kg)	830	1,390	1,565	12,295
Seating capacity	2	4	5	51
Battery (energy)	LI-ion (9.2 kWh)	LI-ion (16.4 kWh)	LI-ion (24 kWh)	LI-ion (95 kWh)
Inlet Position	LH side	Front side	LH & RH side	Rear side
Max. Speed	60 km/h	130 km/h	140 km/h	85 km/h

Test results and analysis

Charging mode compared with driving mode

The measurement was taken from horizontal and vertical polarization of receiving antenna and on the left and right sides of the vehicle. Therefore need to perform 4 times mode for emission test. The detector of EMI receiver applies quasi-peak detector measurements and the bandwidth is 120 kHz

The horizontal distance between the antenna and vehicle is $10 \pm 0.2\text{m}$ for test vehicle A, B & C(NEV & Passenger EV), $3 \pm 0.05\text{m}$ for test vehicle D.(EV-Bus) For measurement at 3m antenna distance, 10 dB is added to the 10m limit. The graph presented as below shows a representative result among 4 test modes.

Figure 8 was measured from vertical polarized antenna on the left side of the test vehicle(NEV). [10]

The result is shown in Figure 8. According to the test Results, electromagnetic waves were partially measured high while driving or charging under 200MHz measurement frequency. It was not nearly emitted over 200MHz. It was measured high at the cruise driving mode except for 30~40MHz and 80~100MHz frequency band

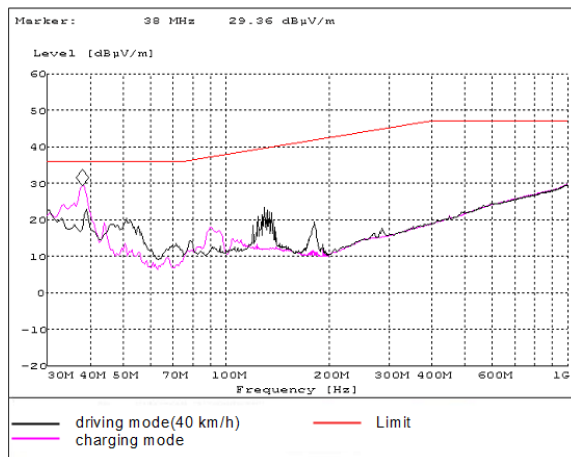


Figure 8. Test vehicle A (Left side of vehicle)

Figure 9 was measured from vertical polarized antenna on the right side of the test vehicle(EV). The result is shown in Figure 8. All measurement frequency of the 30~200MHz was measured electromagnetic waves high at charging mode. The charging mode was measured approximately 30 dB higher than the cruise driving mode. [11]

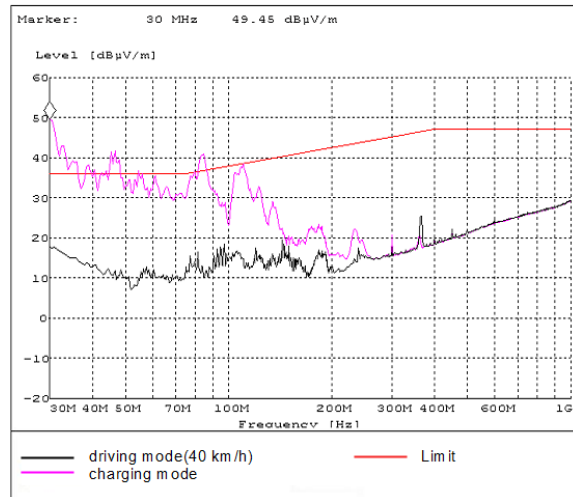


Figure 9. Test vehicle B (Right side of vehicle)

Fig. 10 was measured from vertical polarized antenna on the right side of the test vehicle.

The result is shown in Figure 10. According to the test results, all of the measurement has been measured lower than limit value and also the electromagnetic waves in driving mode was almost emitted higher than charging mode.

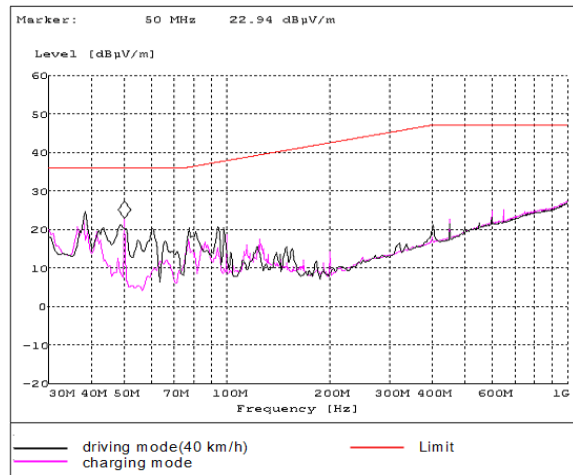


Figure 10. Test vehicle C (Right side of vehicle)

Figure 11 was measured from vertical polarized antenna on the right side of the test vehicle(EV-bus). Most of the electromagnetic waves in driving mode were measured higher than charging mode

and then the peak value in driving mode was approximately 37.8dBuV/m at 108.5MHz.

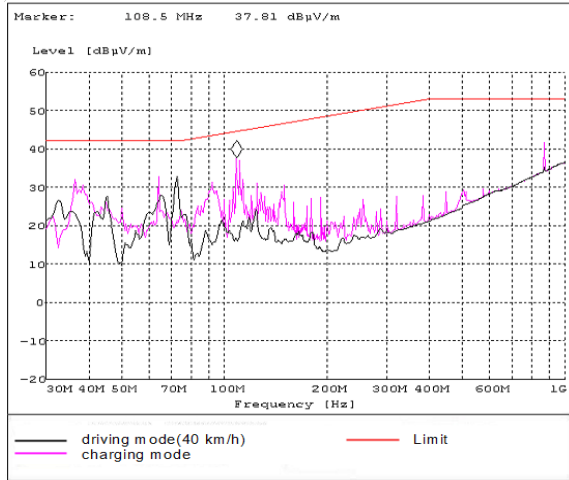


Figure 11. Test vehicle D (Right side of vehicle)

According to this experiment, the results from the two methods(driving & charging) are compared. Also the measured graphs show that electro-magnetic wave is radiated from the vehicle while charging. The results demonstrate that EV needs to be measured in charging mode including driving mode for vehicle safety.

Measurement of the inlet located on the front(or rear) on charging

According to ECE/Trans/WP.29/GRE/2010/54, as shown in Figure 7, the evaluation has to conduct both sides (left and right side of vehicle) regardless of inlet position. And the test method of inlet located on the left and right sides of the vehicle is specified but on the front and rear sides of the vehicle is not exactly stated.

The experiment results show comparisons of the left (or right) with the front (or rear) side of vehicle for emitting the electromagnetic waves.



Figure 12. Test –setup between vehicle and antenna

The test vehicle A is a small electric vehicle equipped with inlet on the left side of the vehicle. Figure 13 is a result of comparing the measured value on the front and left of vehicle from the antenna while charging. The graph shows that two measured results are roughly similar because of small size car and low capacity OBC(On board charger).

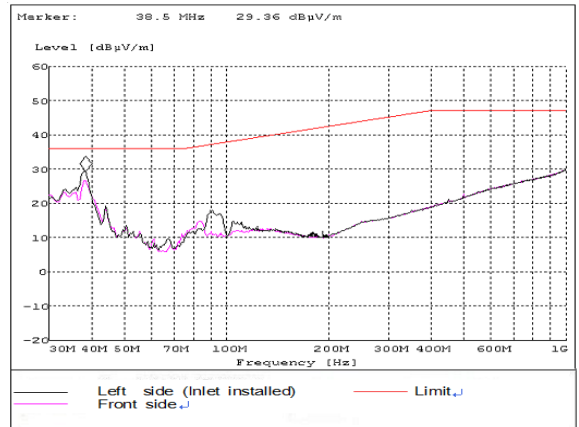


Figure 13. Test vehicle A (Left & Rear side of vehicle)

The test vehicle B is an electric vehicle equipped with inlet for AC charger on the front of the vehicle.

Figure 14 is a result of comparing the measured value on the front and right of vehicle from antenna. Below 85MHz frequency, the value on front installed the inlet has been measured greater than the side specified on standard. It is estimated that the charging device and OBC is located in front of the vehicle.

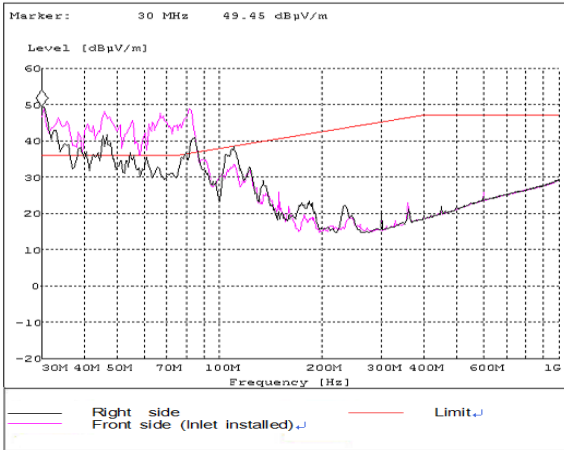


Figure 14. Test vehicle B (Front & Right side of vehicle)

The test vehicle B is an electric vehicle equipped with inlet both sides of the vehicle.

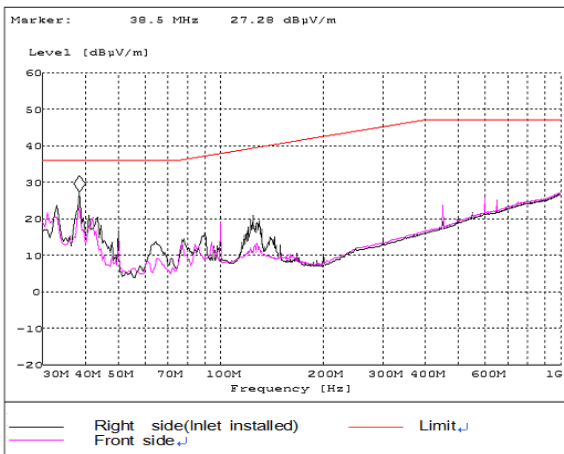


Figure 15. Test vehicle C (Right & Front side of vehicle)

Figure 15 is a result of comparing the measured value on the right and front side of the vehicle. According to the results, the right side was measured slightly higher than the front side.

The test vehicle D is an electric vehicle equipped with inlet at the rear of the vehicle. Figure 16 is a result of comparing the measured value on the rear and left side of the vehicle. According to the results, on the rear of the vehicle installed the inlet was measured higher than the left specified on standard. It seems the results of this test is caused by the charging device and OBC which are located in rear of the vehicle.

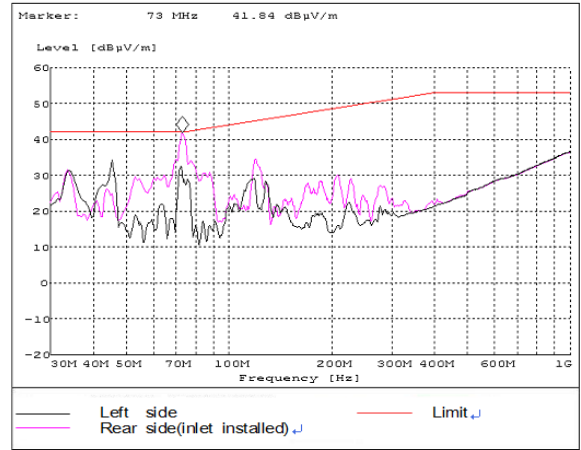


Figure 16. Test vehicle D (Rear & Left side of vehicle)

The table 3 is illustrated the difference between the two data in the frequency of 30~100MHz about 4 kinds of vehicles. The calculated values are the average of the values measured by every 10MHz for the brief analysis. It is presented that how much deviation between on both sides specified on standard and on front(or rear) position installed inlet for AC charger of vehicle

The test vehicle A is measured high approximately 5.05dB in 90~100MHz frequency band at the left side inlet mounted. The test vehicle B is measured high, about 12.56dB in 60~70MHz frequency band at the front side inlet mounted. The test vehicle D is measured high about 15.23dB in 80~90MHz frequency band at the rear inlet mounted.

Table 3.

Comparison of Measurement Orientation

Frequency Band [MHz]	Test vehicle A (Inlet position : left)			Test vehicle B (Inlet position : Front)			Test vehicle D (Inlet position : Rear)		
	Left side [dBµV/m]	Front [dBµV/m]	Deviation (Left-FR)	Right side [dBµV/m]	Front [dBµV/m]	Deviation (Right-FR)	Left side [dBµV/m]	Rear [dBµV/m]	Deviation (Left-RR)
30 ~ 40	23.99	22.71	1.28	39.48	42.96	-3.48	24.49	23.17	1.32
40 ~ 50	14.39	14.88	-0.49	36.36	44.15	-7.79	23.78	21.38	2.41
50 ~ 60	9.83	9.83	0.00	33.26	41.22	-7.96	15.57	26.54	-10.97
60 ~ 70	7.77	6.80	0.96	31.59	44.15	-12.56	17.71	29.51	-11.80
70 ~ 80	9.36	10.18	-0.82	32.49	44.21	-11.72	24.63	36.01	-11.38
80 ~ 90	13.51	12.69	0.82	36.63	41.02	-4.39	14.31	29.55	-15.23
90 ~ 100	15.80	10.75	5.05	28.55	30.21	-1.66	16.35	19.40	-3.05

Therefore, in case the inlet is located on front (or rear) of the vehicle, the measurement results in charging mode are showed that electromagnetic waves of the test vehicle B were more emitted on the front side than on the right side of vehicle. These results indicate that electromagnetic emission is dependent on the position of inlet.

Measurement of dual inlet

In the case of the inlet located on left and right of the vehicle, the measurement in charging mode was respectively taken by antenna located on the left and right sides of the vehicle.



Figure 17. Both inlets of test vehicle C

This study aims to identify which inlet is properly used for test setup if the inlets are installed on both sides as shown in figure 17.

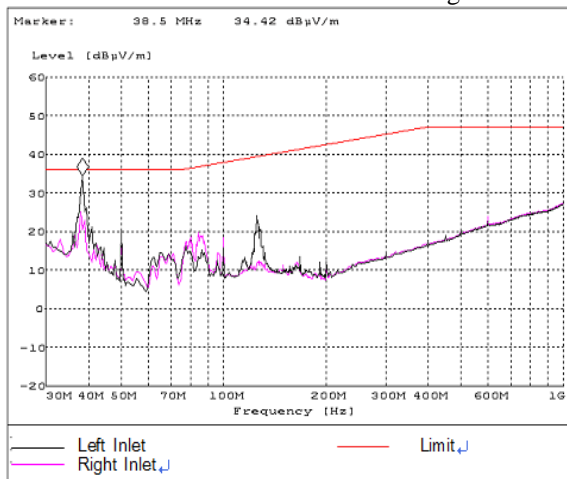


Figure 18. Result of test vehicle C (Left & Right side of vehicle)

The results of this figure 18 show that electromagnetic waves were somewhat more emitted on the left side than on the right. The position of inlet in test vehicle is on the left side from the middle of the bonnet as shown in figure 19.



Figure 19. The position of OBC in bonnet

In conclusion, if the inlets for AC charger are located on both sides of the vehicle, the study has proposed that it would be more appropriate to consider the test setup as the position of the on board charger in vehicle.

CONCLUSIONS

The automobile standard for EMC evaluates only in driving mode. From the result of the test, the electromagnetic waves of driving mode is mostly measured high, but partial frequency bands are occurred in the charging mode. Some of the vehicles in the charging mode emit more electromagnetic waves by comparison with driving mode. The results show that EV needs to be measured in charging mode including driving mode for vehicle safety.

Based on the ECE/Trans/WP.29/GRE/2010/ 54, the measurement of charging mode has to conduct both sides similar to the driving mode. The existing test method reflects to provide protection for residential environment which locates on both side of the road in condition of vehicle driving. But EV's charging condition is static mode (no driving state). The test results show that electromagnetic emission is dependent on the position of inlet. This study suggest

that antenna is required to be positioned on either the front(or rear) side of a vehicle including on the left and right sides, case of the vehicle with inlet located front(or rear).

The measurement of dual inlet shows that which inlet is properly used for test setup, in the case of the inlet located on left and right of the vehicle. This research is to propose that it would be more appropriate to consider test setup position on board charger in vehicle. More researches need to see if this proposal satisfies in other dual conditions.

REFERENCES

- [1] Motor Vehicle Safety Standard of Korea, Article 111-2 “Electromagnetic Compatibility”
- [2] UNECE/TRANS/WP.29/GRE/2010/54, "Proposal for the 04 series of amendments to Regulation No. 10" <http://www.unece.org/trans/main/welcwp29.htm>, 2010.
- [3] Clayton R. Paul., Introduction to Electromagnetic Compatibility, John Wiley & Sons, Inc., 1992.
- [4] UNECE/TRANS/WP.29 “Regulation No. 10 Revision 3” <http://www.unece.org/trans/main/wp29/wp29regs1-20.html>
- [5] IEC, CISPR 12 Ed. 6 “Vehicle, boats and internal combustion engines – Radio disturbance characteristics – Limit and methods of measurement for the protection of off-board”, 2009
- [6] IEC, CISPR 25 Ed. 3 “Vehicle, boats and internal combustion engine driven devices – Radio disturbance characteristics – Limit and methods of measurement for the protection of on-board receivers”, 2000
- [7] ISO 11451-2 Ed. 3 “Road vehicles - Vehicle test methods for electrical disturbances from narrowband radiated electromagnetic energy - Part 2:Off-vehicle radiation sources”, 2005
- [8] SAE J551/2 “The limit and methods of measurement of radio disturbance characteristics of vehicles, Motor boat and spark-ignited engine driven devices”, 1994
- [9] “United Nations Economic Commission for Europe”, UN/ECE, Proposal for the 04 series of amendments to Regulation No. 10, July 2010.
- [10] Kim, S. B., "Considerations for Electromagnetic Compatibility from NEV's Charging mode", KSAE, 2011.
- [11] Kim, S. B., “A study of EMC about EV’s Charging mode”, KSAE, 2012.

APPLICATION OF SYSTEM POWER CONCEPT ON HYBRID ELECTRIC VEHICLES AND ELECTRIC VEHICLES

Dongseok CHOI

Kwangbum LEE, Kihyeon Ryu, Haeboung KWON, Jonghyun LEE

Korea Automobile Testing and Research Institute

Republic of KOREA

Paper Number 13-0324

ABSTRACT

The concept of system power for motor vehicles becomes necessary because multi energy converters and higher efficiency drivetrain are being adapted in advanced motor vehicles for the energy savings and the precise emission controls. This concept is very important in hybrid vehicles due to two different energy converters such as an internal combustion engine and an electric motor. This concept is also applicable to electric vehicles for the efficiency of energy transfer from energy sources to vehicle wheels.

The system power is measured on the powertrain test bed at the state of whole vehicle. It is possible to measure the wheel torque precisely by the direct connection between the power absorber and the end of drivetrain without tires. Two different test methods were developed for the measurement of system power. One is the acceleration at full load under road load (i.e., Method I); the other is the acceleration at full load under the constant vehicle speed (i.e., Method II). Three HEVs and two EVs were tested using the developed test methods. The different types of drivetrain such as an automatic transmission (AT), a continuously variable transmission (CVT) and reduction gear (RG) were equipped in the test vehicles respectively.

Engine speed, coolant temperature, and SOC condition were very important factors for this test in order to produce the maximum power. Method I was much better one for the measurement of system power despite of transient characteristics. The analysis of standard deviation was used for the determination of transient system power at the specific vehicle speed. The criterion for this analysis is the standard deviation of one value, which means that each power value is within +/- two percent of averaged power value.

By measuring system power at the constant vehicle speed, it is shown that the transient power by method I could be maintained during at least 30s. The repeatability of method I was within +/- 5 percent. It is found that this concept and method are applicable and reasonable for the power test of HEVs and EVs.

INTRODUCTION

High efficiency and environmentally friendly vehicles have been developed since the reduction target of green house gases concentrates on the ground vehicles. An electric vehicle (EV) uses one or more traction motors for propulsion. Three main types of electric vehicles exist, those that are directly powered from an external power station, those that are powered by stored electricity originally from an external power sources, and those that are powered by an on-board electrical generator, such as an internal combustion engine or a hydrogen fuel cell. The mass production of those vehicles was started from hybrid electric vehicles (HEVs) and is being extended battery electric vehicles (BEVs) and fuel cell electric vehicles (FCEVs) [1, 2].

Hybrid electric vehicles are possible to drive efficiently by adapting an internal combustion engine and an electric motor. However, much confusion arises in defining which power is used as the maximum power of the engines. Much more electrified hybrid vehicles were inevitably faced with this problem.

Therefore, the concept of system power in terms of power measurement becomes necessary because multi energy converters and different types of drivetrain are adapted in hybrid electric vehicles. This concept of system power in terms of energy saving is applicable to electric vehicles. It shows how much energy transfers from a power source to a vehicle wheels.

System power means the power measured at the vehicle wheels in the powertrain test bed. It is possible to evaluate the power in a whole vehicle state using this concept. In other words, system power is equal to powertrain power because the definition of powertrain contains with energy storage and/or source, an engine, and a drivetrain. Moreover, this concept is irrelevant to an energy source or storage, an engine type, and a drivetrain type.

Meanwhile, it is difficult to conduct the test of maximum engine power due to the adaptation of the security system and the active safety system. Therefore, it is necessary to introduce the concept of system power on high efficiency and

environmentally friendly vehicles such as HEVs and EVs.

OBJECTIVES

This study has two objectives. One is to apply to the concept of system power on HEVs and EVs. The other is to evaluate the energy transfer efficiency for HEVs and EVs using this concept.

EXPERIMENTAL SETUP AND METHOD

Experimental setup

Figure 1 shows schematic of powertrain test bed [3]. The powertrain test bed is possible to measure the wheel torque precisely through the direct connection between the power absorbers and the ends of drivetrain without tires. It consists of four dynamometers, its control and I/O system, a pedal jig for acceleration, and a cooling fan. Each dynamometer as load absorber is a synchronous one with low inertia, maximum power of 290kW, maximum torque of 2500Nm. It is possible to install the vehicle with the wheelbase ranging from 1.8m to 3.8m and the wheel track ranging from 1.2m to 2.2m in this test bed. A pedal jig for acceleration equipped in a driver's seat is specially made in order to adjust an acceleration pedal. The speed of a fan for the vehicle cooling is adjustable with a vehicle speed.

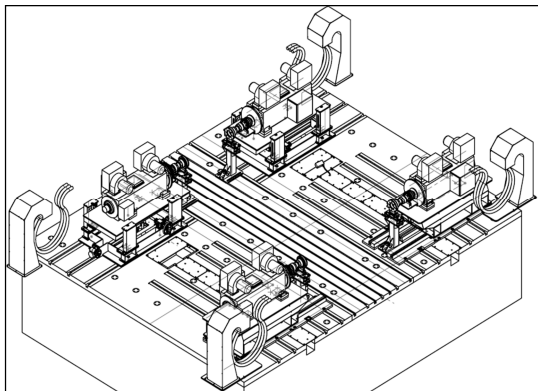


Figure 1. Schematic of powertrain test bed

Methodology

Two different test methods as shown in figure 2 were suggested for the measurement of system power. One is the measurement under road load (i.e., method I); the other is the measurement at the constant vehicle speed (i.e., method II).

Method I rapidly accelerates at full load from the minimum vehicle speed or vehicle standstill to the predefined maximum speed or 60s. This method should measure the friction of drivetrain in the state of neutral gear in order to set the road load properly. Dyno adaptation is completed by subtracting this

frictional resistance from actual road load. This method could be shown dynamic characteristics of powertrain. Due to the nature of the method I, the maximum power is produced within a few minutes. Method I could be had a noise problem due to very short measurement time. For this reason, the determination process using a standard deviation was provided. In order to make easier determination of maximum system power, all data were recorded at 100Hz.

Method II put the full load after the stabilization period of 60s at the constant vehicle speed by the speed control of dynamometer. All data were recorded at 100Hz like method I. This method do not consider the road load. Due to this difference between two methods, the power value by method I is smaller than that by method II.

These methods were also developed using a conventional vehicle with a gasoline engine and a 6-gear automatic transmission [4, 5]. In testing both methods, test vehicles were fully warmed up by running the vehicles at a moderate speed (90-100 km/h) for at least 10 minutes before beginning test.

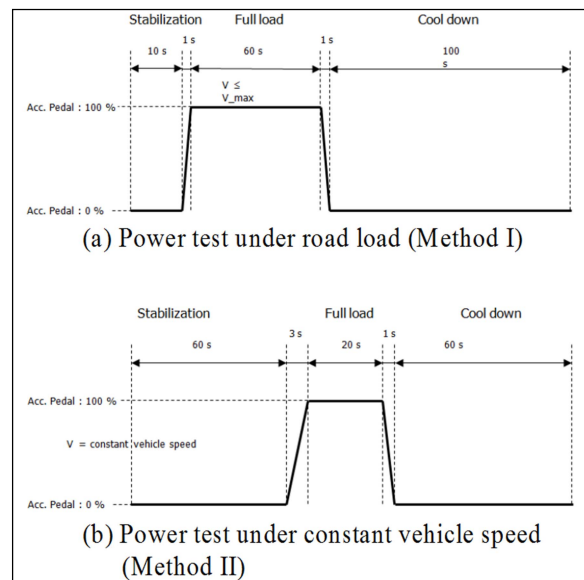


Figure 2. Experimental method

Test vehicles

Five vehicles were tested using Method I and II. Test vehicles were consisted of three different hybrid vehicles and two electric vehicles. Each vehicle had different power of a traction motor and different type of a drivetrain such as an automatic transmission (AT), an electronically controlled continuously variable transmission (ECVT), and a reduction gear (RG). For the case of vehicle C, the system power value was provided by the manufacturer [6].

Table 1.
Specification of powertrain of test vehicles

Power Test Vehicles	Internal Combustion Engine (kW)	Electric Motor (kW)	Drivetrain type
A	133.2	17.6	AT
B	110.4	30	AT
C	55.9	50	ECVT
	System power : 74 kW		
D	-	50	RG
E	-	70	RG

RESULTS AND DISCUSSION

Figure 3 shows the measurement result of system power on vehicle A by method I. Vehicle A is the hybrid electric vehicle, which has the layout connected by the belt between an internal combustion engine and a traction motor. The powertrain consists of a compact electric motor powered by a lithium-ion battery, a 2.4L gasoline engine, and a 6 gear automatic transmission.

Wheel torque shows the typical trend of rapid acceleration at full load. High wheel torque transits to low wheel torque as the gear shifts up. Two jerk points appears in the vehicle speed ranging from 60km/h to 110km/h due to the gear-shift shock. The maximum system power appears around 140km/h. Engine speed is also around 5700rpm at this vehicle speed.

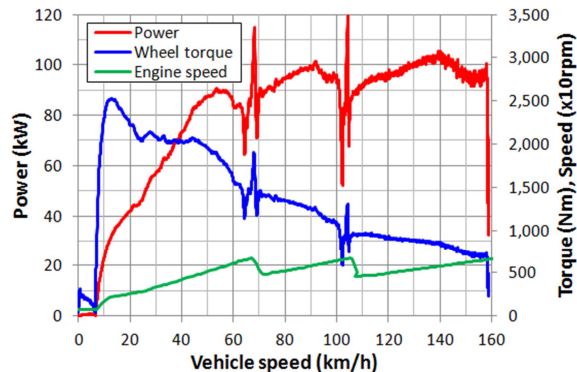


Figure 3. Test result of system power on vehicle A by method I

Each power value was averaged with the vehicle speed. Each vehicle speed was calculated down to the first decimal place. In order to determine the maximum system power, the analysis of standard deviation was used. The criterion for this analysis is the standard deviation of one value, which means that each power value is within +/- two percent of the averaged power value.

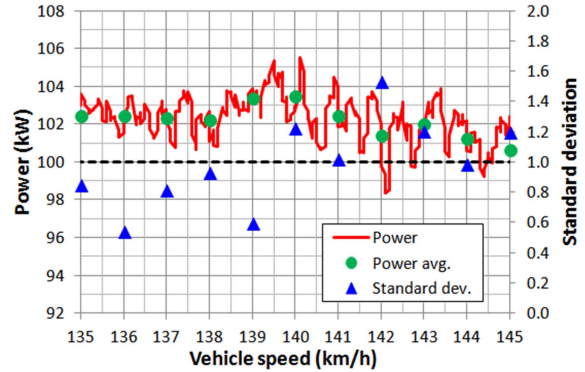


Figure 4. Determination of max. system power by analysis of standard deviation

Figure 4 shows the result of this analysis. Two candidate values at the vehicle speed of 139 and 140 kilometers per hour were shown in figure 4. The standard deviations were 0.6 and 1.2 respectively. Thus, the maximum power value was 103.4kW at 139km/h. This test conducted three times and then the averaged value was 103.8kW at 138km/h.

For the case of method II, the vehicle speed was set in 140km/h and the load was given full within three seconds. The result by method II showed 105.3kW at 140km/h. The difference between two power values is whether road load is considered or not, which is the characteristics of test method. From these results, the transient power measurement by method I is also possible to represent the power performance of the vehicle.

Figure 5 shows the measurement result of the system power on vehicle B by method I. Vehicle B is a parallel type of hybrid vehicle, which has two ways for the power transfer to the wheels. This parallel hybrid system features the clutch and the electric motor positioned between the engine and the transmission. The powertrain consists of a 2.0L gasoline engine, a clutch, an electric motor powered by lithium polymer battery, and a 6 gear automatic transmission.

The wheel torque is a little different with that of the vehicle A due to the different hybrid feature. No jerk point appears in the vehicle B. The first peak of the wheel torque shows the engine torque due to a rapid acceleration. After this peak, the torque by the electric motor affects dominantly by the vehicle speed of 40km/h. The wheel torque is similar with that of the vehicle with a conventional 2.0L gasoline engine [5]. The maximum system power appears around 115km/h. Engine speed was also around 5700rpm at this vehicle speed. Through the analysis of standard deviation for the system power values in the test three times, the maximum system power was 101.6kW at 113km/h.

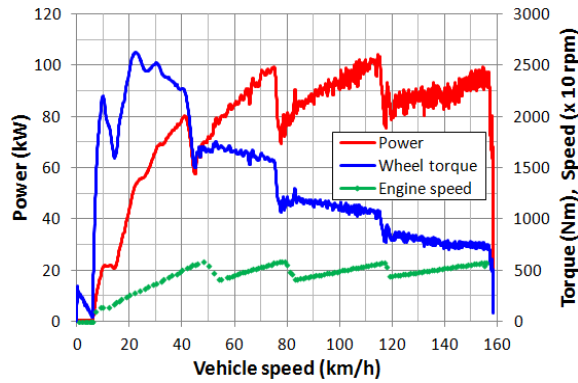


Figure 5. Test result of system power on vehicle B by method I

The test result of vehicle B by method II had significantly different with that of the others. The measurement of system power by method II was conducted at the vehicle speed of 110km/h, 115km/h, and 120km/h. Engine speed at full load was around 4400rpm. Maximum system power was about 90kW at three vehicle speeds above. Thus, vehicle B did not reach the maximum power value measured by method I due to the effect of the control logic on the engine and the electric motor.

Figure 6 shows the measurement result of system power on vehicle C by method I. Vehicle C is also a parallel type of hybrid vehicle. The powertrain consists of a 1.6L gasoline engine, an electric motor of 50kW powered by Ni-MH battery, and an electronically controlled continuously variable transmission.

The wheel torque is quite different with those of the vehicle A and B due to the different hybrid types and transmission features. No step of wheel torque by gearshift appears in vehicle C. The shape of wheel torque until the vehicle speed of 50km/h is similar with the torque shape of the traction motor. Wheel torque below 50km/h has a significant effect on the motor torque, while the wheel torque over 50km/h has a dominant effect on the engine torque. The engine speed of 5000rpm for the maximum engine power was achieved over 90km/h, which means that the maximum system power also outputs over this speed. This power value was approximately 65kW. Through the analysis of standard deviation for the system power values in the test three times, the maximum system power was 68.1kW at 92km/h.

Figure 7 shows the measurement result of the system power on vehicle C by method II. Three candidates for the maximum system power on vehicle C was at the vehicle speed of 90km/h, 100km/h, and 110km/h. Engine speed also reached about 5000rpm over

90km/h. With a little difference, the maximum system power was 70.3kW at 100km/h. The difference between method I and method II is due to the consideration of road load.

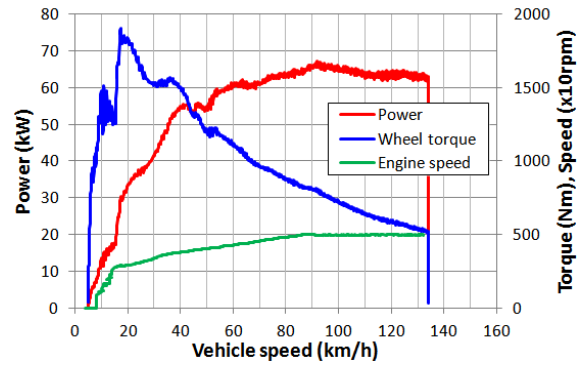


Figure 6. Test result of system power on vehicle C by method I

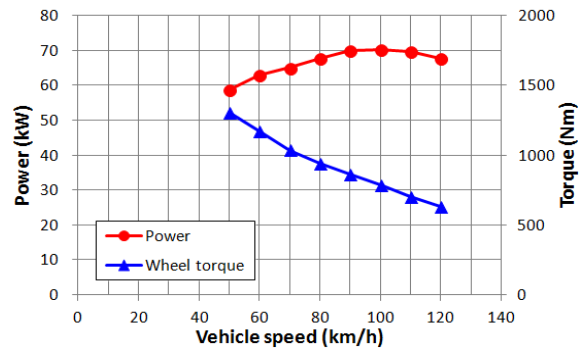


Figure 7. Test result of system power on vehicle C by method II

Figure 8 shows the measurement result of the system power on vehicle D by method I. Vehicle D is an electric vehicle powered by a battery. The powertrain layout of this vehicle is very simple comparing with other test vehicles. The electric power from a lithium polymer battery transfers to the wheel via an electric motor and a reduction gear.

The rapid acceleration at full load was performed at the minimum vehicle speed of 7km/h. Wheel torque shows typical shape of the motor torque due to the simple reduction gear. The motor speed is also proportional to the vehicle speed directly due to the same reason. Wheel torque could be converted into traction force by multiplying a tire radius.

The region below 30km/h shows the operation of continuous wheel torque, which can be produced the maximum wheel torque. The region ranging from 30km/h to 100km/h shows the operation of continuous power, which can be maintained the maximum power continuously. The region over 100km/h shows the operation of weak magnetic field for higher vehicle speed.

The maximum system power could be expected in the vehicle speed ranging from 60km/h to 90km/h. Through the analysis of standard deviation for system power values in the test three times, the maximum system power was 47.6kW at 64km/h.

Figure 9 shows the measurement result of the system power on vehicle D by method II. Four candidates for maximum system power on vehicle D is at the vehicle speed of 60km/h, 70km/h, 80km/h, and 90km/h. With a little difference, the maximum system power was 48.1kW at 80km/h.

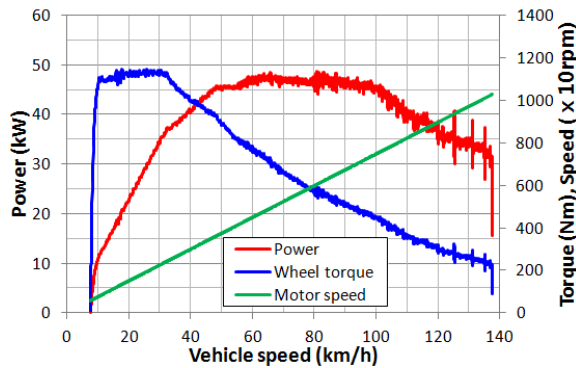


Figure 8. Test result of system power on vehicle D by method I

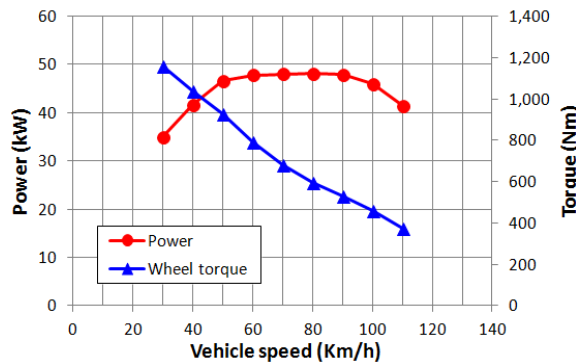


Figure 9. Test result of system power on vehicle D by method II

Figure 10 shows the measurement result of the system power on vehicle E by method I. Vehicle E is also an electric vehicle powered by a battery like vehicle D. The powertrain of this vehicle has very simple layout consisting of a lithium polymer battery, a 70kW electric motor, and a reduction gear. The rapid acceleration at full load was performed at the standstill. The motor speed is also proportional to the vehicle speed directly due to a simple reduction gear. The region of continuous torque was maintained until around 37km/h. The region of continuous power could be shown until around

110km/h. For higher vehicle speed, the operation of weak magnetic field was conducted over 110km/h. Each characteristic region of vehicle E is much more definite than that of vehicle D. The maximum system power could be expected in the vehicle speed ranging from 37km/h to 50km/h. Through the analysis of standard deviation for system power values in the test three times, the maximum system power was 68.7kW at 47km/h.

Figure 11 shows the measurement result of the system power on vehicle E by method II. Two candidates for the maximum system power on vehicle E is at the vehicle speed of 40km/h and 50km/h. With a little difference, the maximum system power was 69.3kW at 50km/h.

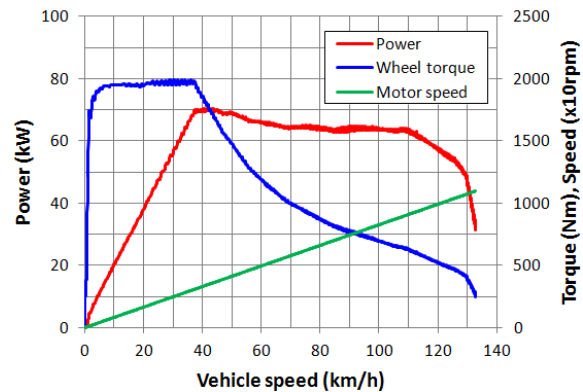


Figure 10. Test result of system power on vehicle E by method I

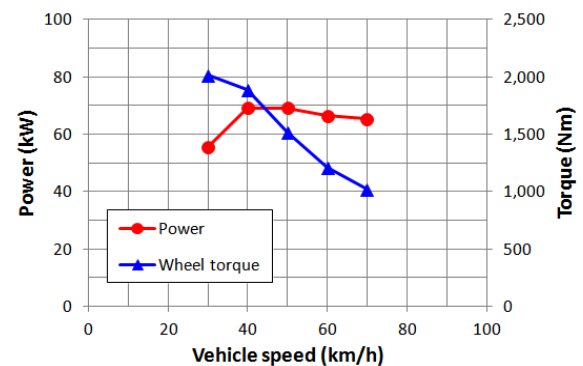


Figure 11. Test result of system power on vehicle E by method II

Table 2 shows the summary of the test results by both methods. The repeatability of method I is within +/- 5 percent of average value. The test values by method II could be considered as reference values without the drivetrain loss in spite of no value on vehicle B. The difference between system power values by method I and those by method II was within +/-5 percent. Thus, method I could be used as

the measurement method for system power on HEVs and EVs.

The efficiency of energy transfer was calculated as follows: For HEVs, the measured value was divided by the power value of an internal combustion engines (ICE) as shown in Table 1. If the specification value of system power is provided by a manufacturer, the specification value was used instead of the power value of an ICE. For EVs, the measured value was divided by the power value of electric motors.

It was found that EVs have high efficiency of more than 95 percent comparing with their motor powers due to simple path of drivetrain. For the case of some HEVs, there was a big gap between the engine power and the system power due to complex drivetrains and different operating regions. It is important that which energy converters such as engines and electric motors are adapted to which drivetrain for higher energy transfer efficiency. Therefore, test method I is available to estimate the energy transfer efficiency for both complex HEVs and simple EVs. In the viewpoint of evaluation of energy transfer efficiency and energy saving such as well-to-wheel efficiency, the concept of system power is very important. Especially, vehicles with multi energy converters such as HEVs are positively necessary this concept.

Table 2.

Test results of system power for test vehicles

Items Test Vehicles	Method I		Method II
	System power [kW/(km/h)]	Efficiency of energy transfer [%]	System power [kW/(km/h)]
A	103.8 / 138	76.7	105.3 / 140
B	101.6 / 113	92.0	-
C	68.1 / 92	121.8, 92.0 ¹⁾	70.3 / 100
D	47.6 / 64	95.2	48.1 / 80
E	68.7 / 47	98.1	69.3 / 50

1) measured value divided by specification value of system power

CONCLUSIONS

The concept of system power was introduced in this paper. This concept was applied to HEVs and EVs for the determination of powers in whole vehicle state. The efficiency of energy transfer was evaluated for these vehicles. Main findings are as follows.

- System power on the vehicles means the power that is measured at the end side of the powertrain without a tier.
- The method of power measurement under road load (method I) was suggested and had the repeatability within +/- 5percent.
- For higher repeatability, it is important to the cooling condition and initial SOC for hybrid electric vehicles.
- The method of power measurement at a constant vehicle speed was used for the confirmation of method I.
- It was possible to apply the concept of system power by method I to HEVs and EVs for the power measurement and the energy transfer efficiency.

ACKNOWLEDGEMENT

This research was supported by a grant (07-Transport System-Future-02) from Transportation System Innovation Program funded by the Ministry of Land, Transport and Maritime Affairs, Republic of Korea.

REFERENCES

- [1] National Renewable Energy Laboratory, "A Vision of our Transportation Future –The Next 30 Years", <http://www.nrel.gov>
- [2] Korean Society of Automotive Engineers, 2012, "Prospection of vehicle technology for year of 2030", KSAE
- [3] AVL, 2009, "Drive train test technology."
- [4] J. Lee, 2008, "The study on the test method of system power in hybrid vehicles", KSAE annual conference, 2104-2109
- [5] D. Choi, 2012, "Development of system power measurement on the vehicles", KSAE annual conference, 1790-1795
- [6] TOYOTA, 2003, "Toyota hybrid system."
- [7] T.D. Gillespie, 1992, "Fundamentals of vehicle dynamics." SAE

A STUDY ON FIRE RESISTANCE TEST PROCEDURE FOR TRACTION BATTERY

Hyuk JUNG
Kyungsam KIM
Kwangbum LEE
Haeboung KWON

Korea Automobile Testing & Research Institute (KATRI)
Republic of Korea
Paper Number 13-0353

ABSTRACT

Market share of electrically propelled vehicle are increasing due to high oil prices and environmental concerns. These electrically propelled vehicles demand to ensure high safety of electric energy storage system, high voltage system and mechanical structure which is equivalent to existing ICE vehicle.

Due to these social demands, global organizations like UN/ECE and ISO are under discussion to make the safety test specification of Lithium-battery, one of rechargeable energy storage systems. KATRI also have researched and developed KMVSS which is for electrically propelled vehicles since 2006, and seven traction battery safety tests have been issued and conducted since 2009. Fire resistance test is to confirm whether traction battery could withstand the intended fire for 2 minutes which is minimum time for evacuating driver and passengers from burning car. This test is considered one of important traction battery safety tests.

In this study, current KMVSS traction battery fire resistance test, draft of ECE R-100 RESS fire resistance test in outside and draft of GTR/SGS-test procedure for hydrogen storage fire test were comparatively analyzed. Subsequently, this study proposed new fire resistance test procedure for traction battery with verification.

INTRODUCTION

In this study, fire tests were conducted with commercialized traction battery or Mock-up.

To check how much of fire heat transferred, metal shielded K-type thermocouples were set up in various position. Position of thermocouples is considered to confirm fire heat profile in each X-Y-Z planes.

To check explosion as a test criteria, visible inspection were carried out with video recording. First test was the current KMVSS fire resistance test. It took more than 5 minutes until stable heat of 890 ~ 900 °C was maintained. Secondly, draft

of ECE R-100 fire resistance test in outside used commercial fuel for positive-ignition engines (gasoline) and flame temperature was about 700 °C at the bottom of DUT. Thirdly, draft of GTR/SGS- hydrogen storage fire test was suitable to meet test flame temperature of 600 ~ 1100 °C. Three fire tests had impressive characters which are wide temperature fluctuation window, control hardness belonging to gasoline as a fuel and suitability to meet test fire temperature.

This study proposes optimized traction battery fire resistance test as a results of comparative test analysis. This optimized test using LPG direct injecting method to attain test temperature easily heats whole bottom area of DUT. Also, this test procedure has another merit which is relatively short time to maintain test temperature condition. After verifying this optimized fire resistance test, KATRI plans on proposing the draft amendment of KMVSS test procedure to the government and UN/ECE GTR/EVS informal group.

KMVSS Article 18-3. Traction Battery

The necessity of the legislation for safety standards of traction battery came to the fore since HEV were propagated to public organizations and provincial governments in the capital region by Ministry of Environment, 2004.

Ministry of Land, Transport and Maritime Affairs consigned KATRI the government project and KATRI carried out research on the development of safety-Assessment Procedures for HEV from October, 2006 to September, 2008.

During this project, KATRI conducted research on not only traction battery, but also all aspects of Hybrid vehicles. Furthermore, we drew deficiencies of the then safety standards and submitted a complement to safety standard proposals. Consequently, Korean government revised the KMVSS 8 Articles in Jan 2009. At this time, revision articles were Definitions, Motor and Transmission System, Brake System, Fuel System, Motor Power and EMC. And newly inserted High

voltage electric device and Traction Battery. And Revised the seven test Procedures according to revision of KMVSS in Feb. 2009.

Table1.
Summary of KMVSS related the traction battery

Article	Description
Article 2 Definition	“Traction Battery” means the storage of electrical energy to propel a vehicle
Article 18-3 Traction Battery (RESS)	General Structural Requirements Traction batteries in a vehicle shall meet each of the following requirements. 1. The batteries shall be isolated from the wall or guard plate. 2. They shall be equipped with functions to prevent an overcharge or over-current exceeding the range specified in the design. 3. Traction batteries shall be free of the possibility for fire or explosion that can take place in physical, chemical, electrical, and thermal shock conditions as notified by the Minister of Land, Transport and Maritime Affairs.

Table2.
Summary of KMVSS test procedure for traction battery safety(Annex 1 -Part 48)

Test	Procedure	Specimen	Criteria
Drop	Drop from 4.9 m high	package or system	Fire & Explosion
Immersion	Immerse completely in the sea water	package or system	Fire & Explosion
Over - charge	Charge up to 150% SOC	System	Fire & Explosion
Over - discharge	Discharge with 1C rate	System	Fire & Explosion
Short circuit	Closed circuit with total resistance of 50 mΩ or less for 1 hour	System	Fire & Explosion
Heat Exposure	Exposed to 80 °C heat for 4 hour	package or system	Fire & Explosion
Fire Resistance	Exposed to flame of 890 to 900 °C for 2 min.	package or system	Explosion

KMVSS Test Procedure Annex 1.48. Traction Battery Safety Test
48.6.7 Fire Resistance Test

1. Test purpose

The purpose of current KMVSS fire resistance test is to confirm the safety of traction battery to secure an evacuation time for driver and passengers when vehicle is on fire. Test procedures are as follows.

2. Test procedures

The following requirements and conditions shall apply to the test

(a) Discharge the traction battery completely at room temperature and then charge until target SOC with rated current.

(b) At the beginning of the test, the SOC shall be adjusted to a value in the maximum charged SOC among the vehicle normal operating range. however, if there is no standardized SOC, the SOC shall be adjusted to a value in the 80 percent.

(c) Measure the voltage of traction battery.

(d) The traction battery shall be placed on the test equipment and then bottom area of the traction battery shall be directly heated by flames.

(e) Set the flame temperature at 890°C to 900°C shall be maintained for 2 minutes.

(f) Check the explosion of traction battery during the test and then measure the voltage of traction battery after the test

3. Review

The component of fire resistance test equipment in KATRI is as shown Figure1. Combustion method of this equipment is a top open burner type which maintains a flame temperature of 890°C to 900°C by supply of LPG and air with PID control.



Figure1. Fire resistance test equipment and test scene according to current KMVSS test procedure

The current procedure of KMVSS fire resistance test is appropriate for a small scale of HEV traction battery when a flame temperature is adjusted and a test specimen is placed on the test equipment. However, a problem comes up when EV traction battery is tested, because it is so large and heavy that a test specimen is hard to be placed on the test equipment. Also, a flame temperature is difficult to adjust because top of the burner is open. Consequently, KATRI recognized the need of the revision on the current test procedure and examined the validity of the application of ECE R-100 fire resistance test draft and GTR/HFCV-SGS Hydrogen Storage Fire Test procedure.

Table3 shows traction batteries for EV which are currently under the mass production and development in Korea.

Table3.
Example of traction battery specification of electric vehicle in Korea

Appearance	specification
	RAY (M1) Li-ion 1.7×1.1×0.3m , 300kg 360v, 75Ah
	SM3 Z.E. (M1) Li-polymer 1.3×0.7×0.8m, 250kg 360v, 65Ah
	ELEC-CITY (M3) Li-polymer Sub Pack. 1.5×0.9×0.4m , 150kg, 380v, 250Ah
	E-PRIMUS (M3) Li-polymer Sub Pack. 1.65×0.7×0.5m, 320kg, 613v, 140Ah
	QTPE-BUS (M3) Li-ion 1.9×1.1×0.5m, 620kg 591V, 70Ah

Draft of ECE R-100 Fire Resistance Test

This test procedure, based on existing ECE R-34 [“Uniform provisions concerning the approval of vehicles with regard to the prevention of fire risks” / 5. Requirements for liquid fuel tanks / Annex 5. Testing of fuel tanks made of a plastic material / Appendix 1 Test of resistance to fire], was suggested by SP Technical Research Institute of Sweden. Test procedures are as follows.

1. Test purpose

The purpose of draft of ECE R-100 fire resistance test procedure is to verify the resistance of the REESS, against exposure to fire from outside of the vehicle due to e.g. a fuel spill from a vehicle (either the vehicle itself or a nearby vehicle). This situation should leave the driver and passengers with enough time to evacuate. Test procedures are as follows.

2. General test conditions

The following requirements and conditions shall apply to the test:

(a) the test shall be conducted at a temperature of at least 0 °C,

(b) at the beginning of the test, the SOC shall be adjusted to a value in the upper 50 percent of the normal operating SOC range,

(c) at the beginning of the test, all protection devices which effect the function of the Tested-Device and are relevant for the outcome of the test shall be operational.

3. Test procedures

A vehicle based test or a component based test shall be performed at the discretion of the manufacturer:

(a) Vehicle based test

The Tested-Device shall be mounted in a testing fixture simulating actual mounting conditions as far as possible; no combustible material should be used for this with the exception of material that is part of the REESS. The method whereby the Tested-Device is fixed in the fixture shall correspond to the relevant specifications for its installation in a vehicle. In the case of a REESS designed for a specific vehicle use, vehicle parts which affect the course of the fire in any way shall be taken into consideration.

(b) Component based test

The Tested-Device shall be placed on a grating table positioned above the pan, in an orientation according to the manufacturer's design intent.

The grating table shall be constructed by steel rods, diameter 6-10 mm, with 4-6 cm in between. If needed the steel rods could be supported by flat steel parts.

The flame to which the Tested-Device is exposed shall be obtained by burning commercial fuel for positive-ignition engines (hereafter called "fuel") in a pan. The quantity of fuel shall be sufficient to permit the flame, under free-burning conditions, to burn for the whole test procedure. The fuel temperature shall be ambient temperature.

The fire shall cover the whole area of the pan during whole fire exposure. The pan dimensions shall be chosen so as to ensure that the sides of the Tested-Device are exposed to the flame. The pan shall therefore exceed the horizontal projection of the Tested-Device by at least 20 cm, but not more than 50 cm. The sidewalls of the pan shall not project more than 8 cm above the level of the fuel at the start of the test.

The pan filled with fuel shall be placed under the Tested-Device in such a way that the distance between the level of the fuel in the pan and the bottom of the Tested-Device corresponds to the design height of the Tested-Device above the road surface at the unladen mass if paragraph (1) is applied or approximately 50 cm if Paragraph (2) is applied. Either the pan, or the testing fixture, or both, shall be freely movable.

During phase C of the test, the pan shall be covered by a screen. The screen shall be placed 3 cm +/- 1 cm above the fuel level measured prior to the ignition of the fuel. The screen shall be made of a refractory material, as prescribed in Annex. There shall be no gap between the bricks and they shall be supported over the fuel pan in such a manner that the holes in the bricks are not obstructed. The length and width of the flame shall be 2 cm to 4 cm smaller than the interior dimensions of the pan so that a gap of 1 cm to 2 cm exists between the flame and the wall of the pan to allow ventilation. Before the test the screen shall be at least at the ambient temperature. The firebricks may be wetted in order to guarantee repeatable test conditions.

If the tests are carried out in the open air, sufficient wind protection shall be provided and the wind velocity at pan level shall not exceed 2.5 km/h.

The test shall comprise of three phases B-D, if the fuel is at least at temperature of 20 °C. Otherwise the test shall comprise four phases A-D.

(a) Phase A: Pre-heating (Figure 2)

The fuel in the pan shall be ignited at a distance of at least 3 m from the Tested-Device. After 60 seconds pre-heating, the pan shall be placed under the Tested-Device. If the size of the pan is too large to be moved without risking liquid spills etc. then the Tested-Device and test rig can be moved over the pan instead.

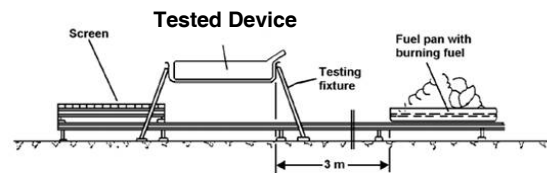


Figure 2. Phase A: Pre-heating

(b) Phase B: Direct exposure to flame (Figure 3)

The Tested-Device shall be exposed to the flame from the freely burning fuel for 70 seconds.

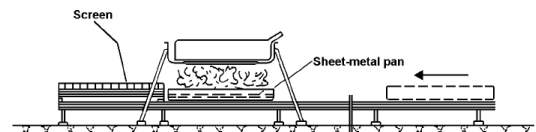


Figure 3. Phase B: Direct exposure to flame

(c) Phase C: Indirect exposure to flame (Figure 4)

As soon as phase B has been completed, the screen shall be placed between the burning pan and the Tested-Device. The Tested-Device shall be exposed to this reduced flame for a further 60 seconds.

Instead of conducting Phase C of the test, Phase B may at the manufacturer's discretion be continued for an additional 60 seconds.

However this shall only be permitted where it is demonstrable to the satisfaction of the Technical Service that it will not result in a reduction in the severity of the test.

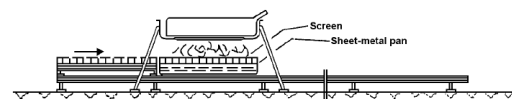


Figure 4. Phase C: Indirect exposure to flame

(d) Phase D: End of test (Figure 5)

The burning pan covered with the screen shall be moved back to the position described in phase A. No extinguishing of the Tested-Device shall be done. After removal of the pan the Tested-Device shall be observed until such time as the surface temperature of the Tested-Device has decreased to ambient temperature or has been decreasing for a minimum of 3 hours.

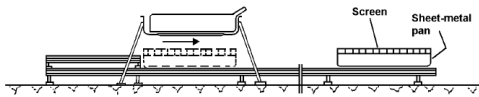


Figure 5. Phase D: End of test

4. Review

As examined previously, ECE R-100 fire resistance test procedure is very complicated compared to KMVSS.

KATRI participated in UN/ECE WP29 RESS informal meeting to amend ECE R-100 and suggested our opinions to make fire resistance test carried out outside because currently KATRI does not have an indoor facility for fire resistance test.

Figure 6 shows vehicle based fire resistance test scene according to the draft of ECE R-100 by SP Technical Research Institute of Sweden at 3rd RESS informal meeting in April, 2011.



Figure 6. Fire resistance test scene according to the draft of ECE R-100(vehicle based)

Draft of ECE R-100 Fire Resistance Test in Outside

1. Test purpose

KATRI verified whether Fire Resistance Test in outside was possible or not according to fire resistance test procedure specified in the draft of ECE R-100. For the test, Mock-up DUT fitted to the size of NEV traction battery was manufactured and the dimension of pan, type of fuel, quantity of fuel and wind velocity condition for outdoor test were set up to satisfy requirements of the draft of ECE R-100. Moreover, the test was carried out under the condition of only direct exposure to flame. Verification of the temperature distribution and problems in test procedure was achieved by measuring the temperature of eight points around DUT.

2. Test Configurations

Figure 7 and Table 4 shows the dimension of DUT and pan, temperature measuring point and wind speed measuring point for the test.

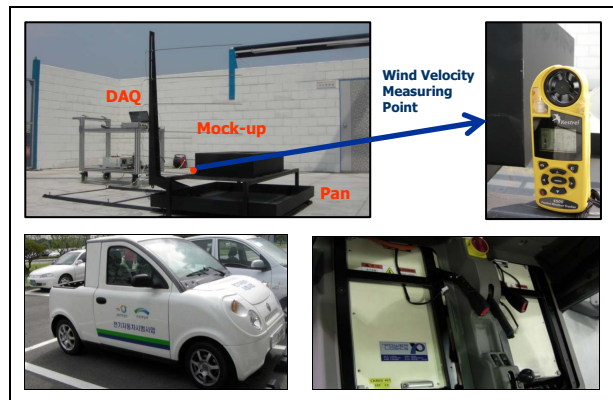


Figure 7. Test Configurations

Table4.

Test conditions of ECE R-100 Fire Resistance Test in Outside

Test conditions
• Mock-up simulates real DUT size : 920 x 605 x 206 mm
• DAQ get 8 temp. channels <ul style="list-style-type: none"> - Under the DUT (center & side) - Middle of DUT (external) - 200, 500, 800, 1100 mm above the DUT
• Pan exceed the horizontal projection of the every DUT side by 25 cm (Draft : 20 ~ 50 cm)
• K-type sheath Thermocouple(3.2 mm)
• Initial ambient temp : 32.2 °C
• Wind speed : about 0.5 m/sec (Draft : not exceed 2.5 km/h(= 0.69 m/sec))
• Fuel quantity : 25 lit./m ²

3. Test Result

This tests are carried out only direct exposure to flame condition according to draft of ECE R-100 fire resistance test procedure in outside. Test procedure and Temp. Data were acquired for 120 sec. Test scene and results of each points measuring flame temperature are as follows.



Figure 8. Fire resistance test scene according to draft of ECE R-100 in Outside



Figure 9. Flame temperature at each point

4. Review

Despite of the weak wind, temperature curve cannot be easily stabilized. Even if initial wind velocity is lower than draft limitation, heat generated by flame causes turbulence due to the evaporation rate and difference of thermal distribution. In this test, reasonable flame temperature data could not be acquired because of

turbulence except just one point. It is #1 point (in Figure 9) that located at the bottom of DUT. Average temperature was about 700 °C during the test. This temperature is very important to decide the heating condition on the draft amendment of KMVSS fire resistance test procedure.

As a test result, KATRI recognized the difficulty of doing the test according to the draft of ECE R-100 fire resistance test procedure in outside. If we adopt the draft, then KATRI and vehicle or battery manufacturer have to construct an explosion proof facility for indoor test including a large ventilation and emission and waste water disposal facility with an enormous expense.

Draft of GTR/HFCV-SGS HYDROGEN FUELED VEHICLE “Test Procedures for Service Terminating Performance in Fire”

1. Test purpose

This regulation specifies safety-related performance requirements for hydrogen-fueled vehicles. The purpose of this regulation is to minimize human harm that may occur as a result of fire, burst or explosion related to the vehicle fuel system and/or from electric shock caused by the vehicle’s high voltage system. Test procedures are as follows.

2. Definitions

The hydrogen container assembly consists of the compressed hydrogen storage system with additional relevant features, including the venting system (such as the vent line and vent line covering) and any shielding affixed directly to the container (such as thermal wraps of the container(s) and/or coverings/barriers over the TPRD(s)).

Either one of the following two methods are used to identify the position of the system over the initial (localized) fire source:

Method I: Qualification for a Generic (Non-Specific) Vehicle Installation

If a vehicle installation configuration is not specified (and the qualification of the system is not limited to a specific vehicle installation configuration) then the localized fire exposure area is the area on the test article farthest from the TPRD(s). The test article, as specified above, only includes thermal shielding or other mitigation devices affixed directly to the container that are used in all vehicle applications. Venting system(s) (such as the vent line and vent line

covering) and/or coverings/barriers over the TPRD(s) are included in the container assembly if they are anticipated for use in any application. If a system is tested without representative components, then retesting of that system is required if a vehicle application specifies the use of these type of components.

Method 2: Qualification for a Specific Vehicle Installation

If a specific vehicle installation configuration is specified and the qualification of the system is limited to that specific vehicle installation configuration, then the test setup may also include other vehicle components in addition to the hydrogen storage system. These vehicle components (such as shielding or barriers, which are permanently attached to the vehicle's structure by means of welding or bolts and not affixed to the storage system) must be included in the test setup in the vehicle-installed configuration relative to the hydrogen storage system. This localized fire test is conducted on the worst case localized fire exposure areas based on the four fire orientations: fires originating from the direction of the passenger compartment, cargo/luggage compartment, wheel wells or ground-pooled gasoline.

In addition, the container is subjected an engulfing fire without any shielding components as described in paragraph "Engulfing fire test".

3. Test conditions

The following test requirements apply whether Method 1 or 2 (above) is used:

(a) The container assembly is filled with compressed hydrogen gas at 100 percent of NWP. The container assembly is positioned horizontally approximately 100 mm above the fire source.

Localized Portion of the Fire Test

(b) The localized fire exposure area is located on the test article furthest from the TPRD(s). If Method 2 is selected and more vulnerable areas are identified for a specific vehicle installation configuration, the more vulnerable area that is furthest from the TPRD(s) is positioned directly over the initial fire source.

(c) The fire source consists of LPG burners configured to produce a uniform minimum temperature on the test article measured with a minimum 5 thermocouples covering the length of the test article up to 1.65m maximum (at least 2

thermocouples within the localized fire area, and at least 3 thermocouples equally spaced and no more than 0.5 m apart in the remaining area) located 25 mm + 10 mm from the outside surface of the test article along its longitudinal axis. At the option of the manufacturer or testing facility, additional thermocouples may be located at TPRD sensing points or any other locations for optional diagnostic purposes.

(d) Wind shields are applied to ensure uniform heating.

(e) The fire source initiates within a 250 mm + 50 mm longitudinal expanse positioned under the localized exposure area of the test article. The width of the fire source encompasses the entire diameter (width) of the storage system. If Method 2 is selected, the length and width shall be reduced, if necessary, to account for vehicle-specific features.

(f) As shown in Figure 10, the temperature at the thermocouples in the localized fire area are increased continuously to at least 600 °C within 3 minutes of ignition, and a temperature of at least 600 °C is maintained for the next 5 minutes. The temperature in the localized fire area shall not exceed 900 °C during this period. Compliance to the thermal requirements begins 1-minute after entering the period with minimum and maximum limits and is based on a 1-minute rolling average of each thermocouple in the region of interest. (Note: The temperature outside the region of the initial fire source is not specified during these initial 8 minutes from the time of ignition.)

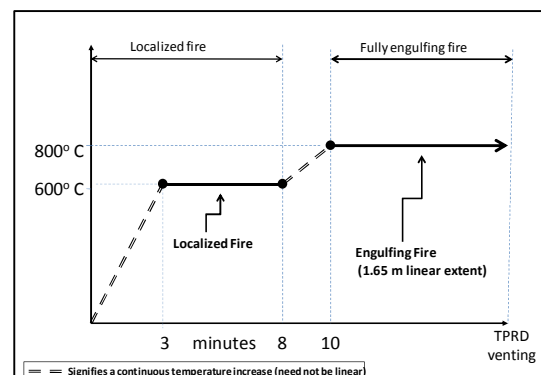


Figure 10. Profile of the flame temperature

4. Test Procedures

Engulfing Portion of the Fire Test

(g) Then within the next 2-minute interval, the temperature along the entire surface of the test article shall be increased to at least 800 °C and the fire source is extended to produce a uniform temperature along the entire length up to 1.65 meters and the entire width of the test article (engulfing fire). The minimum temperature is held at 800 °C, and the maximum temperature shall not exceed 1100 °C. Compliance to the thermal requirements begins 1-minute after entering the period with constant minimum and maximum limits and is based on a 1-minute rolling average of each thermocouple.

(h) The test article is held at temperature (engulfing fire condition) until the system vents through the TPRD and the pressure falls to less than 1 MPa. The venting must be continuous (without interruption), and the storage system must not rupture. An additional release through leakage (not including release through the TPRD) that results in a flame with length greater than 0.5 m beyond the perimeter of the applied flame must not occur.

5. Review

KATRI applied the above test to hydrogen storage tank of hydrogen fuel cell vehicle being developed through “Research on the development of safety-Assessment Procedures for HFCV” and the following picture shows hydrogen storage fire test equipment and test scene.

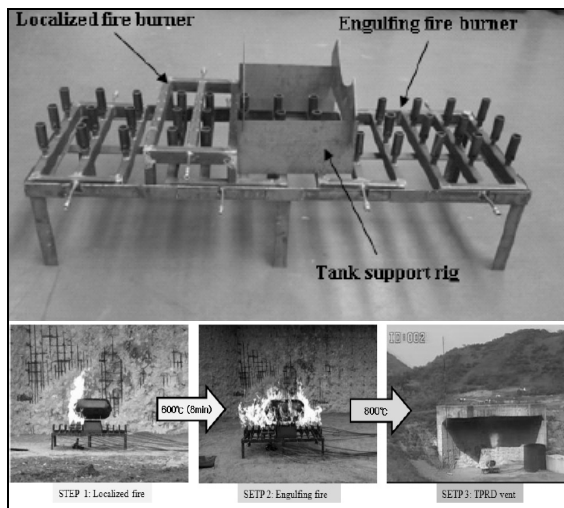


Figure 11. GTR/SGS-hydrogen storage fire test equipment and the test scene

Furthermore, KATRI paid attention to the combustion process and flame temperature control of GTR/SGS-test procedure for hydrogen tank in fire for the amendment of fire resistance test procedure of KMVSS traction battery as fire resistance test in outside was difficult on conditions according to the draft of ECE R-100.

As a result, it was possible to keep 800~1100 °C of flame temperature control as being able to regulate LPG and air content, be less influenced by wind as LPG was injected by a nozzle, and immediately extinguish the fire by fuel cut-off valve. Also, the speed of evaporation and difference of thermal distribution did not occur.

Draft Amendment of KMVSS Test Procedure

KATRI reflected flame temperature control of GTR/SGS-test procedure for hydrogen tank in fire to draft amendment of KMVSS test procedure and developed the test equipment verifying the measurement of temperature distribution and operational problems.

1. Test procedures

(a) The traction battery shall be placed on the test equipment. The traction battery shall be horizontal.

(b) The number of temperature sensors shall be at least 5. The sensor locations shall be representative locations which cover the whole area of traction battery. The sensor shall be placed 25 ± 10 mm downward from the bottom of traction battery.

(c) Whole bottom area of traction battery shall be uniformly heated by flames.

(d) Temperature shall reach 800 °C within 30 sec from ignition. Flames with temperature of 800 °C shall be maintained for 2 minutes, after that fuel supply shall be stopped. After 2 hours from the stop of fuel supply, the test shall be terminated. The temperature of flames shall not exceed 1100 °C.

(e) Check the explosion of traction battery during the test.

2. Development of the test equipment

The dimension of the flame part for fire resistance test equipment was manufactured 2m x 2m in order that pack unit test for a large size of EV traction battery should be possible.

In addition, fire resistance test equipment was structurally possible to move into the flame part after the preparation of a test specimen so that the installation of a test specimen was easy and the interval of nozzles supplying LPG and air simultaneously was placed densely so that temperature should reach over 800 °C sufficiently. Moreover, detachable windbreak was installed to minimize wind effects and it was possible to extinguish the fire from control station by remote ignition and a cut off of fuel supply. Figure 12 represents the developed fire resistance test equipment.



Figure 12. Fire resistance test equipment according to the draft amendment of KMVSS test procedure

3. Test result

After manufacturing fire resistance test equipment, K-type thermocouple (1.5mm) was installed on five measurement points which could represent the whole dimension of a test specimen at the position of 25 mm from the bottom of a test specimen for mock-up fire resistance test.

Mock-up DUT was moved into the flame part and then, the temperature of all five points reached 800 °C, which is the lowest limit of flame temperature, within 14 sec from supply of LPG and ignition and flames with temperature of 800 °C was maintained, satisfying the test conditions. The overall average temperature recorded 914°C and the maximum flame temperature was 1052°C until the stop of fuel supply.



Figure 13. Test Configurations

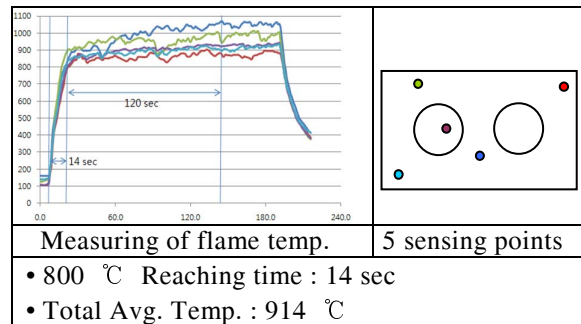


Figure 14. result of each points measuring flame temperatures

4. Review

Consequently, problems of the current KMVSS fire resistance test procedure, such as placement of large traction battery for EV and adjustment of a flame temperature, were completely resolved through the draft amendment of KMVSS fire resistance test procedure. And the developed test equipment satisfied the test conditions in regard to the draft amendment of test procedure.

CONCLUSIONS

The current procedure of KMVSS fire resistance test is appropriate for a small scale of HEV traction battery when a flame temperature control is adjusted and a test specimen is placed on the test equipment. However, a problem comes up when EV traction battery is tested, because it is so large and heavy that a test specimen is hard to be placed on the test equipment. Also, a flame temperature is difficult to adjust because top of the burner is open.

Consequently, KATRI recognized the need of the revision on the current test procedure and examined the validity of the application of ECE R-100 fire resistance test draft and GTR/HFCV-SGS Hydrogen Storage Fire Test procedure.

As examined previously, ECE R-100 fire resistance test procedure is very complicated compared to KMVSS.

KATRI carried out test according to draft of ECE R-100 fire resistance test procedure in outside and recognized difficulty to test by the draft. Despite of the weak wind, temperature curve could not be easily stabilized. Even though initial wind speed was lower than draft limitation, heat generated by flame caused turbulence due to the evaporation rate and difference of thermal distribution. However, reasonable flame temperature was acquired about 700 °C at the bottom of DUT in this test.

If ECE R-100 draft was adopted, then KATRI and vehicle or battery manufacturer have to construct an explosion proof indoor test facility including a large ventilation, emission and waste water disposal facility with an enormous expense.

KATRI performed test to hydrogen storage tank of hydrogen fuel cell vehicle being developed through “Research on the development of safety-Assessment Procedures for HFCV”

KATRI reflected flame temperature condition of GTR/SGS-test procedure for hydrogen tank in fire to the draft amendment of KMVSS test procedure. Major contents are heating temperature condition (800 °C ~ 1100 °C), number of measuring point (at least 5) and DUT setting method. This heating temperature condition is more severe than ECE R-100 draft. And KATRI developed the test equipment through verifying conditions of flame temperature.

Consequently, problems of the current KMVSS fire resistance test procedure, such as placement of large traction battery for EV and adjustment of a flame temperature, were completely resolved through the draft amendment of KMVSS fire resistance test procedure. And the developed test equipment satisfied the test conditions in regard to the draft amendment of test procedure.

Lastly, KATRI proposes the test procedure according to Draft amendment of KMVSS which is simple, effective and economically viable while achieving the purpose of fire resistance test.

ACKNOWLEDGEMENT

This research was supported by a grant(07-Transport Sytem-Future-02) from “Transport System Innovation Program”, “Monitoring Program of Electric Vehicles” and “World Harmonization Program for Motor Vehicle Safety Standard” funded by the Ministry of Land, Transport and Maritime Affairs, Republic of Korea.

REFERENCES

- [1] KMVSS. 2009. “Traction battery.” Article No. 18-3
- [2] KMVSS Test Procedure. 2009. “Traction battery safety test.” Annex 1- Part No 48
- [3] UN/ECE/TRANS/WP.29/GRSP/RESS. 2012. “Battery electric vehicle safety.” Draft of Regulation No.100, 45-49
- [4] ECE/TRANS/505/Rev.1/Add.33/Rev.2. 2012, “Uniform provisions concerning the approval of vehicles.” ECE Regulation No.34, 29-34
- [5] UN/ECE/TRANS/WP.29/AC.3/SGS. 2011. “Hydrogen Fueled Vehicle.” Draft of Global technical regulation No. xx, 82-86
- [6] Sang-Hyun KIM, 2011, “Hydrogen Storage System of Fuel Cell Vehicle(I).” Trans. of the Korean Hydrogen and New Energy Society, 2011, Vol. 22, No. 4, 520-526

OPTIMIZING VEHICLE STRUCTURE ARCHITECTURES FOR LIGHT TRUCKS

Eduardo del Pozo de Dios

Applus IDIADA

Spain

Juan José Alba

University of Zaragoza

Spain

Oscar Cisneros

Centro Zaragoza

Spain

Massimiliano Avalor

Alessandro Scattina

Politecnico di Torino

Italy

Aritz Esnaola

Mondrauto

Spain

Giorgio Pochettino

Italdesign-Giugiaro

Italy

Paper Number 13-0363

ABSTRACT

Electric Vehicles (EVs) have experienced an incredible fast evolution. In the last few years almost every car manufacturer has presented its own EV prototype or fully functional vehicle and developing dedicated vehicles instead of the classical “General Purpose” concept is becoming more common. Most Electric Light Trucks existing already in the market still adopt the classic powertrain lay-out used in thermal engine vehicles. The EC co-funded OPTIBODY project is developing new modular structure architecture for a European L7e category vehicle focused on safety improvement and exploring the capabilities of modularity applied to safety and reparability.

The OPTIBODY vehicle has been designed using a modular structure architecture composed of a chassis, a cabin and several add-ons. The cabin will provide improved levels of comfort, protection and ergonomics to the user and the add-ons will provide protection in case of frontal, side and rear impact, including also crash compatibility and interaction with vulnerable road users.

Europe, U.S.A., Canada, Japan and Australia were targeted for the initial analysis of the electric light vehicle worldwide situation to achieve the objectives of the project. The current light trucks fleet, accidentology and the requirements to be fulfilled by the vehicles were analyzed in the

previous regions. The chassis, the cabin and the add-ons have been designed using new light materials and a modular concept to improve self and partner protection safety. The thermal engine has been removed and substituted by electrical in-wheels engines, and the extra space has been used to improve frontal impact and vulnerable road users protection.

The requirements for certification of both L7e and low-speed vehicle categories in Europe and North America are very low in terms of safety and there is no mandatory crash test to evaluate neither pedestrian protection nor impact performance. OPTIBODY project has proposed frontal, side, rear and pedestrian impact tests and they have been used as targets to design the OPTIBODY vehicle to improve self and partner protection. Frontal crash test simulations showed an improvement in the cabin integrity and self and partner protection, as well as an improved pedestrian protection due to the extra space available, the use of new materials and the design of the add-on. The OPTIBODY vehicle adhered to the US commitment of Part 581 Zone, improving the crash compatibility of the vehicle. The use of modular architectures and new materials also improved the reparability of the vehicle.

The OPTIBODY project is developing a new modular architecture for L7e vehicles that will provide an improvement in self and partner protection and reparability. Modularity has been

only considered in this vehicle category and its applicability to other categories should be considered. L7e vehicles in Europe and low speed vehicles in the US have very poor safety requirements for certification. The OPTIBODY project is a good opportunity so show a great improvement in self and partner protection for L7e vehicles and also to explore how electric vehicles can improve the current levels of safety and the benefits of applying modularity to safety and reparability fields.

INTRODUCTION

Electric Vehicles have experienced an incredible fast evolution during the last years and almost every car manufacturer has presented its own prototype. Some of these manufacturers even have fully functional vehicles on the roads, showing the increasing importance that electric vehicles have in the automotive industry.

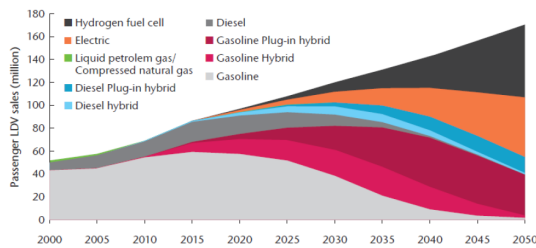


Figure 1. Prediction of annual light duty vehicle sales, according to its technology (International Energy Agency).

Last trends in electric vehicles design show the increasing importance of dedicated vehicles instead of the classic general purpose concept so manufacturers are developing specific vehicles for urban logistics, urban mobility, etc. The current status of the technology impose very light vehicles to optimize energy consumption, so most of the full electric vehicles that we are and we will see on the roads in the near future will still run in urban areas and, in consequence at low-to-medium speed in short range displacements.

For all these reasons, the European Commission co-funded OPTIBODY project (Optimized Structural components and add-ons to improve passive safety in new Electric Light Trucks and Vans –ELTVs-) project is focused in ELTVs that are worldwide homologated as N1 and N2 vehicles and, in Europe, also include the L7e category (Directive 2002/24CE).

Most of the existing ELTVs adopt the powertrain lay-out used in classic internal combustion engine vehicles. Very conservative solutions and technologies are used in their development, mainly because it is done by small and medium sized companies. However, bigger companies are already introducing new solutions in the design of this type of vehicles, such as the implementation of in-wheel motors. In this particular solution the internal combustion engine is replaced by at least two electric motors located in the hub of the wheels. This new design provides a considerable amount of space in the former location of the engine. This space is no longer necessary to accommodate awkwardly-shaped mechanical components.

Introducing these changes in the frontal part of the vehicle, the engineers can concentrate their efforts towards improving the performance and safety when the new frontal part of the vehicle is being designed. Simplifying the vehicles enables engineering teams to perform changes that were considered impossible in the past. These changes include eliminating the entire engine block, reducing the weight, totally flat floor design, chassis design focused on passengers' safety and frontal design focused in vulnerable road users' safety. All these modifications, as well as the possibility of implementing specific systems and add-ons will increase the vehicle passive safety of ELTVs and, more in general, of electric vehicles.

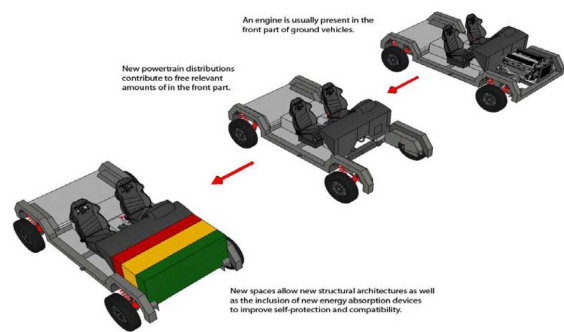


Figure 2. Evolution of vehicle fronts (from classic cars to EVs) and the resulting possibility to use the front for the installation of new safety components

The OPTIBODY vehicle is based on a new structural concept for ELTVs composed of a chassis, a cabin and a number of specific add-ons. The chassis will act as a key structural supporting element for any other components in the vehicle. The cabin will improve current levels of EVs'

comfort, occupant protection and ergonomics. Finally, a number of add-ons will bring specific self-protection in case of front, rear and side impacts, as well as in case of rollover. Additionally, these add-ons will also provide partner protection in case of interaction with other vehicles (crash compatibility) or vulnerable road users (such as pedestrians, cyclists and motorcyclists).

The main objective of the OPTIBODY project is to improve the passive safety of vehicles under the European category L7e. Additionally, theoretical concepts will be shaped as a pilot demonstrator. In order to achieve the main goal of the project, the OPTIBODY concept needs to reach the following specific objectives:

- Enhance vehicle's passive safety
- Enhance crash compatibility
- Optimize the reparability in small crashes
- Optimize ergonomics and space distribution for passengers and main components accessibility
- Improve maintainability

In addition, to these objectives, the OPTIBODY project will also propose the establishment of some requirements for impact-safe ELTV's and will study the applicability of the project results such as the modularity to other vehicle categories, such as N1, N2, M1, M2, etc.

Vehicle included in the OPTIBODY vehicle category (L7e in Europe and Low Speed Vehicles in the U.S.) have very high fatality ratios when crashing with other vehicle categories due to their typically light design and much less restrictive regulations than the existing for passenger cars. The improvement of the passive safety requirements for self and partner protection of this vehicle category is, therefore, the main goal of the project. Some of the structural modifications will include removing the thermal engine to incorporate new load paths and energy absorbing add-ons in vehicle's frontal end. The FP6 project APROSYS already studied the enhancement of pedestrians, cyclists and infrastructure protection based on different add-ons. The OPTIBODY project will implement these add-ons in a much less restrictive concept of modular vehicle than the classic vehicle concept provided with thermal engines.

In order to optimize the damaged parts reparation or substitution cost, reparability will be introduced as a key factor in the design of the different add-ons. Ergonomics and accessibility will be also considered as key factors in the design of the vehicle. Finally, some technical requirements for an "OPTIBODY" quality marking will be determined.

The OPTIBODY concept will aim to improve and provide innovative solutions for three main areas:

1. Pedestrian protection, using the former thermal engine space available to incorporate new optimized front parts.
2. Crashworthiness and compatibility. Self-protection and partner protection can be improved by developing optimized crash energy absorbing add-ons.
3. Reparability. As a modular concept, OPTIBODY will take an extra advantage of reduction of architectural constraints and will make reparability and maintenance procedures easier and more cost efficient.

In the automotive industry, for conventional vehicles as well as for electric vehicles, "crashworthiness" is a measure of the vehicle's structural ability to plastically deform and still maintain a sufficient survival space for its occupants in crashes involving reasonable deceleration load. "Compatibility" is a term that refers to the "quality" of structural interaction in collisions, and this "quality" depends on several factors that are common to all kind of vehicles and means the good performance of traffic participants among each other in the event of an accident.

This paper describes the methodology that is currently been used in the OPTIBODY project and the preliminary results from the analysis of the ELTV regulations in the major geographical areas, the analysis of accidents involving ELTVs and the ongoing work that is been currently carrying out for the chassis, cabin and add-ons design.

VEHICLE DEFINITION

The quadricycles are the vehicles included in the European vehicle category L7e, also referred to as 'Heavy quadricycles'. They are defined by Framework Directive 2002/24/EC as motor vehicles with four wheels "other than those referred to (as light quadricycles), whose unladen mass is not more than 400 kg (category L7e) (550 kg for vehicles intended for carrying goods), not including the mass of batteries in the case of

electric vehicles, and whose maximum net engine power does not exceed 15 kW.” Vehicles included in this category shall be considered to be motor tricycles and shall fulfill the technical requirements applicable to motor tricycles of the European category L5e unless specified differently in any of the separate Directives.

The OPTIBODY vehicle is intended to be a urban vehicle for carrying goods. In this case, as being design to be equipped with exchangeable superstructures, the total mass of these superstructures shall not be taken into account for the calculation of the unladen mass and shall be considered to be part of the payload. The basic type of vehicle (chassis cab), on which the above mentioned superstructures are designed to be fitted, shall fulfil all the prescriptions established for category L7e quadricycles for transportation of goods. The superstructure is considered to be exchangeable if it can be easily removed from the chassis cab without the use of tools and the manufacturer shall provide in the information document: the maximum permitted dimensions, the mass, the limits for the position of the centre of gravity and a drawing with the position of fixing devices. In table 1 the European Directives that regulate the L7e vehicle category are listed.

The L7e vehicles in Europe are limited to an unladen mass of 550 kg without batteries and a maximum payload mass (Payload = maximum technically permissible mass - mass in running order - 75 kg driver) of 1000 kg. The mass in running order is not limited. The dimensions are limited to a length equal or less than 4.0 m, a width equal or less than 2.0 m and a height equal or less than 2.5 m.

The maximum speed for this category of vehicle is not limited and the approval test is optional. A declared value from the manufacturer is accepted. The maximum net power is limited to 15 kW. No official verification test is required but a statement from the motor manufacturer according to standard IEC 60034-1 must be provided.

Table1.European Directives for L7e vehicle category

DIRECTIVE	TOPIC
2002/24*1137/2008	Whole vehicle type
93/14*2006/27/EC	Braking
93/30/EEC	Fitting of audible warning device
93/33*1999/23/EC	Protective devices intended to prevent the unauthorized use of the vehicle
93/93*2004/86/EC	Masses and dimensions
95/1/I*2006/27/EC	Maximum speed
95/1/II*2002/41/EC	Maximum power and torque
97/24/1/III*2006/27/EC	Fitting of tyres
97/24/3*2006/27/EC	External projections
97/24/4*2006/27/EC	Installation of rear-view mirrors
97/24/EC Chapter 8	Electromagnetic compatibility
97/24/10/EC	Coupling devices
97/24/11*2006/27/EC	Safety belts and anchorages
97/24/12*2006/27/EC	Glazing, windscreen wipers, windscreen
2000/7/EC	Speedometer
2009/62/EC (former 93/94*1999/26/EC)	Space for the mounting of the rear registration plate
2009/67/EC (former 93/92*2000/73/EC)	Installation of lighting and light-signalling devices
2009/80/EC (former 93/29*2000/74/EC)	Identification of controls, tell-tales and indicators
2009/139/EC (former 93/34*2006/27/EC)	Statutory markings

The passive safety requirements for a bodied quadricycle are limited to three-point seatbelts for all seats with some requirements concerning the location of the effective anchorage points to the H point. A resistance test on the vehicle structure consisting in applying simultaneously 675 kg in the upper and lower seatbelt sections of the seats of the same row and verifying the resistance of the structure is required. No requirements of the performance of the vehicle in a crash are established.

In the United States, the vehicles fitting in the European L7e category are considered as Low Speed Vehicles (LSV) and are regulated under the safety standard FMVSS 500.

Low-speed vehicle (LSV) means a motor vehicle that is 4-wheeled, whose speed attainable in 1.6 km (1 mile) is more than 32 kilometers per hour (20 miles per hour) and not more than 40 kilometers per hour (25 miles per hour) on a paved level surface, and whose gross vehicle weight rating (GVWR) is less than 1,361 kilograms (3,000 pounds). In this case the maximum speed is limited as well as the maximum permissible weight.

In terms of passive safety, the vehicle equipment required by the FMVSS500 standard is a Type 1 (lap belt) or Type 2 (Lap and harness belt) seat belt assembly conforming to Sec. 571.209, Federal Motor Vehicle Safety Standard No. 209.

Requirements for Low speed vehicles in Canada are similar to the ones existing in the U.S. The safety standard, by which these vehicles are assessed, is the CMVSS500 on low-speed vehicles. The main differences of the CMVSS500 with respect to the US Standard are that Low Speed Vehicles in Canada do not use fuel as an on-board source of energy, are required to fit a Slow Moving vehicle emblem and that some Canadian provinces may not allow Low-speed vehicle registration, and some others may impose additional requirements to the ones set forth in the CMVSS500.

In Australia there is no vehicle category equivalent to the European L7e quadricycles. A goods vehicle with a "Gross Vehicle Mass" not exceeding 3.5 tonnes is deemed as a Light Goods Vehicle (NA). The vehicle could be classified as sub-category NA1 (Light Goods Vehicles not exceeding 2.7 tonnes). The passive safety requirements in this case are more restrictive than in the US and Europe.

In Japan there is no vehicle category equivalent to the European L7e quadricycles either. A vehicle within the dimensional limits of Length 3.4m x Width 1.48m x Height 2.0m and with a displacement of 660cc or less if the vehicle has internal combustion engine is considered a mini-sized motor vehicle. For electric vehicles there are no requirements regarding the motor output. Japanese vehicle manufacturers are obeying their voluntary guidelines for mini-sized EV that the motor output is not more than 47kW but there is no such obligation for EVs exported by foreign manufacturers.

ACCIDENT ANALYSIS

After reviewing the legal requirements for the construction of the OPTIBODY vehicle, the identification of the most common accident scenarios in which the L7e vehicles are involved was studied. One of the main problems when analyzing accidents involving the OPTIBODY vehicle is the lack of vehicle category harmonization when the different existing databases are considered. Depending on the database, the vehicle category is defined as "vans and lorries", "lorries under 3.5 tonnes", etc. This made very complicated to compare results from the different databases considered.

Focusing in the OPTIBODY vehicle category, there are two important issues to address: self-protection and vulnerable road user protection. Most pedestrian fatalities occur inside urban areas, where the OPTIBODY vehicle is most likely to be circulating. In EU19 the pedestrian fatalities account for 20% of the total number of fatalities and the number grows to 27% when the inside urban areas are considered. When passengers of lorries are considered, the number of fatalities is considerably lower, between 3% and 4% in the last decade. It is important to remark that the percentage of lorries and pedestrian fatalities inside urban areas in EU 19 has grown up in spite of the number of fatalities has decrease in these years. In the "lorries under 3.5 tonnes" the inside urban areas fatalities account for 15% of the total number of fatalities.

Good transport vehicles under 3.5 tonnes accidents in 2009 were analyzed and a total of 12958 incidents with at least one of these vehicles were found causing 139 fatalities. 24.53% of these fatalities were pedestrians, 10.06% were drivers of the vehicle and 5.66% were passengers. When injuries are considered, 17.96% were drivers, 7.28% were passengers and 5.45% were pedestrians, highlighting that the pedestrian accidents are much more severe and more fatalities are associated to this type of accident. For the vehicle occupants, the frontal, frontal-lateral crash and collision with obstacle (including stopped vehicle) were the scenarios with higher number of fatalities, accounting for 75% of the driver fatalities and more than 55% of the passenger fatalities. In terms of injuries they accounted for 57% of the injured drivers and 56% of the injured passengers.

A more detailed study was performed in the Italian region of Piamonte category using the "*Regione Piemonte database*" provided by the "*Istituto Italiano di Statistica*". This database was the only

one found that includes one category of vehicle, category #21, which refers to quadricycles. In 2009 and 2010, 1 person died in accidents that involved quadricycles in this region and 78 suffered injuries of different severity. In the same period of time, 17 fatalities and 1083 injured people were associated with vehicles included in the trucks category.

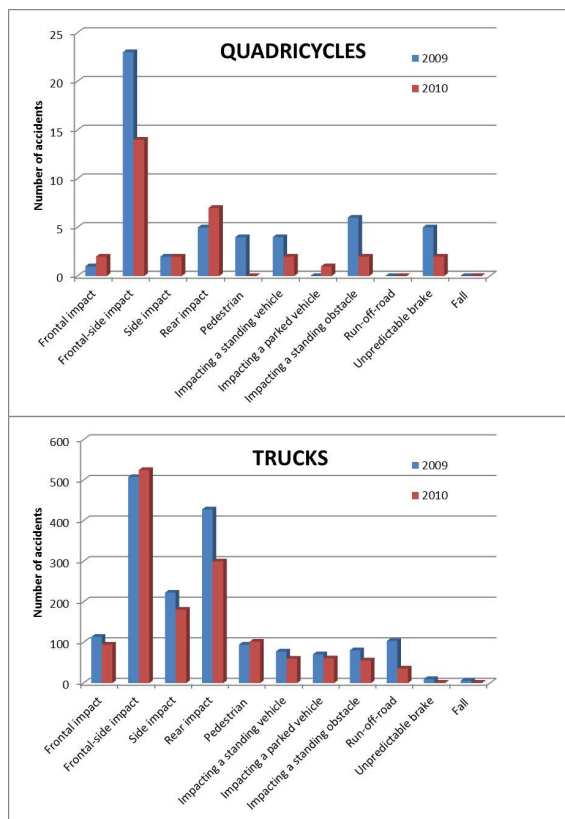


Figure 3. Total number of trucks and quadricycles accidents per type of crash in the Piemonte region

Other geographical areas

NHTSA (National Highway Traffic Safety Administration) initiated a research program to investigate the problem of aggressive vehicles in multi-vehicle crashes. The goal of this research program is to identify and characterize compatible vehicle designs with the intention that improved vehicle compatibility will result in large reductions in crash related injuries. Specifically, the objective is to identify those vehicle structural categories, vehicle models, or vehicle design characteristics which are aggressive based upon crash statistics and crash test data. LTV-to-car collisions are one specific, but growing, aspect of this larger problem. The

magnitude of this problem then is not only due to the aggressivity of LTVs in crashes, but also the result of the dramatic growth in the LTV fraction of the U.S. fleet.

In two-vehicle crashes involving a Passenger Car and a LTV, particularly in head-on collisions, 3.6 times as many passenger car occupants were killed as LTV occupants. When LTVs were struck in the side by a passenger car, 1.6 times as many LTV occupants were killed as passenger car occupants. On the other hand, when passenger cars were struck in the side by LTVs they were killed 18 times more than LTV occupants.

The damaged body parts in crashes involving cars and LTVs were also analyzed. The most damaged body regions were the head (25% for cars and 23% for LTVs) and upper extremities (20% and 22%). For the lower extremity, the percentage of injuries is higher for LTVs (20%) than cars (16%). Regarding the chest injuries are lower for LTVs (10%) than cars (14%). Adding together the three most commonly injured body regions in cars (head, upper and lower extremity), they represent 61% of the injuries whereas in the case of LTVs they represent 65% of the injuries.

Injuries in U.S. and Australia side crashes are very similar. Main damages were focused in the upper extremities (23% in U.S. and 20.3% in Australia) and head (21.8% and 24.5%). On the other hand the main differences concern to the spine and chest. U.S. injuries represented 9.7% for spine and 13.4% for chest, while, Australian percentages changes to 14.7% and 7.3%, respectively.

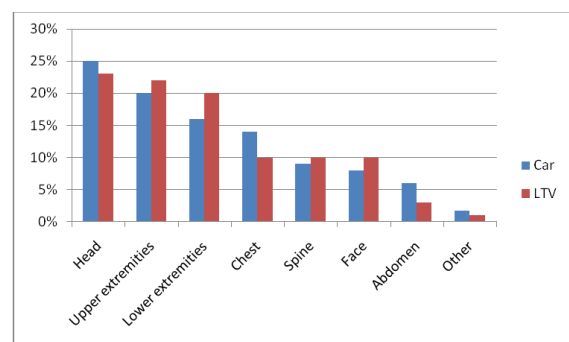


Figure 4. Total number of trucks and quadricycles accidents per type of crash in the Piemonte region

DESIGN OF THE VEHICLE

Currently, the OPTIBODY project is focused in the design of the chassis, cabin and add-ons of the vehicle, as well as the identification and selection of the energy storage and the powertrain. Regarding the powertrain, two in-wheel motors with a maximum power of 15 kW were considered. The battery pack will be placed on the rear axle, on the vehicle structure behind the cabin.

Design of the chassis

The design of the structure includes selecting the materials and also establishing the crash targets that the structure must fulfill based on the regulatory and accident analysis. Different structural architectures are being considered as well as different materials (High strength steel, aluminum, composites, etc.). For the materials selection, aspects like the Greenhouse Gas (GHG) Emissions for production are also considered in addition to the classic selection criteria as weight, strength, etc.

In order to fulfill all the design requirements, the frame of the vehicle was thought in a very simple way made of two main rails and a series of transverse beams welded to them (Figure 5). All these parts are made with aluminum extruded profiles; this solution allows reducing the weight and containing the costs, compared to, respectively, a common steel solution and a normal production aluminum car body. The frame is divided in two main parts. The rear one, aimed at the transportation of goods and, under the floor, the battery housing. The front part is aimed at carrying the cabin, the powertrain devices and to manage the energy in the case of impact. The two parts are joined together by bolts: this solution improve the modularity of the vehicle, because it is possible to exchange the front cabin part with different rear equipment. In the rear part a series of crash boxes and a longitudinal crash beam are fixed to the main rails in order to improve the safety and to protect the batteries in case of side impact. For these two components high strength steels is adopted to improve the energy absorption. Also the cabin is a wireframe structure made of aluminum extruded profiles joined by welding. The cabin is welded on the front structure. To manage the energy during impact, the front part is divided in two main portions. The front one, made with a stamped high strength steel crash boxes and crash beam, is aimed to absorb energy at low speed impact (16 km/h). Behind this part, the second portion is a front rail aimed to absorb energy in impact at higher speed (36 km/h). Crash box, front rail and main rail are joined together with

bolts in order to improve the reparability. Different solutions in terms of shapes and materials both for the front and side crash boxes and crash beams were taken into considerations. The final solutions are optimized to obtained the best crashworthiness behavior and consequently to maximize the energy absorption. . The same approach in terms of materials and structural behavior is being considered for the add-ons.

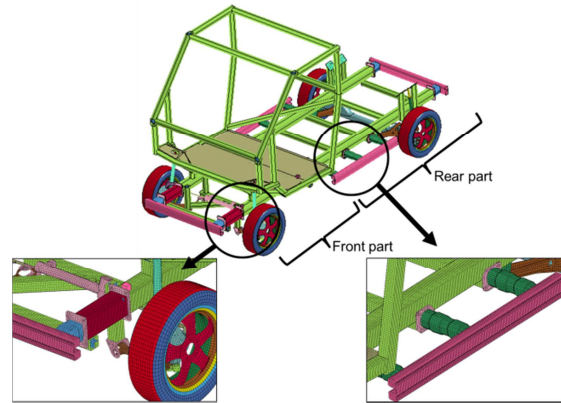


Figure 5. OPTIBODY 3D model chassis. In detail the front and side crash structures.

One of the main objectives of the project is to enhance crash compatibility in the OPTIBODY vehicle category. For that, as shown in Figure 6, the Primary Energy Absorbing Structures (PEAS) of the vehicle fulfill the option 1 specifications of the USA standard 49 CFR Part 581. These specifications require that the light truck's PEAS shall overlap at least 50% of the Part 581 zone and at least 50% of the light truck's PEAS shall overlap the Part 581 zone.

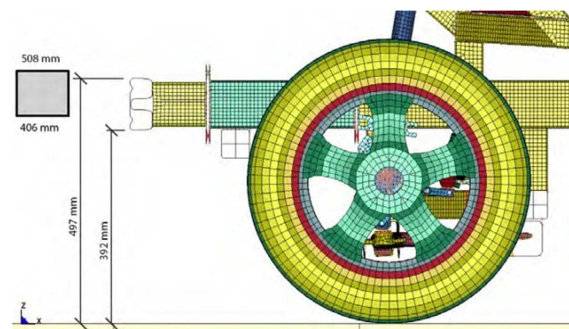


Figure 6. PEAS height compared with 49 CFR Part 581 specifications

Design of the cabin

When this work is being prepared, the design of a cabin for the OPTIBODY concept is still at a very preliminary stage. The cabin is intended to bring an ergonomic and safe space for occupants so, in case of accident, deformations of the structure and intrusion of components must be avoided.

At this moment, the work is concentrating on the protection of the cabin against rollover loads. This test is performed by applying a static load on the top of the cabin. The finite element model is already developed and first results are being used to optimize this design.

Global frontal and side crash tests will bring additional information to understand the behavior of the structure.

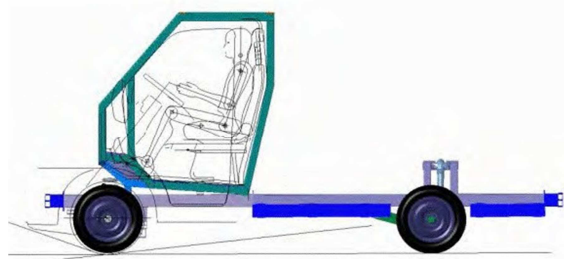


Figure 7. Driver position inside the new cabin

DESIGN OF THE ADD-ONS

Since the thermal engine is no longer needed, new space is available to accommodate the frontal add-on and other potential energy absorber devices. To design the frontal add-on for pedestrian protection, a numerical hybrid III 50th male dummy model is being used in a frontal centered impact simulation. The add-on geometry is being designed to avoid a direct impact of the head against the cabin or the windscreen.

The APROSYS European project considerations concerning the deflection of the pedestrian to one side of the road in case of a run over accident are also considered: a rounded circular shape was adopted in the contact area with the legs.

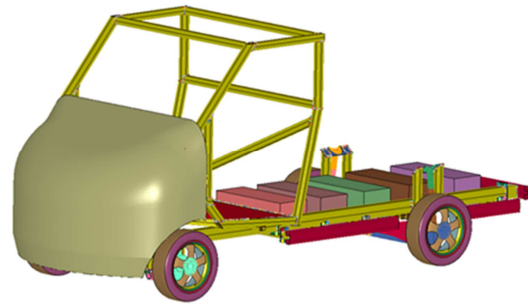


Figure 8. Frontal add-on positioned on the OPTIBODY concept.

Simultaneously, physical impact tests are being performed in order to validate the numerical simulations. These impact tests are carried out by means of simple point impactors that facilitate the analysis of the behavior of the structure during the impact. In this way, data on damaged area, impact speed or energy absorbed are available to be compared to those coming from identical simulated tests.



Figure 9. Impact test simulation for the frontal add-on.

When good numerical-experimental correlation is achieved, the process to optimize geometry and materials will start.

In the current add-on design, a configuration of a glass-fiber skin with internal foam is being used to optimize the energy absorption and the HIC15 values. The total add-on weight has been kept below 30kg

CONCLUSIONS

Most of the existing ELTVs adopt the powertrain lay-out used in classic thermal engine vehicles. OPTIBODY has been defined as a new structural concept of ELTVs composed of a chassis (the key structural supporting element), a cabin and a number of specific add-ons, which will bring specific self and partner protection in case of front, rear, side impacts and rollover.

The OPTIBODY vehicle has been defined as an Electric light trucks that have specific regulatory status in Europe as L7e quadricycles, and in USA/Canada as Low Speed Vehicles. In both Japan and Australia, these vehicles are not identified as a particular case and approval requirements are those of upper categories, and thus more demanding (including crash tests). In Europe and the North America areas no crash test is mandatory. In the US the maximum speed of the vehicle is limited while in the other geographical areas no restriction on speed is established. In Europe, the only passive safety requirement is the seat belt in all seated positions and the testing of the seat belt anchorages.

The accident analysis to determine the most common accident scenarios highlighted the lack of harmonization when the category of the vehicle is codified in the databases. The Piemonte Region database in Italy was found the only one that the OPTIBODY consortium could access with the quadricycle vehicle category registered. The small number of fatalities and injuries in accidents involving this category of vehicles in this particular region might be due to: safety measurements integrated in the vehicles, small mass, low speed, and the fact that they mostly circulate in urban areas and/or that the number of vehicles in this category is very small. Frontal-side impact (frontal with offset) and rear impact are by far the most frequent types of accidents. However, frontal impact and pedestrian accidents are much more severe causing more casualties and injuries than the other types of prevailing accidents. The number truck accidents and the number of fatalities associated with those accidents are significantly higher than for quadricycles. Especial effort need to be done to reduce the number of pedestrian accidents in both quadricycle and truck cases. These numbers are in line with the European road accident statistics, where a total of 155 of the deaths related with vans and lorries under 3.5 tones occurred in urban areas. Accidents in urban areas represent a high number of deaths and they require especial attention due to the urban use that the OPTIBODY vehicle will have.

The chassis of the vehicle has been designed using aluminum as base material for the main frame of OPTIBODY. The frame was divided in two different parts to enhance the modularity of the vehicle since it is possible to change the transportation of goods part of the vehicle while keeping the same cabin and frontal protection structure. The compatibility issue was found a key design concept and the vehicle Primary Energy Absorbing Structures (PEAS) have been design to meet the standard 49 CFR Part 581, that has been also considered by the FIMCAR (Frontal Impact and Compatibility Assessment Research) project in Europe.

The cabin is still under design to create a safety space for the occupants while improving the level of comfort of the vehicle. At the moment of writing this paper, efforts in the cabin safety design are focused in the rollover performance of the vehicle.

The add-ons concept that was previously considered in projects such as APROSYS has been implemented in the OPTIBODY concept. The frontal add-on is mainly focused in pedestrian protection while lateral and rear add-ons are improving safety performance optimizing the energy absorption through crash boxes made of high strength steel in lateral and side impacts.

OPTIBODY is being defined as a new modular structure concept to take benefit of the singularities of electric vehicles to fully design a new ELTV focused in the improvement of self and partner protection, reparability and modularity.

ACKNOWLEDGMENTS

The authors would like to acknowledge the European Commission that co-funded this project through the FP7 program. The authors wish to acknowledge the Partners of the OPTIBODY consortium for their contributions.

The OPTIBODY consortium comprises: University of Zaragoza, Politecnico di Torino, PIMOT, IDIADA Automotive Technology, Centro Zaragoza, AMZ, Italdesign - Giugiaro, BELLA, SSAB and Mondragón Automoción.

REFERENCES

- [1] Transport Safety Council, CARE: Community Road Accident Database
http://ec.europa.eu/transport/road_safety/specialist/statistics/care_reports_graphics/index_en.html
- [2] International Transport Safety Data & Analysis Group. Annual report 2010. www.irtad.net/
- [3] International Road Federation Global Database 2009, "World Road statistics 2002-2007"
Geneva
- [4] NHTSA. Traffic Safety Facts 2007: a compilation of motor Vehicle Crash Data from the Fatality Analysis Reporting System and the General Estimates System
- [5] The Aggressivity of Light Trucks and Vans in Traffic Crashes, Hampton C. Gabler and William T. Hollowell, SAE International, 1998. Paper: 980908
- [6] Gabler, H.C., Fitzharris, M., Scully, J., Fildes, B.N., Digges, K. and Sparke, L., "Far Side Impact Injury Risk for Belted Occupants in Australia and the United States", Proceedings of the Nineteenth International Conference on Enhanced Safety of Vehicles, Paper No. 05-0420, Washington, DC. 2005
- [7] Scarboro, M., Rudd, R., Sochor, M., "Near-Side Occupants in Low Delta-V Side -Impact Crashes: Analysis of Injury and Vehicle Damage Patterns". Enhanced Safety Vehicles 07-0225. Lyon, France: National Highway Traffic Safety Administration; 2007.
- [8] IATSS, Road Accidents Statistics, Japan 2007

EFFECTS OF LOW NOISE EMISSIONS OF ELECTRICAL VEHICLES FOR PEDESTRIAN ACCIDENT RISKS

Heiko Johannsen

Gerd Müller

Verein für Fahrzeugsicherheit Berlin e.V.

Germany

Paper Number 13-0394

ABSTRACT

Following the political discussion of global warming and the political objective to support green mobility, in particular electric mobility, there is a substantial discussion whether or not electrical vehicles are dangerous for pedestrians based on their low noise level. This paper aims at answering the question regarding the specific injury risk resulting from electrical vehicles.

The study is based on two pillars. On the one hand there is the analysis of published accident data regarding the impact velocity dependent injury risk of pedestrians. On the other hand noise emissions of the same car with electrical propulsion system, gasoline propulsion system and diesel propulsion system in constant speed and acceleration are acquired.

Car noise emissions are caused by the propulsion system but also by the tyres and aerodynamic effects. The study shows that significant differences in noise emissions only exist in high acceleration phases and low speed conditions. Based on the accident data analysis both situations do not appear to be important with respect to severe injuries (low speed) and accident risk (high acceleration). In total it is estimated that the number of killed or seriously injured pedestrians will not change with the largely introduction of electrical vehicles. Accidents that are felt not to be dangerous may occur more often with silent propulsion systems.

INTRODUCTION

Based on the discussion regarding global warming a solution for road transport currently discussed worldwide is the use of electrical vehicles. However, besides the advantage of low CO₂ emissions an important drawback is discussed. That is the potential larger risk for pedestrian accidents resulting from lower noise emissions.

In order to better understand this risk, it is important to compare the noise emissions of vehicles with different propulsion systems and to

assess possible differences taking into account the accident situation of pedestrians.

BACKGROUND

Against the background of current discussions on climate change, the widely use of electric vehicles is strongly encouraged by the political side. Thus, for example the German government has set the target that there will be 1 million electric vehicles on Germany's roads by the year 2020. This includes electric vehicles (EV) as well as hybrid electric vehicles (HV). HVs are vehicles that combine a conventional engine with an electric drive. While on the one hand electric vehicles can be sold only in very limited numbers, as their economical operation is still difficult, it is indicated that the use of these vehicles in everyday conditions results in a different problem. Due to the fact that electric motors emit almost no noise, EVs are more difficult to notice, especially for cyclists and pedestrians, compared to vehicles with an internal combustion engine (ICE). What leads on one side to a significant increase in quality of life for people who live in heavily travelled roads may mean on the other side that vehicles are not recognised early enough what might increase the accident risk for these vehicles especially with respect to pedestrian accidents and cyclists accidents. Consequently, this raises the question whether or not there is a need of an artificial noise generator for electric vehicles and hybrid vehicles in certain operating conditions.

REGULATION

To deal with the described issue of the low noise level of electric vehicles the Informal Work Group on Quiet Road Transport Vehicles (QRTV) of GRSP has worked out a recommendation for quiet vehicles in terms of road noise. The focus here is the so called Audible Vehicle Alerting System (AVAS). The system describes a device, which has to be installed on the vehicle to emit sounds to inform other road users on a moving vehicle. Basic intent of this recommendation is to pass it as a Global Technical Regulation (GTR), with the aim to find a common worldwide regulation [ECE/WP.29].

The American National Highway Safety Administration (NHTSA), made also a proposal for regulation for minimum sound levels for hybrid and electric cars. The draft is summarised in the FMVSS 141 and refers to a range of speed up to 18 miles per hour (29 km/h). At speeds above this limit, the driving noise can be regarded as predominant, so that an additional noise source is not necessary. NHTSA estimates that if this proposal were implemented there would be 2.800 fewer pedestrian and cyclists injuries over the life of each model year of hybrid cars, trucks and vans and low speed vehicles, as compared to vehicles without sound [NHTSA, 2013].

ANALYSIS OF PEDESTRIAN ACCIDENTS

The objectives of the analysis of pedestrian accidents were to define relevant test scenarios for the noise emission tests, to rate the noise emission test results with respect to accident data and to compare the performance of combustion engine cars with electrical vehicles. The analysis is mainly based on literature.

Most of the pedestrian accidents are happening inside towns, however, injury severity is considerably higher outside towns, see Figure 1.

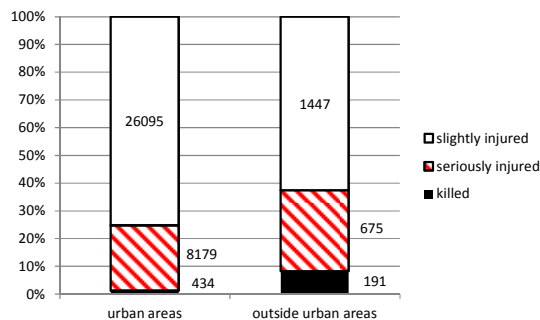


Figure 1. Pedestrian injury severity depends on accident location, German national accident data 2011 [DESTATIS, 2012].

Most of the accidents are happening in situations, where it can be expected that the car driver did not accelerate the car directly before the critical situation occurred; in 59% of the cases the accident occurred in situations outside crossings and in 4% in situations outside crossings but in curves, see Figure 2. In both situations it can be expected that the car is driving with constant speed. In the cases where the car was running straight ahead in crossings, it is unclear whether or not the car was accelerated before the accident situation; both scenarios are possible: starting up after red light or giving priority and running with constant speed. In the 10% of the cases where the car turned before the accident, acceleration of the car can be considered as being likely.

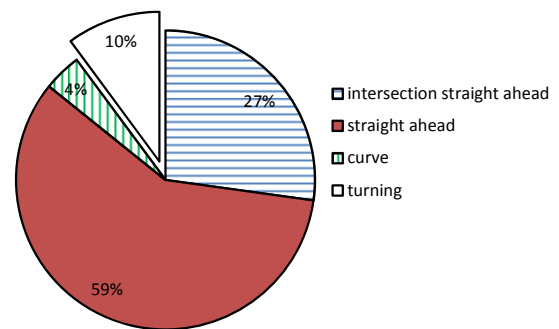


Figure 2. Locations of pedestrian accidents in the road network according to GIDAS 1999 - 2005 [Otte, 2007].

When analysing MAIS 3+ accidents, there are less accidents after the car turns and more in intersections with the car going ahead, Figure 3.

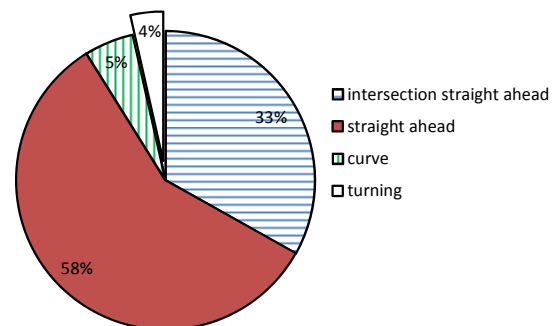


Figure 3. Locations of pedestrian accidents (MAIS 3+) in the road network according to GIDAS 1999 - 2005 [Otte, 2007].

The data is confirmed by UK data (STATS19 from 1997 – 2001) showing 74.4% of the pedestrian accidents happening in areas without pedestrian crossing facilities, and approx. 78% of the vehicles were moving straight ahead while approx. 20% of the vehicles were turning, reversing, starting up, stopping, parking etc. [Parker, 2005].

Based on typical accident situations observed in the accident data base of the German insurance organisations GDV Niewöhner et al. [Niewöhner, 2011] defined scenarios for testing of pedestrian detection systems, see Figure 4.

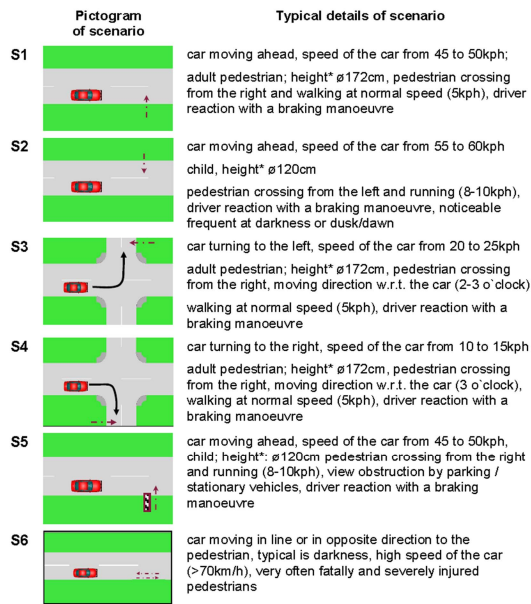


Figure 4. Scenarios for testing of pedestrian detection systems based on GDV accident data [Niewöhner, 2011].

The collision speed in the GIDAS sample ranges from 0 to approx. 70 km/h, see Figure 5. However, when taking into account injury severity severe injuries occur mainly for impact speeds above 20 km/h and fatalities cannot be expected below 50 km/h, see Figure 6.

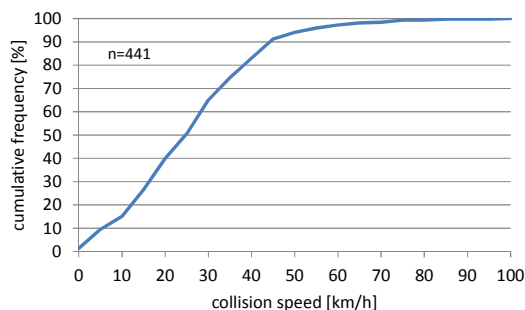


Figure 5. Collision speed, GIDAS data 1999 to 2004 [Oehler, 2005].

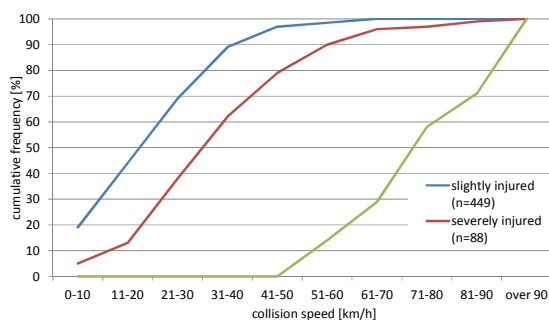


Figure 6. Injury severity depending on collision speed [Kühn, 2006].

Furthermore it needs to be considered that the collision speed is often reduced due to pre-impact braking. Driving speeds up to 20 km/h are occurring in approx. 15% of the accidents, see Figure 7.

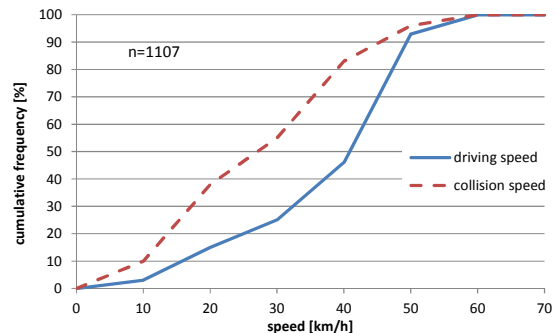


Figure 7. Driving and collision speed in pedestrian impacts [Otte, 2007].

TRL compared the risk of being involved for electrical/hybrid electrical vehicles and vehicles with internal combustion engines and concluded that the risk is equal for both propulsion types based on STATS19 data [Morgan, 2011]. However, it needs to be taken into account that for hybrid electrical vehicles it is unclear whether or not the combustion engine was running at the time of the accident. Depending on the concept of the hybrid vehicle the combustion engine is either used to propel the car directly or is just used to charge the battery. The noise emissions for both concepts are completely different.

A query concerning German national data resulted in a complete number of purely electrical vehicles being involved in any accident of 29 for 2011. Therefore it was concluded that further analysis of these cars would not result in reliable results.

In summary the accident analysis shows that a large number of pedestrian accidents are happening in situations in which the car is going straight, likely with constant speed. However, there are also accidents with cars that were accelerating prior the critical situation. In the majority of accidents the car had an initial speed of more than 15 km/h which is in line with the collision speed in accidents with severely or fatally injured pedestrians.

COMPARISON OF NOISE EMISSIONS OF CARS WITH DIFFERENT PROPULSION SYSTEM

Measurement of Sound Level

To measure the vehicles sound level, there exist different methods. For approval to the European market, vehicles are tested according to the regulation 70/157/EEC. Depending on the vehicle

it passes a sound-level meter in a distance of 7.5 meter in a defined operation status. The test are repeated and considered as valid if the difference of the measurements does not exceed 2 dB(A). The sound level of vehicles intended for the carriage of passengers and comprising not more than nine seats including the driver's seat there may not exceed 82 dB(A) [70/157/EEC].

Further noise measurement regulations are described in the SAE standard J/2889/1 [SAE]. The paper specifies an engineering method for measuring the minimum noise emitted by road vehicles. Here the real operating conditions of the vehicle with its background noise are respected.

Comparison of noise emissions of vehicles with different propulsion system

To investigate the real difference of noise between different power train concepts three vehicles with different drive concepts were compared. For this measurement a BMW E-Mini (EV), a diesel-powered BMW Mini and a BMW Mini with petrol engine were used. The tests were conducted in accordance with regulation 70/157/EEC (see above). A comparison of the three vehicles in terms of its technical data is shown in Table 1.

Table 1.
Properties of tested vehicles

Vehicle type, description	MINI Cooper D Clubman	MINI Cooper	MINI E
Engine	4 cylinder/ 16V	4 cylinder/ 16V	electric motor
Cubic capacity	1600 ccm	1600 ccm	(Max. speed 13000 min ⁻¹ ; isolation: Class H, double-insulated)
Nominal power/ rated speed	80 kW at 4000 min ⁻¹	88 kW at 6000 min ⁻¹	150 kW at 7000-8000 min ⁻¹
Max. torque/ number of revolutions	240 Nm at 1750-2000 min ⁻¹	160 Nm at 4250 min ⁻¹	220 Nm at 0-5000 min ⁻¹

The results of the noise measurement according to 70/157/EEC have shown that the E-Mini, with a noise level of 73 dB(A), is quieter than the diesel- and the petrol-Mini with 77 dB(A) and 84 dB(A). These values were measured in the second gear with 75% of full power, wherein E-Mini in the corresponding operating condition were used. In all three cases the measured sound levels are above the values that are specified on the registration document. The differences may be due to the fact

that the ground was wet at the time of measurement, which increases the rolling noise of tires normally.

Table 2.
Maximum pass-by noise level Mini tests

Speed [km/h] Gear	Maximum noise level, dB(A)		
	Mini diesel	Mini petrol	Mini electric
5 (1. Gear)	*	53	*
10 (1. Gear)	57	58	50
20 (2. Gear)	60	58	58
30 (2. Gear)	66	66	63
30 (3. Gear)	*	63	
50 (3. Gear)	71	70	70
50 (4. Gear)	71	*	
70 (3. Gear)	76	75	75
70 (5. Gear)	75	74	

*measurement invalid

The measurement of road noise at different speeds showed a mixed picture. At speeds below 20 km/h, the electric vehicle is clearly quieter; above this speed it is difficult to identify differences between the cars (Figure 8).

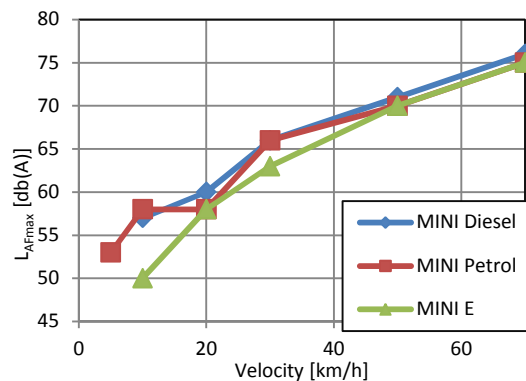


Figure 8. Sound level for different speeds.

It can be assumed that, above a speed of 20 km/h, the driving noise is dominant and noise from the engine, regardless of its type, plays only a minor role.

Thus, according to the objective measurement results of the sound recording significant differences between electric vehicles and conventional vehicles can be observed only at low speeds.

Zeitler et al. [Zeitler, 2010] analysed the distance to a pedestrian when an approaching car (driving speed 10 km/h) was audible recognised under different environmental noise levels. In summary independent of the environmental noise level the electrical car was recognised very late, above 47 dB(A) not until the car approached the position of the pedestrian, see Figure 9. The hybrid car that

was used in ICE mode was recognised later than the ICE car and the hybrid vehicle that was used in electrical mode was noisier than the electrical car but less noisy than the ICE car.

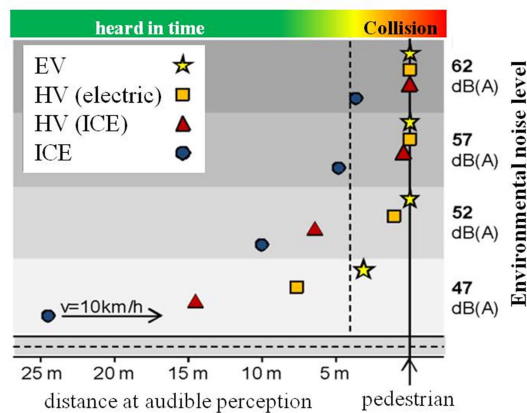


Figure 9. Distance to vehicle when detecting it [Zeitler, 2010].

Tests Conducted by TRL The tests results described below were conducted and published by [Morgan, 2011]. In this investigation two test rows were conducted. On the one hand objective noise measurements, where the noise level of different cars was recorded and on the other hand subjective noise assessments, where probands were asked about their noise perception. It is important to note, that TRL did not distinguish between EV and HE. They were combined to E/HE (electrical and hybrid electrical) vehicles.

For the measurement tests three different test were conducted: A “steady-speed pass-by test”, where a car passes the microphone with a constant speed, a “Pull-away from rest test”, where the car accelerated in front of the measurement device and a “Low-speed parking test”, where vehicles were both driven forwards and reversed out of a conventional parking space at typical speeds.

Table 3.
Maximum pass-by noise levels at microphone position M3 [Morgan, 2011]

Vehicle	Maximum noise level, dB(A)			
	7-8 km/h	20 km/h	30 km/h	50 km/h
ICE-01	57	62	69	77
ICE-02 *	65	74	75	81
ICE-03	51	62	68	77
ICE-04	58	66	73	81
E/HE-01	56	64	70	79
E/HE-02	53	63	70	77
E/HE-03	52	63	70	76
E/HE-04	56	66	72	80

*not included in the analysis below

The results of the pass-by test showed no significant differences between electric vehicles and cars with combustion engine (Table 3).

The E/HE vehicles were from 2 dB(A) quieter to 1 dB(A) louder than the ICE vehicles. On average, the E/HE vehicles were only 1 dB(A) quieter than the ICE vehicles. The quietest ICE vehicle is comparable to the quietest of the E/HE vehicles. For the E/HE vehicles, the spread is less than that for the ICE vehicles. At higher speeds, the range across all vehicles is more consistent because road noise becomes the dominant source. In Figure 10 the maximum sound level is shown where it can be seen that all vehicles have a similar trend.

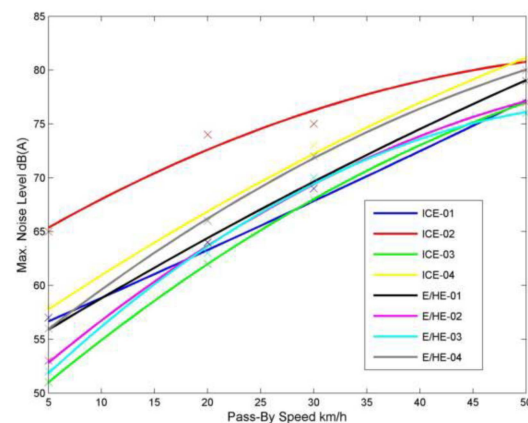


Figure 10. Maximum noise levels for steady-speed pass-by measurements [Morgan, 2011].

The results of the pull-away tests showed, that for low acceleration the electric vehicles were a bit quieter than the ICE vehicles (1 dB(A) in average) and for the higher acceleration the electric vehicles were in average 2 dB(A) quieter.

The parking manoeuvres showed that the absolute noise levels for the majority of the vehicles were not significantly above the background noise levels at the test location.

The objective measurements indicated that for lower speeds where powertrain noise is the dominant source, electric vehicles are in average 1 dB(A) quieter than ICE cars. However, it has to be noted that background noise levels at these speeds are typically only 3dB(A) below the noise level of the vehicles. That means if there is a certain problem with silent cars it possibly should be discussed for all cars and not only for electric vehicles.

The subjective tests of [Morgan, 2011] were conducted with 10 vision-impaired participants using a series of audio samples of both vehicle types (electric and ICE), which were moving at different speed and were performing different

manoeuvres, which were pass-by at 20 to 50 km/h and a vehicle manoeuvring out of parking spaces. The participant's task was to identify when they became aware of the presence of the vehicle and to find out if they were able to distinguish the vehicle type. The exercise assumed that, for the most part, the vision-impaired participant was a pedestrian standing at the kerbside, as if waiting to cross the road. The background noise was divided into two scenarios: urban area and semi-rural environment.

In the analyses of the results the risk exposure, based on the assumption that there is always some element of risk for road crossing pedestrians, was assessed. Risk exposure was deemed to be 'increased' if the presence of the vehicle was detected at a distance less than typical safe stopping distances or not detected at all. The results showed that the likelihood of increased risk exposure is 1.4 times greater in a semi-rural environment for electric vehicles than for ICE vehicles, irrespective of vehicle speed or manoeuvre, and 1.3 greater in an 'urban' environment. Irrespective of the background environment, the study indicates that the likelihood of increased risk exposure was 1.4 greater for E/HE vehicles than ICE vehicles. The risk exposure for pass-by tests increases with decreasing speed. Under steady-speed conditions, participants were more than twice as likely to correctly identify ICE vehicles as E/HE vehicles in a rural scenario and almost twice as likely to correctly identify the vehicles in an urban scenario. When the vehicles were accelerating from stationary, subjects were far more easily able to identify both vehicle types.

In summary it can be said that the objective tests of the TRL study [Morgan, 2011] confirmed the tests with the Minis. From a speed of 20 km/h or above, there is nearly no difference in terms of noise levels between ICE and electric vehicles. At lower speeds electric vehicles are quieter. The result that noise emissions are equal above 20 km/h is also confirmed by Zeitler et al. [Zeitler, 2010].

By contrast the subjective tests of the TRL study [Morgan, 2011] with vision-impaired people have shown that the risk of insufficient perceptibility of electric vehicles is higher than for ICE. This applies in principle to all performed manoeuvres.

NOISE PERCEPTION

The comparison of the noise emissions of different propulsion systems with the subjective assessment whether or not a car was recognised opens the questions for the deviation between both. In principle the following hypotheses are discussed:

- the A-weighted sound pressure level is not suitable for the evaluation of the detectability of the noise emitter,
- humans are mainly using the engine noise in order to distinguish between moving objects (cars) and stationary objects
 - o this vehicle detection strategy is trained following the experience on the road and can be adopted to future changes
 - o the strategy is a result of psycho-acoustic capabilities and cannot be adopted

It is likely that a combination of the hypothesis is causing the discrepancy.

There are three main sources for noise emissions in a car. These are the engine noise, the aerodynamic noise and the noise resulting from the wheel-to-road contact. While the first one is different in EV compared to vehicles with internal combustion engine the two latter ones are similar in both propulsion types.

Noise emissions of cars are evaluated using the A-weighted sound pressure level that represents equal noise perception across the frequencies at 40 phon, resulting in heavy filtering in the range of 10 – 100 Hz.

When analysing the frequency band from the TRL study, it is obvious that the vehicles with internal combustion engine show a peak in the loudness in the frequency range between 10 – 100 Hz, see Figure 11. These peaks are resulting from the noise of the internal combustion engine. It can be expected that E/HE-02 is a hybrid electrical vehicle with the internal combustion engine running at the time of measurement.

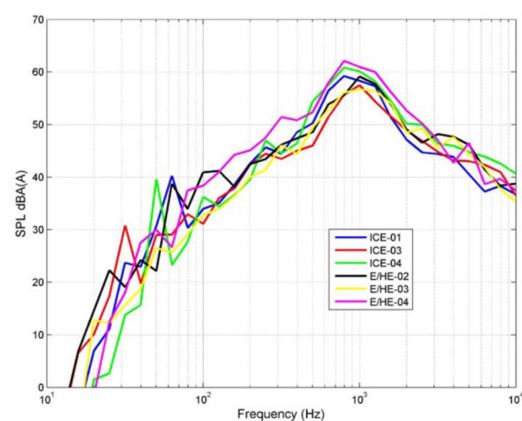


Figure 11. One third octave spectra corresponding to maximum noise level at a pass-speed of 20 km/h [Morgan, 2011].

In contrast to the statement of TRL that the differences in the spectral content do not suggest any difference how a pedestrian would be able to differentiate between vehicle types, the peaks from

the combustion engine and exhaust, although weighted in the dB(A) assessment relatively low result in an important difference in the noise perception of a vehicle. Similar results were described by Zeitler et al. [Zeitler, 2010]. It is questionable whether or not the A-weighted sound pressure levels are suitable for assessing the audible vehicle perception by pedestrians.

This analysis suggests that the engine noise is very important for the perception of the noise emitter. However, it remains questionable whether or not pedestrians can train themselves to better perceive vehicles with electric propulsion system. With respect to the aerodynamic noise it can be expected that it is impossible to distinguish between any stationary object that is passed by the wind or a car that moves through the air. Besides this the tire noise seems to be unique and can likely replace the engine noise in the vehicle perception. However, this needs to be further analysed taking into account psycho-acoustic evaluation.

DISCUSSION AND CONCLUSION

The objective noise measurements within this study and the study conducted by TRL show that the noise emission of ICE and EVs is equivalent constant speeds above 20 km/h using the A-weighted sound pressure. Below 20 km/h the ICE noise dominates the vehicle's noise emissions, this is also the case for accelerating vehicles.

Today, the noise of the combustion engine appears to be the main source for the audible detection of vehicles. The absence of the engine noise might lead to wrong assessment of the situation even for EV driving faster than 20 km/h. However, it is expected that the tire noise can replace the engine noise in the perception of cars if the latter one disappears.

The analysis of accident data showed that pedestrian accidents mainly occur in situations where the car driver is going straight ahead and where constant speed of the car can be expected. Accidents with slight or severe injuries are very seldom for vehicle driving speeds below 20 km/h. When transferring these data to the noise emission results, it is obvious that for those situations where EVs are significantly less noisy pedestrian accidents do not occur very often (vehicle is accelerating when approaching the pedestrian) or are not considered to be of high severity.

In total the pedestrian accident risk might increase with the large scale introduction of EVs, but it is not expected that the injury risk for pedestrians is increasing from that measure.

For future developments like the introducing of AVAS for electrical vehicles one needs to consider that there will be more than only one electrical vehicle driven on the road and the artificial noise may accumulate to an unacceptable level [Genuit, 2012]. To get a better understanding of vehicle noise perception further investigation is needed. Especially the need of artificial sound generators should be discussed with respect to accident data.

ACKNOWLEDGEMENTS

The noise emissions of the BMW MINIs were assessed in cooperation with BsSB GmbH Berlin – SCHALLTECHNISCHES BÜRO.

REFERENCES

- Carter, E.: "Definition of Vehicle and Pedestrian/Cyclist Impact Conditions – UK National Epidemiological Studies on Pedestrian and Cyclist Accidents", APROSYS SP3 Report, AP-SP31-001R-BASC, 2005
- DESTATIS (Statistisches Bundesamt): "Fachserie 8 Reihe 7 Verkehrsunfälle 2011", Juli 2012 (in German)
- ECE/WP.29: "Draft Recommendations for a Global Technical Regulation Regarding Audible Vehicle Alerting Systems for Quiet Road Transport Vehicles"; ECE/TRANS/WP.29/GRB/2012/6; Economic and Social Council; www.unece.org; 04.03.2012
- Genuit, K.; Fiebig, A.: „Die Relevanz der Psychoakustik für die E-Mobility“, 38. Deutsche Jahrestagung für Akustik – DAGA 2012, Darmstadt, 2012 (in German)
- Kühn, M.; Fröming, R.; Schindler, V.: "Fußgängerschutz – Unfallgeschehen, Fahrzeuggestaltung, Testverfahren" Springer Verlag, 2006 ISBN 978-3540343028
- Morgan, PA.; Morris, L.; Muirhead, M.; Walter, LK.; Martin, J.: "Assessing the perceived safety risk from quiet electric and hybrid vehicles to vision-impaired pedestrians" PUBLISHED PROJECT REPORT PPR525, TRL, 2011
- NHTSA: FMVSS 141: Minimum Sound Requirements for Hybrid and Electric Vehicles, 2012
- Niewöhner, W.; Roth, F.; Gwehenberger, J.; Gruber, C.; Kuehn, M.; Sferco, R.; Pastor, H.; Nagel, U.; Stanzel, M.: "Proposal for a Test Procedure of Assistance Systems regarding Preventive Pedestrian Protection" Proceedings to 22nd ESV Conference, Washington, 2011, paper no. 11-0393

Oehler, R.: "Epidemiology Report", APROSYS SP3 Report, AP-SP31-001R-DC, 2005

Otte, D.; Huefner, T.: "Relevance on Injury Causation of Vehicle Parts in Car to Pedestrian Impacts in different Accident Configurations of the Traffic Scenario and Aspects of Accident Avoidance and Injury Prevention" Proceedings of ESV Conference 2007, Paper no. 07-0176

SAE: "Measurement of Minimum Noise Emitted by Road Vehicles"; SAE standard; Product Code: J2889/1; Revision Number: A; Date Published: 2012-05-14

Zeitler, A.; Liebing, R.; Kerber, S.: „Sounddesign im Dienste der Wahrnehmbarkeit von leisen Fahrzeugen“; 36. Deutsche Jahrestagung für Akustik – DAGA 2010, Berlin, 2010 (in German)

70/157/EEC: Council Directive 70/157/EEC of 6 February 1970 on the approximation of the laws of the Member States relating to the permissible sound level and the exhaust system of motor vehicles

SAFETY OF LITHIUM ION BATTERIES IN VEHICLES – STATE OF THE ART, RISKS AND TRENDS

Lars Hollmotz

cpcMomentum GmbH & Co.KG

Germany

Paper Number 13-0395

ABSTRACT

The safety of lithium ion batteries in vehicles is a priority of the automotive industry. The focus of the development activities are the reduction of the risks and the improvement of the safety concepts and systems.

In the last few years some incidents and accidents have taken place; a short overview about the state of the art of lithium ion battery technology on cell and battery level with focus on safety features, the risks, the statistical relevance and occurred incidents or accidents will be given.

An overview about dangerous events (worldwide) with lithium ion batteries for vehicles will be given (for cars as well as for test facilities); this overview is limited to data that is publicly available. A statistical significance based on this data will be shown; it includes the total number of vehicles in the relevant markets and an outlook for the future. In conclusion, the absolute number of safety relevant events is low because of the low number of electric and hybrid vehicles on the market. The absolute risk is low as well. The risk of safety-related incidents per electric or hybrid vehicle is much higher. Ultimately it depends on the used trigger; if vehicle accidents are seen as the trigger for battery incidents, the risk is low.

Using a bottom-up safety assessment approach in which the estimated risks for the cell, module, and

battery are described, and the hazard levels and risk levels for their use in vehicles are determined will give an excellent overview. A description of additional and possibly future relevant safety features like changes in cell chemistry (additives, improved separators or flame retardant electrolytes) will be included. Furthermore, an assessment of these additional relevant safety features will be given. This main finding of this assessment is that the safety level of a lithium ion battery depends mainly on the cell chemistry and its capacity. The use of additives can improve the safety, but will lead to lower capacity and performance and result in higher prices. Other additional features won't have any impact regarding battery safety.

From this it is possible to define requirements for the safety of vehicles regarding: package, crash behaviour, and functional safety. The current safety level of electric and hybrid vehicles (concepts and characteristics) will be shown and discussed.

Finally information about new technology and trends for lithium batteries will be given, including information about relevant safety characteristics.

This study is limited to lithium ion batteries used in electric and hybrid vehicles.

INTRODUCTION

According to the sales numbers of hybrid electric vehicles and electric vehicles (in sum XEV's) as well as the attention given by the public, the hype of the e-mobility seems to have died down. Despite this, car manufactures continue to develop these kind of vehicles.

Lithium ion batteries are used in drive trains for these vehicles for energy storage reasons. Of the various technologies available, lithium ion technology is the preferred technology (power and energy density) despite any negative concerns regarding cost and safety.

For this reason it is necessary to know the real risk, challenges, and countermeasures to resolve any problems and to ensure safe mobility.

STATISTICAL RELEVANCE – INCIDENTS AND ACCIDENTS

In 2012, there were 42.9 million passenger vehicles recorded in Germany (according to the data of the German departure for statistics).

Currently 52,183 HEV's and EV's are in use in Germany. The market share of XEV's is 0.09% in 2011 and 0.12% in 2012 (according to all vehicles in Germany). The goal to have 1 million EV's by 2020 still stands. [1]

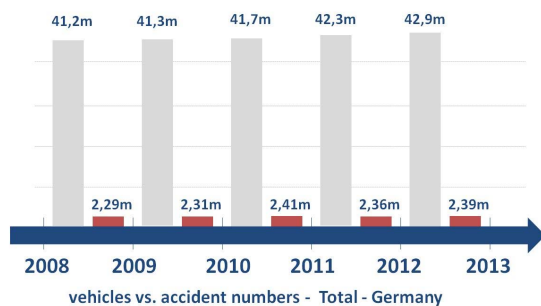


Figure 1: Vehicle numbers [1]

The expected number of accidents for cars in Germany is 2.390.000; out of this 303.000 are accidents with injuries of persons. That is of about 12,68%. [1]

From a former study done in 2011, the share of accidents involving XEV's with injured persons is about 0.05% to 0.08% (2007 to 2011) of all accidents with injuries.

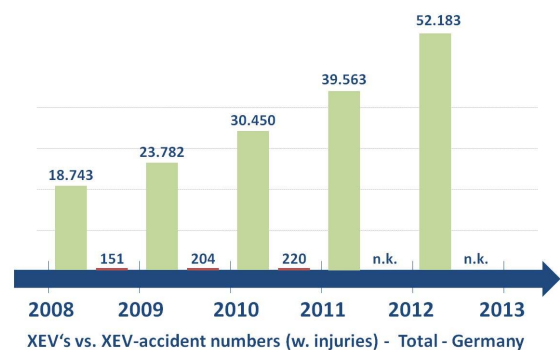


Figure 2: Accidents w/o XEV's [1]

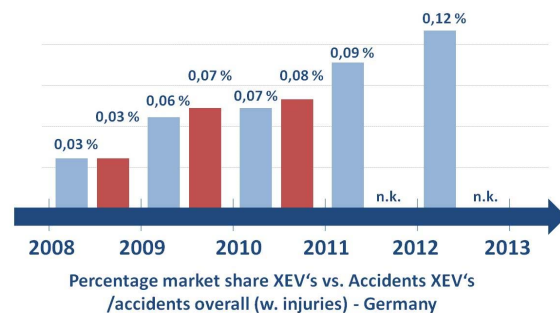


Figure 3: Accidents w/o XEV's according to market share [1]

This shows a strong, yet unsurprising correlation between the total numbers of cars and XEV's, and the accident numbers. The crash severity could seem a little bit lower due to the preferred use of XEV's in urban areas.

The overall risk for an incident due to a battery problem seems to be quite low. This is a result of the low numbers of existing vehicles.

It is important to distinguish between incidents that were the result of technical malfunctions and incidents that were a result of crashes involving vehicles.

According to several studies, the amount of technical reasons that cause accidents in Germany is below 10 % (most of which are tire defects), while accidents due to human error are over 85%.

The implication of this is that, in the case of an accident, the protection of a battery in a vehicle is of utmost importance.

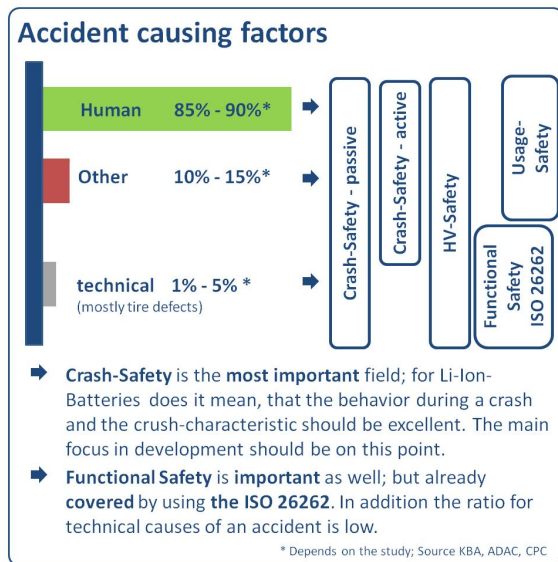


Figure 4: Accident causing factors [2]

The functional safety to avoid incidents due to technical reasons is covered by the development activities and processes of the car manufacturers. This includes different safety fields, like functional safety and the requirements outlined by ISO 26262, high voltage safety and the safety during use and during repairs or maintenance.

If we consider actual accidents involving batteries (both lithium Ion and NiMH), we find that the absolute number during transport and use didn't increase, while the number of vehicle accidents and

incidents due to battery problems is increasing. This is from the increased number of XEV's in the field, but it is not above the expected numbers from the current market share of XEV's.

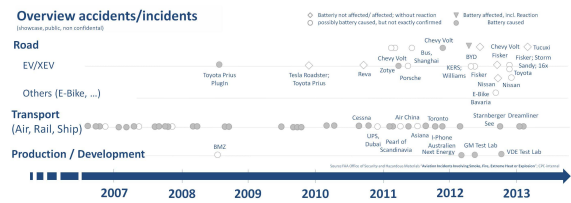


Figure 5: Accident and incidents with batteries involved (public available data only) [3]

The rate of accidents with involved battery but without any dangerous reaction of the battery is of about 25%. This shows that the implemented safety systems of the vehicle and the protection of the battery system worked very well.

In approximately 66% of the accidents the battery probably caused the event. Out of this the safety system of the battery doesn't seem to work properly; this shows that the risk can be reduced by improved safety systems as well as risk assessment processes.

This seems to be opposite to the statistic overview given above with just 1% to 5% of the accidents because of technical issues. It just shows the actual state of the art and the risks of the battery technology and gives a direction for the main focus for future developments.

Noteworthy is that the absolute number of accidents didn't increase with respect to the absolute number of battery cells produced during the past few years, or with respect to the increase in market share. Considering these statistics, it seems that the safety level of the batteries produced and quality of the batteries are not only getting better, but also that the

safety systems and requirements are working very well.

ASSESSMENT METHOD FOR THE SAFETY OF ELECTRIC AND HYBRID VEHICLES

To get an idea of the safety level of vehicles, especially vehicles with an electric power train, it is necessary to understand what the triggers for dangerous situations are as well as the reaction of the vehicle and its occupants.

For this, the methodology of the ICE 61511 is used and adopted to the vehicles. As shown in figure 5 the system is split into several (technology driven) levels; for an electric vehicle, there is the cell chemistry level, the cell level, the battery system level, and the vehicle level, as well as the environment influences by the infrastructure (safety lanes, charging stations) and the rescue and first responder level.

For each of these levels, the risks need to be evaluated. Some of the risks are mentioned below:

- electrical risk (short-cut)
- fire and explosion
- danger due to chemical reactions
- chemical risk due to toxic liquids and gases
- thermal danger due to high temperatures
- mechanical risk because of the higher weight of the battery components

Several technologies to improve the safety of the whole system can be used and are already implemented. Some of these will be discussed below.

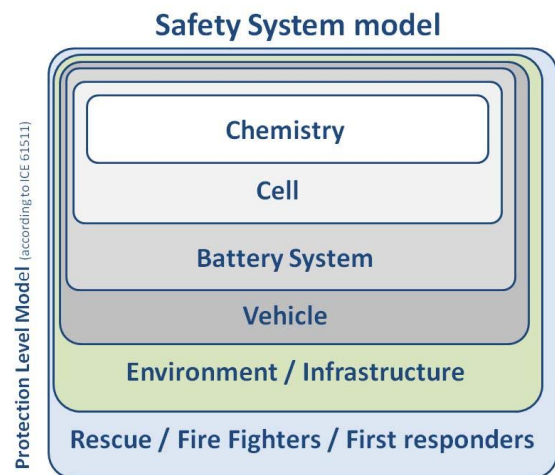


Figure 5: Safety model for XEV's with the different safety levels

On the level of the cell chemistry, it is important which kind of material is used for the cathode, the anode, the separator and the electrolyte. The combination of materials used dictates the thermal stability, the lifetime, the charging- and discharging characteristics, as well as the reaction during an external physical impact.

For the cathode, LiFePO_4 and LiMn_2O_4 are the most safe chemistries, while LiCoO_2 is known as less safe. This is based on tests regarding thermal stability. These tests simulate the reaction of the cell chemistry during an increase in temperature, and in the event of a thermal runaway. Usually heating (external and self heating) is triggered by internal or external short-circuits. The choice of the material chemistry is the basis for the overall safety of the whole system.

Another important aspect of overall safety is given by the anode chemistry used, the electrolyte and the type of the separator.

For the separator currently ceramic, semi ceramic and membranes (mostly polyethylene or polypropylene) are in use. The ceramic separator type

seems to be better out of the safety point of view because of the higher resistance according to physical and thermal influences. On the other hand it's not possible to fold it (doesn't work for cylindrical or prismatic cells with folded layers) and it shows a lower performance according to energy and power.

On the cell level, the cell form that is used is important. Common cell designs are: pouch cells, prismatic cells, and cylindrical cells. The cell form is important because the cell housing is what protects against impacts and intrusions.

The prismatic and cylindrical cells show more mechanical stability than the pouch cells. Using a pressure safety vent makes it possible to avoid a burst or explosion of the cell by reducing the internal pressure. For the pouch cells, overpressure can be reduced via defined cut lines; this helps to guide the gas flow.

For the battery system, the design of the housing is also important. The battery management system controls and checks the performance (temperature, current, voltage, isolation etc.) of the battery during the use.

Another important feature is the choice of the cooling system. In general, air cooling and liquid cooling systems are most common. However, some systems work without cooling devices. Additionally, the cooling system can be used as heating device for low temperatures areas.

The choice of the cooling system depends on the expected use (power batteries for hybrid vehicles or energy focused applications for pure electric vehicles) as well as the expected local weather and temperatures (tropical climate, arctic climate ...).

The positioning and the packaging of the battery, as well as integrated additional protection and deformation elements are part of the vehicle level. Deformation of the battery housing should always be avoided.

In the case of a deformation of the housing and the cells an explosion (because of gas leakage) or fire can take place.

An example for this explanation is the Chevy Volt incident after a crash test in 2011. Besides the handling with the battery (which was not according to the guidelines of the manufacturer; the battery should be secured after a crash and shouldn't be in the vehicle for a lot of days afterwards) the intrusion of the battery caused the following reactions like the leakage of coolant and the short circuits with the result of a vehicle fire.

Sometimes the battery housing is integrated into the vehicle structure and has to fulfill other functions. This might be a little bit concerning, especially in this case where it is crucial that the interface between vehicle and battery be designed properly.

The positioning of the battery is also important for Emergency responders. This is part of the outermost safety level according to the used methodology.

If the battery is packaged under the hood, it is relatively easy to extinguish a fire. It is much more difficult if the battery is positioned in the rear part of the vehicle or directly in the middle under the vehicle.

Lastly, it should be noted that it is necessary to provide emergency responders with information about the vehicle, the position of the emergency disconnect device, the position and type of the used

battery, as well as information about the position of the high voltage harness.

For a realistic assessment of the safety of a battery system in an electric vehicle (XEV) the risk of each system level should be figured out.

The first step involves an analysis of each parameter and the main influencing factors must be indentified.

By using the definition for risks from the ISO 26262, the final risk is the product out of severity, probability and controllability. The following values for the different factors for the levels cell chemistry, cell and battery system are adopted by ISO 26262 and are proposed in this study for the use of the assessment:

Severity:

- S0 EUCAR -Level 0-3
- S1 EUCAR -Level 4-5
- S2 EUCAR -Level 6-7
- S3 EUCAR -Level not predictable

Probability:

- E1 Very low probability ($\leq 0,001$)
- E2 Low probability ($\leq 0,01$)
- E3 Medium probability ($\leq 0,1$)
- E4 High probability (≤ 1)

Controllability:

- C0 controllable in general
- C1 Simply controllable
- C2 Normally controllable
- C3 Difficult controllable

As example an assessment for a 5kWh battery system like described below will be shown.

The system characteristics are:

- prismatic cells with safety vents and LiFePO_4 at the cathode side, hard carbon for the anode and an ceramic separator
- liquid cooling system
- BMS; controls temperature and voltage, able to balance the cells
- stabile metal housing with safety vents
- passing all tests according UN transportation requirements on cell and safety level
- production of more than 1 million cells with a failure rate in the range of $6 \square$
- used in prototype applications without any incidents or failures

The worst case scenario is S1 (it is the goal for future lithium ion systems); the probability for an incident is low (E2) and might be very low basing on the information about the history and the controllability can be assessed as C2.

The overall risk can be defined by using a matrix adapted according to the ISO 26262 matrix. An example of this is shown in figure 6.

		C1	C2	C3
S0	E1	Level 1	Level 2	Level 2
	E2	Level 2	Level 3	Level 3
	E3	Level 2	Level 3	Level 4
	E4	Level 3	Level 3	Level 4
S1	E1	Level 3	Level 3	Level 4
	E2	Level 3	Level 3	Level 4
	E3	Level 3	Level 3	Level 4
	E4	Level 3	Level 3	Level 4
S2	E1	Level 3	Level 3	Level 4
	E2	Level 4	Level 4	Level 4
	E3	Level 4	Level 4	Level 4
	E4	Level 4	Level 4	Level 4

Figure 6: Assessment matrix

The final definition of the risk leads to requirements for the sample application, wherein the battery will

be used. For example, a level 3 system needs to be positioned in a safe part of the vehicle there is no risk for intrusion. Furthermore, it might be needed to pass additional crash test.

The same methodology can be used for the definition of safety requirements for transport, application in aircrafts or ships, for prototype applications, as well as for the identification and the safety of testing facilities.

The main point is that the risk depends on several factors. It cannot be figured out just by knowing that a lithium ion battery is used in an electrical car. The overall risk depends on more factors that have to be taken into account.

TECHNICAL TRENDS

For the future in cell chemistry level, lithium-air and lithium-sulfur systems might be very interesting. With both systems it is possible to store more energy than what is currently possible. This is the reason further developing this. The hope is to get more range, but more energy means less safety on the cell level. Because of the higher risk on cell level, it is important to improve the safety of the battery system and the vehicle system.

Another very interesting topic is the research on flexible cells; this might work very well if high accelerations or intrusion of the battery housing occurs and the flexible cell doesn't break.

For cooling systems, it seems that air-cooling for an electric vehicle might work well. Some reduced systems cool only the outside of the cell housing or only the top or bottom.

In general, the strategy should be developed according to the following [4, 5]:

1. Cell and battery level

- Pre-emption – avoid thermal runaway
- Detection – warning of potential failure
- Intervention – stop thermal runaway
- Containment – minimize damage

2. Vehicle Level

- Safe driving
- Preventive Protection
- Adaptive Protection
- Secure and rescue

The strategy is in general the same; safe use, prevention by detection, reaction if needed and securing after an incident by minimizing the damage.

CONCLUSION

The use of lithium ion batteries in vehicles is not only important for the e-mobility future, it is the key to any future success for electric vehicles. It doesn't matter for which kind of vehicles it will be used.

There are several risks that exist, such as chemical risk or electrical risk. It is important to understand the technology and the reactions of the material, and the cell and the cell system during an accident. With this knowledge, it is possible to design a safe system.

An approach for a method to assess risks and to define requirements for the safety levels is outlined within this paper.

From statistical data of actual accidents, it seems that the risk for electric and hybrid vehicles to be involved in an accident is similar to that of conventional vehicles. There have yet to be found any studies that are focused on the crash safety of batteries because of the high number of non-technical reasons for accidents. It is important to focus on the accelerations and intrusions, but the reaction of batteries according to acceleration is not known completely; especially when it is combined with aging and different states of charge.

The technical risks are covered by developing according to ISO 26262.

The technical trends are gravitating toward higher energy and power densities; but in general, more energy means less safety.

Despite any potential drawbacks, it is possible to design safe battery applications and safe electric and hybrid vehicles if the risks are taken into account and the systems are designed properly.

REFERENCES

- [1] KBA - Kraftfahrtbundesamt, 2013
- [2] CPC internal, using data by ADAC, KBA, EU; 2012
- [3] FAA Office of Security and Hazardous Materials "Aviation Incidents Involving Smoke, Fire, Extreme Heat or Explosion"; 2012
- [4] Brian Barnett; Conference "BatterySafety" Las Vegas, 2011
- [5] Schöneburg, R., Unselt, T.: Sicherheitsstrategien im Spannungsfeld zwischen Sicherheit, Leichtbau und Wirtschaftlichkeit, ATZ agenda, Mobilität von morgen – Ideen und Konzepte, Oktober 2012, S. 30

A METHOD TO ESTIMATE DEFORMATION ENERGY LEVELS OF BATTERY AND FUEL CELL SYSTEMS DEPENDING ON THEIR LOCATION BY USING REAL ACCIDENT DATA (GIDAS)

Christian T., Erbsmehl

Verkehrsunfallforschung an der TU-Dresden GmbH
Germany

Paper Number 13-0444

ABSTRACT

Due to an increasing number of hybrid and electric vehicles in traffic the safety of battery packages as well as of fuel cells becomes more and more interesting. It is another reason to develop appropriate safety ideas to protect all traffic participants and rescue teams of possible threats. In order to reach high safety levels for possible accidents very hard cases protect the high voltage systems or fuel cells in cars. To meet the future safety requirements those housings are subject to various safety tests.

To point out some key requirements for the testing procedures the approach of the FaSeA study has to be continued with the focus on energy levels depending on the installation location of batteries or fuel cells. The aim of this publication is the design and development of a well defined 3-dimensional deformation energy model, which can be used to specify the testing requirements for future battery and fuel cell development or testing.

The model is designed on the basis of the German-In-Depth-Accident-Study (GIDAS) database, which contains about 20.000 deformed cars including the crash energies as a result of a detailed reconstruction of every single accident.

These deformations are then used to form a 3-dimensional-deformation-frequency-model using a similar method like the FaSeA project. After designing this deformation frequency model all deformations and crash energies of the reconstruction are being merged in the energy model. As a last step the energy model will be used to explain some example fuel cells or batteries regarding their installation location.

The paper will provide a better understanding for the development and the design of battery packages or fuel cells. It will also explain a method for specifying

battery package and fuel cell test requirements depending on the vehicle type and the installation location.

INTRODUCTION

Placing battery -packs, fuel cell systems or high-voltage parts in a car is a big issue in the construction process of actual and future cars. Thus gives the necessity to find out some possibilities for getting the deformation energy levels depending on the installation location of those systems or parts. The following paper will give further possibilities for getting information about energy-levels based on a existing method to get deformation frequency models.

3D-deformation models

Basis of the developed method is the creation of 3-dimensional-deformation-models, which is also explained in a previous publication [1]. To create such deformation models out of the accident database GIDAS two important steps have to be done: First step is the calculation and interpolation of the database deformation values and the second step is the 3-dimensional description of those deformations.

Calculation and interpolation In the GIDAS database deformation values for every accident participating car are coded. The deformation values are investigated following the next schemes.

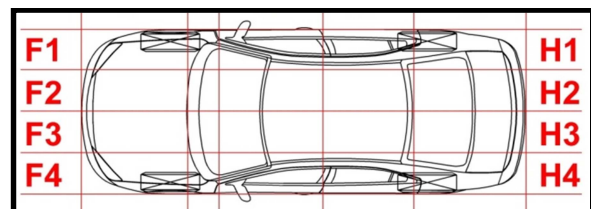


Figure 1: Deformation at front and rear

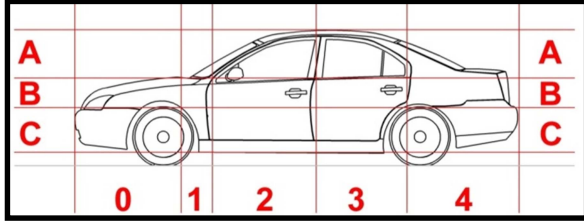


Figure 2: Deformation at the side

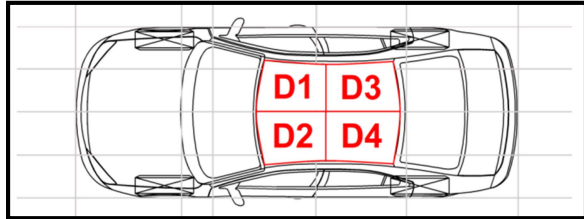


Figure 3: Deformation at the roof

The investigation of following those shemes by finding out the deformation depth of every zone delivers a scaled overview about the whole deformation at the car.

A linear interpolation of the deformation steps delivers deformations lines. The deformation line of the vehicle front or rear is shown in Figure 4.

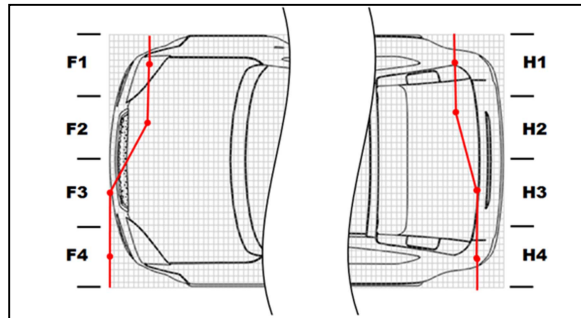


Figure 4: Deformation line of front and rear

The deformation lines of the vehicle side are result of a 2-dimensional interpolation step. First dimension of this interpolation are the deformation lines of the vehicle side of the top view.

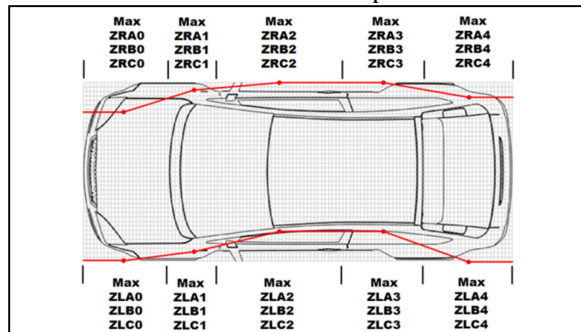


Figure 5: Side deformation lines (topview)

Second interpolation dimension are the deformation lines of the vehicle side of the rear view.

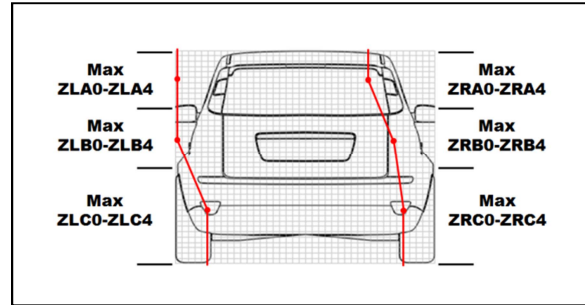


Figure 6: Side deformation lines (rear view)

Last interpolation is done for the vehicle roof (see Figure 7)

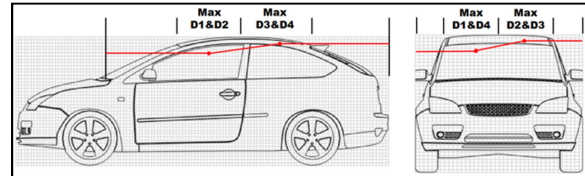


Figure 7: Deformation interpolation at the roof

The resulting deformation lines are afterwards blended with a vehicle Voxel-model which is explained in the next chapter.

Basic car-voxel-model To calculate and print the calculated 3-dimensional deformations a basic model is needed. This basic model will be a 3-dimensional vehicle-model. To build up this vehicle model a 3-dimensional (120x40x40) Voxel matrix is blended with a vehicle shape (Figure 8).

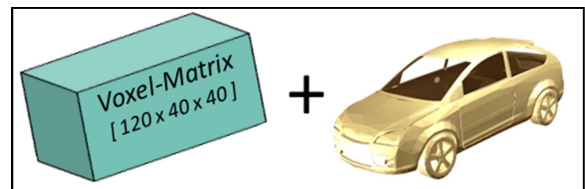


Figure 8: Blending process for basic-voxel-model

The result of this blending process is a 3-dimensional vehicle-voxel-matrix (Figure 9).

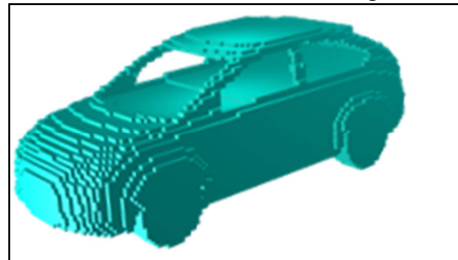


Figure 9: Basic car-voxel-model

Blended results The basic-car-voxel-model and the interpolation planes are blended to get the resulting 3-dimensional-deformation-model. Figure 10 shows an example vehicle out of the GIDAS-database.



Figure 10: Deformed real vehicle (GIDAS) [6]

The calculated result blended with the car-voxel-model is shown in Figure 11. This figure shows four plot variations of the deformation model of the example car.

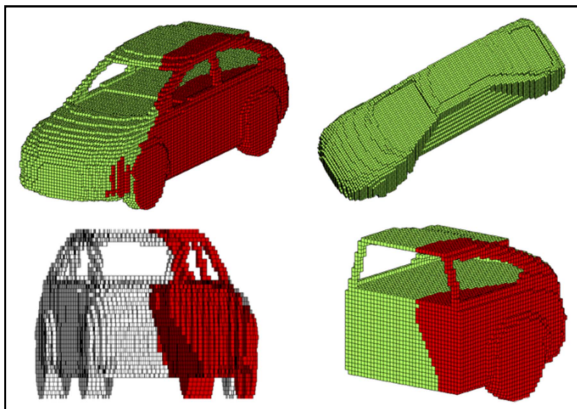


Figure 11: Vehicle-deformation-model

3D-Energy-models (EES-models)

The GIDAS-database also includes information about the deformation energy of every collision. This deformation energy is coded as a speed value called the EES (energy equivalent speed).

Deformation energy It is possible to calculate the deformation energy (E_{ges}), using the equation of the kinetic energy by the vehicles crash mass (m) and the EES-value (EES).

$$E_{ges} = \frac{m}{2} * EES^2 \quad (1)$$

The calculation of the deformation energy is followed by an own distribution approach.

Energy distribution approach Main point of the distribution approach is the fact of the increasing force (F) by the deformation distance during a crash until the maximum compression is reached.

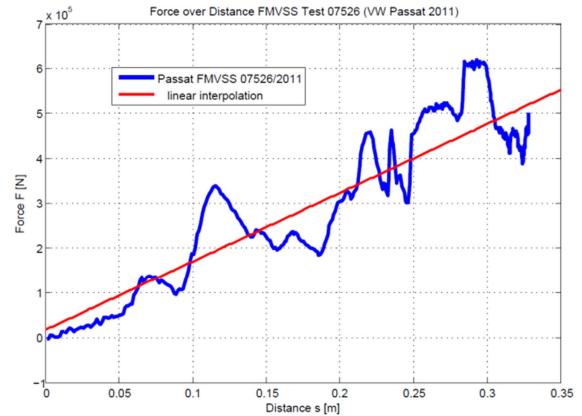


Figure 12: Force over distance, NHTSA [2]

Figure 12 shows the force over the distance during a crash test of a VW Passat in the NHTSA FMVSS 208 Nr. 07526 [2]. Based on this the integration of a linear increasing force is a quadratic increasing deformation energy (Figure 13).

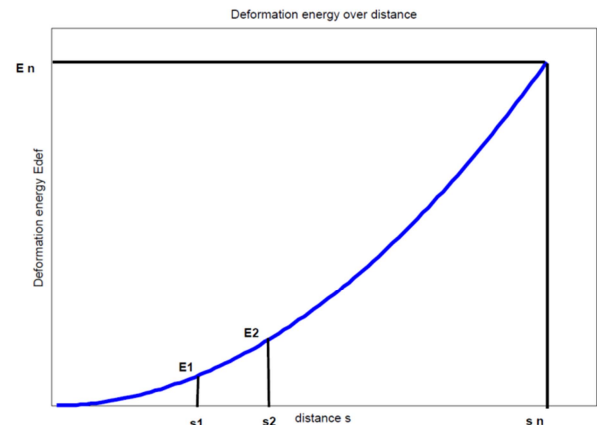


Figure 13: Deformation energy over distance

The whole deformation energy (E_{ges}) is the sum of the single energies in all distance steps (i). Thus the following equation can be set.

$$E_{ges} = \sum_{i=1}^n E_i \quad (2)$$

where $i = 1, \dots, n$.

To calculate the distribution of this deformation energy a simple quadratic equation and a weighting factor (b_i) is used.

$$E_i = b_i \cdot a \cdot s_i^2 \quad (3)$$

The deformation distance (s) is taken out of the deformation area of the vehicle and the direction of the impact pulse. The direction of the impact pulse is coded in the GIDAS-database as well and is called the “VDI 1”. This parameter divided in 12 clockwise parts for every “VDI 1” direction an energy distribution matrix is calculated as a 2-dimensional matrix [120 x 40].

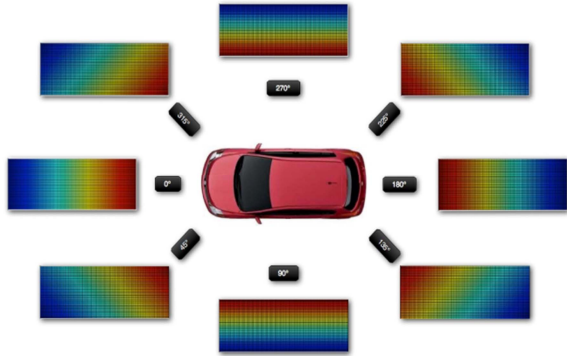


Figure 14: energy distribution by VDI 1

This energy distribution matrix is taken into a 3-dimensional model, which matches the basic-voxel-matrix.

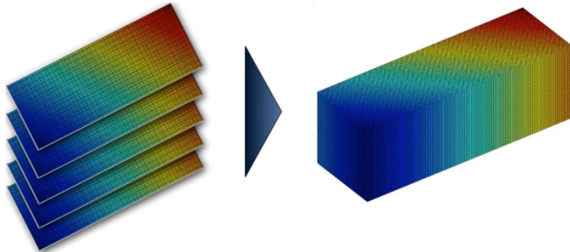


Figure 15: 3-dimensional energy distribution matrix

This 3-dimensional energy distribution matrix is blended with the vehicle shape and the deformations, similar to the basic-voxel-matrix.

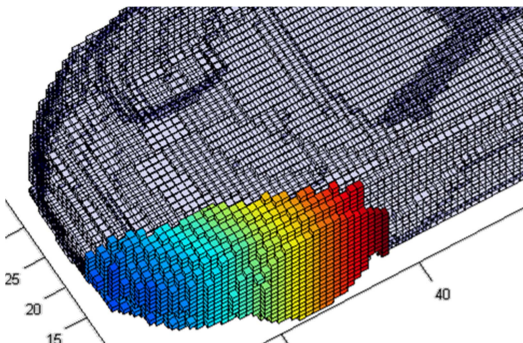


Figure 16: 3-dimensional energy distribution direction

Figure 16 shows an example of this distribution direction. With the number of deformed voxel, the distribution direction, the length and the width of the vehicle it is possible to calculate the deformation distance (s) of the actual deformation.

Due to the very asymmetric distribution of the deformation volume during the real crash (e.g. Figure 11), a weighting factor (b_i) has to be created.

$$b_i = \frac{anz_i}{Vox_{total}} \quad (4)$$

where anz_i are the deformed voxel in each deformation distance step s_i

and Vox_{total} the number of totally deformed voxel in the collision.

This is necessary because there might be a larger deformation volume in some first deformation distance steps than in the following ones.

The placement of equation (3) and (4) into equation (2) delivers the following equation.

$$E_{ges} = a \cdot \frac{1}{Vox_{total}} \sum_{i=1}^n anz_i \cdot E_i \quad (5)$$

To calculate the term a the equation has to be transposed.

$$a = \frac{E_{ges} \cdot Vox_{total}}{\sum_{i=1}^n anz_i \cdot s_i^2} \quad (6)$$

In the next step the deformation energy of each distance step (k) is calculated by the following equation.

$$E_k = \frac{E_{ges}}{\sum_{i=1}^n (anz_i \cdot s_i^2)} \cdot anz_k \cdot s_k^2 \quad (7)$$

, where $k = 1, \dots, n$.

Last step is the calculation of the deformation energy for every single voxel (E_{Voxel}) with the following term.

$$E_{Voxel,k} = \frac{E_k}{anz_k} \quad (8)$$

Grouping the results After the calculation of the deformation energy of each voxel in the whole deformation at one vehicle the results for every vehicle have to be grouped. The fact that the deformation energy of each vehicle depends on the vehicle mass leads to the conclusion, that a grouping of this value delivers wrong information. Thus, a mass free energy value is needed. The best way to set a mass free energy level value in a model is the EES (energy equivalent speed) as used before to calculate the deformation energy. The EES-value of every voxel can be calculated by using the crash mass of the vehicle which is coded in the GIDAS-database.

$$EES_{Voxel} = \sqrt{\frac{2 \cdot E_{Voxel,k}}{m}} \quad (9)$$

After the calculation of the EES-value of every voxel in the deformation area of one vehicle a mean value for each voxel location in a vehicle shape can be calculated regarding all vehicles in the group.

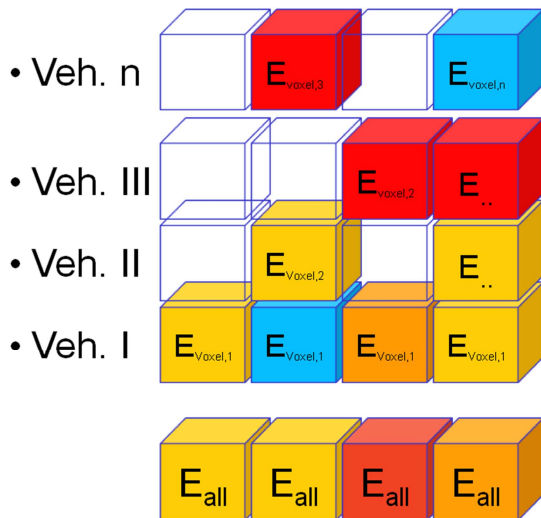


Figure 17: calculation of the mean EES of a vehicle group

Figure 17 shows the scheme of the calculation of the mean values of a vehicle group.

Vehicle groups The development of the passive safety elements in vehicles causes a variation of the deformation and crash behavior between older and newer cars.



Figure 18 EuroNCAP Test Opel Corsa B 1997[3]

Figure 18 shows an old EuroNCAP crash-test with an Opel Corsa B from 1996.



Figure 19: EuroNCAP Test Audi A6 2011 [3]

And figure 19 shows an EuroNCAP crash-test with a newer Audi A6 from 2011. In both tests the EES-value is 64 km/h. But there are two main differences between the tests.

1. The year of construction
2. The vehicles mass

Thus, the basis for the distribution of the EES has to be divided in four groups:

1. Younger, light vehicles
2. Younger, heavy vehicles
3. Older, light vehicles
4. Older, heavy vehicles

The borders for the groups are taken out of the particular distributions of the year of construction and the vehicle weight of the basic dataset.

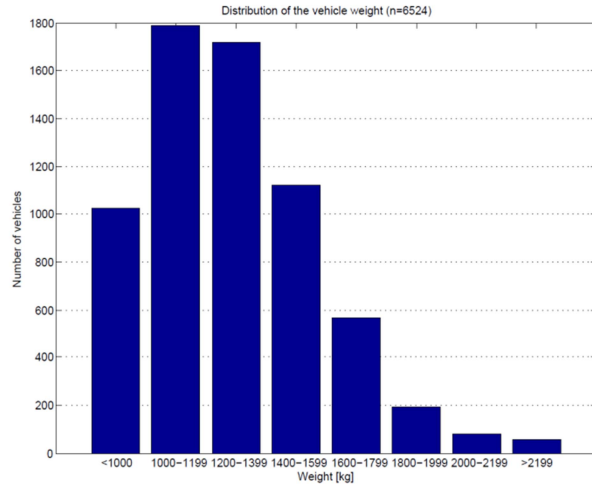


Figure 20: Distribution of the vehicle weight

Figure 20 shows the distribution of the vehicle weight in the basis-dataset. The spread is from 618kg to 3015kg and the median is at 1244kg. Thus, all vehicles with a weight up to 1300kg are light vehicles and vehicles with a weight of more than 1300kg are heavy vehicles.

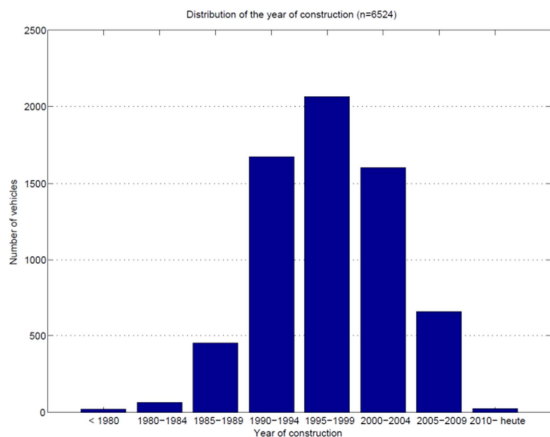


Figure 21: Distribution of the year of construction

Figure 21 shows the distribution of the year of construction of the basis-dataset with the minimal value at 1961 and a maximum value at 2011. The median is at 1997. Based on this median all vehicles which are built up to the year 1997 are old vehicles and all vehicles which are built from 1997 to 2011 are new vehicles.

Results The results of the energy and EES distribution for all four groups deliver the following results for example for young heavy vehicles.

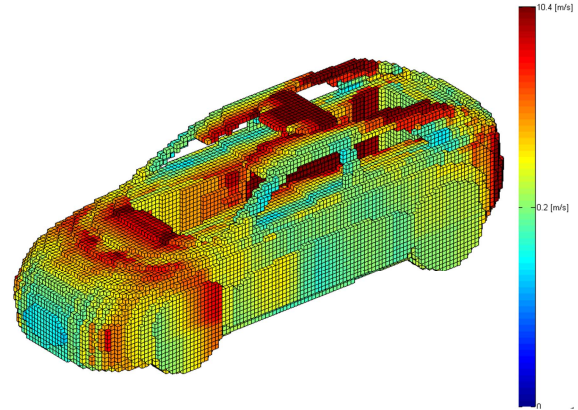


Figure 22: EES distribution of young heavy vehicles

In Figure 22 a distribution of EES values per voxel is shown. The dark red areas have an EES value up to 0.4 [m/s] per voxel and the lighter blue areas have an EES-value down to 0.1 [m/s] per voxel. A more precise overview about the result gives a top view where all EES-values in z-direction are averaged.

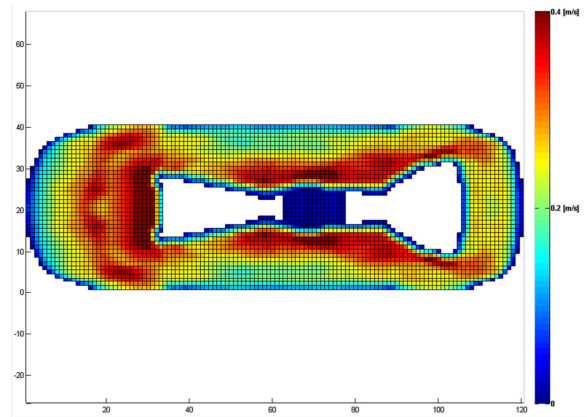


Figure 23: EES distribution (top view, young, heavy)

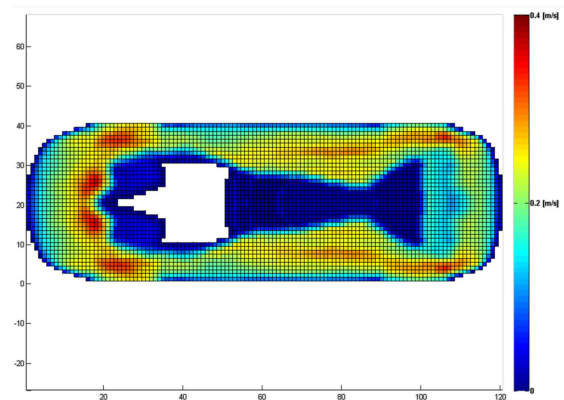


Figure 24: EES distribution (top view, young, light)

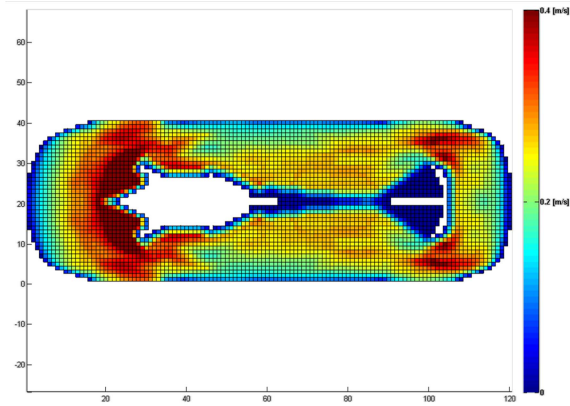


Figure 25: EES distribution (top view, old, heavy)

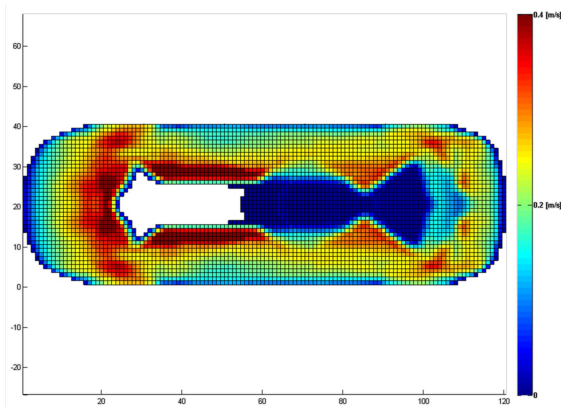


Figure 26: EES distribution (top view, old, light)

These four results show very good the different EES distributions of the four groups. Especially the engine, the absorbing deformation elements and of course the axles have a relative high EES distribution. A difference between newer and older vehicles can also be seen at the sides.

Usage of the Energy (EES) models

There are many ways the Energy (EES) models can be used. Exemplary uses can be: to point out the stiffness of GIDAS vehicles for an automated crash calculation, to build up an EES-catalog or to validate reconstruction calculations. This paper will give a possibility how these models can be used to get some first ideas for testing battery or fuel cell systems or to determine the energy level at their installation locations.

Crash Tests For validation of these EES models a simulative crash test can be done. Therefore a FMVSS 208 with 52 km/h against a rigid barrier is chosen. The EES distribution of an

old heavy car delivers the vehicle model for this test. The vehicle mass is defined with 2000 kg.

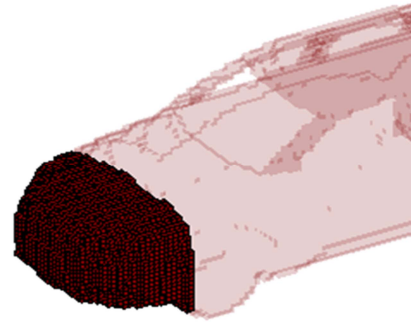


Figure 27: Vehicle deformation after validation crash test FMVSS 208

A similar real test with the number 3455 of a Honda Accord is shown in the figure below.



Figure 28: NHTSA Crash Test 3455 [5]

Both pictures show equivalent deformations. The absorbed crash energy is shown in another picture.

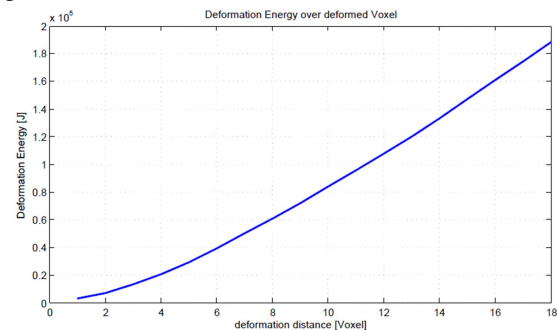


Figure 29: Deformation energy during the crash simulation

This deformation energy over deformation distance matches also good with the energy recorded in FMVSS 208 crash tests.

Rebuilding of the system For further analysis with installed battery and fuel cell systems a geometric definition of the volume of interest is needed.

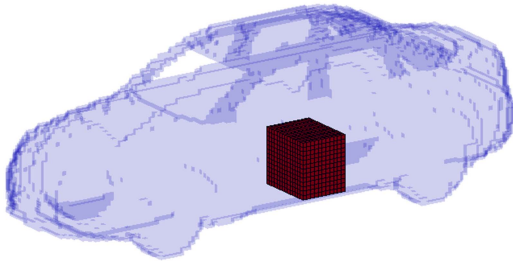


Figure 30: geometric definition of volume of interest

The example volume is defined at the back of the vehicle shape between the wheels (Figure 30).

Calculation of the resulting deformations

The first analysis which can be done with 3D Energy or EES models is to analyze how the crash behavior of all recorded real accidents in the GIDAS database will be modified by using very stiff battery packs or fuel cell systems. To analyze this crash behavior the volume of interest or the installation location of one car is configured very stiff and the crash is simulated again. The next figure shows a calculated example accident, which is a side collision with high speeds.

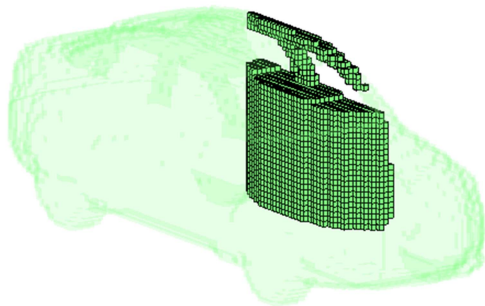


Figure 31: deformation behavior of the pushed vehicle without stiff cells

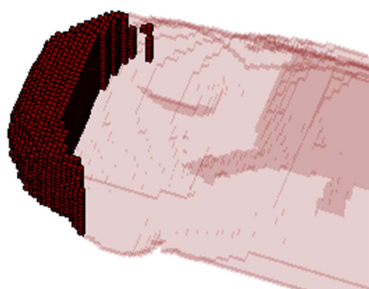


Figure 32: Deformation behavior of the striking vehicle without stiff cells

After that calculation the pushed car is equipped with a very (exorbitant) stiff element at the left side (Figure 30). And the same crash is simulated again. The results of this second crash are shown in the next figure.

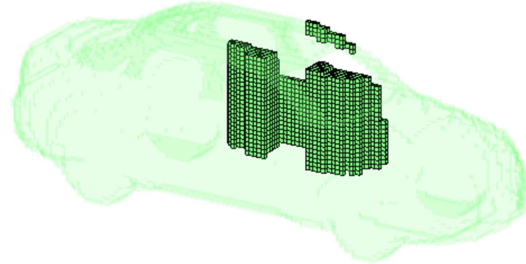


Figure 33: deformation behavior of the pushed vehicle equipped with stiff cells

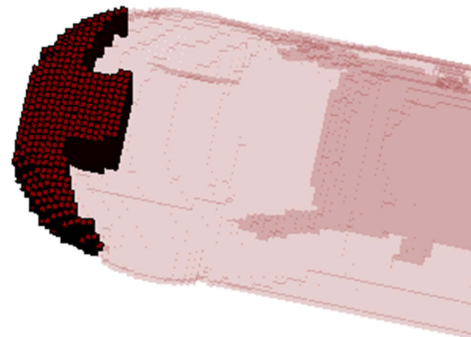


Figure 34: Deformation behavior of the striking vehicle equipped with stiff cells

The last both pictures show, that the deformation behavior in the real crashes will be very different depending on the stiffness level of the battery packs and fuel cells in future vehicles. This may have further influences to the development of new cars, battery packs or fuel cells.

Calculation of resulting energy levels The next possibility how the Energy (EES) models can be used for battery and fuel cell safety development is the possibility to find out which energy level in the deformed zones of the vehicle is important. Or what does the battery packs and the fuel cells have to absorb. This question can be answered again with the definition of a volume of interest or installation location in the car. After this definition all deformation energy is distributed as explained before and the area of interest is recorded in detail. This means, that the still left deformation energy at the area of interest is coded into a several matrix without calculating a mean value. At the end there will be maximum energies

relative to the installation location. The next picture shows an example battery pack between the rear axle of a vehicle.

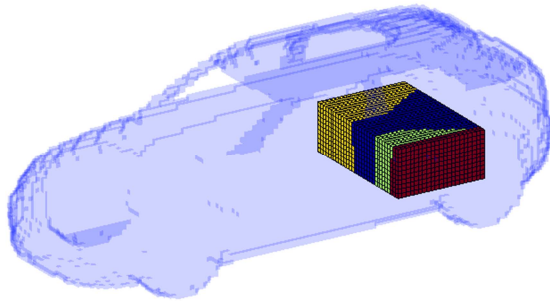


Figure 35: Energy level of battery pack example 1

In Figure 35 the left deformation energy at the chosen installation location is shown. The picture gives the possibility to check, where the critical areas for the installation of battery packs or fuel cell systems are. For this example there are three levels of left deformation energy, using a 2000kg vehicle.

1. Green – 15.210 J
2. Orange – 21.160 J
3. Red – 51.840 J

This is only an example result to show the possibilities of the energy (EES) models method.

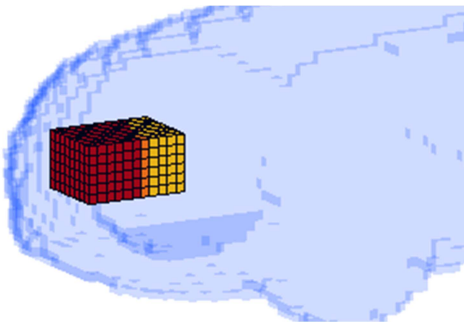


Figure 36: Energy level of battery pack example 2

Figure 36 shows the battery pack in the front of the vehicle with the following energy levels for a 2000 kg vehicle.

1. Yellow – 11.560 J
2. Orange – 15.210 J
3. Red – 23.040 J

These deformation energy levels are much lower than the energy levels between the rear axle but there is a much higher deformation frequency at this location. So the analysis of the safety of the installation location of battery packs and fuel cell

systems should be also done in dependency of the deformation frequency at the vehicle out of the real accident scenarios e.g. GIDAS.

CONCLUSIONS

This paper gives an overview about new methods to get a better understanding of the installation locations of battery packs or fuel cell systems. Basis of the method are deformed vehicles of the GIDAS database. The deformations of those vehicles are calculated into 3-dimensional deformation models. The deformation energy of the particular deformation is then distributed by an own new approach with 3-dimensional energies (EES) models as a result. Those models can then further be used to point out relevant information of the safety of the installation locations of fuel cell systems or battery packs according to real accidents. At last three important issues can be taken out of the analysis.

1. 3-dimensional energy (EES) models can deliver statements to the safety of fuel cell systems and battery packs
2. The safety of the installation location of those systems has to be analyzed for
 - a. Deformation behavior
 - b. Energy levels
 - c. Deformation frequency
3. The development of stiff fuel cell systems or battery packs may have a principle influence to real accident scenarios

REFERENCES

- [1] Erbsmehl, Große, Bakker, 2011. „Analyse von Einbautagen für Hochvoltssysteme und Energiespeicher im Fahrzeug auf Basis von Unfalldaten“ VDI Fahrzeugsicherheit (Berlin, Oct 5-6)
- [2] NHTSA, FMVSS 208 Nr. 07526
- [3] EuroNCAP, 1997
- [4] EuroNCAP, 2011
- [5] NHTSA, FMVSS 208 Nr. 3455
- [6] GIDAS Project, German In-Depth Accident Study, <http://www.gidas.org>, 2011.